

PHYSICAL HYDROGRAPHY OF THE VIENNA POWER PLANT SITE

Part I: Computations of the
Distribution of Effluent
Discharged from the Vienna
Electric Generating Station
into the Nanticoke River

Part II: Computations of the
Distribution of Contaminant
Introduced into Chicone
Creek in Groundwater

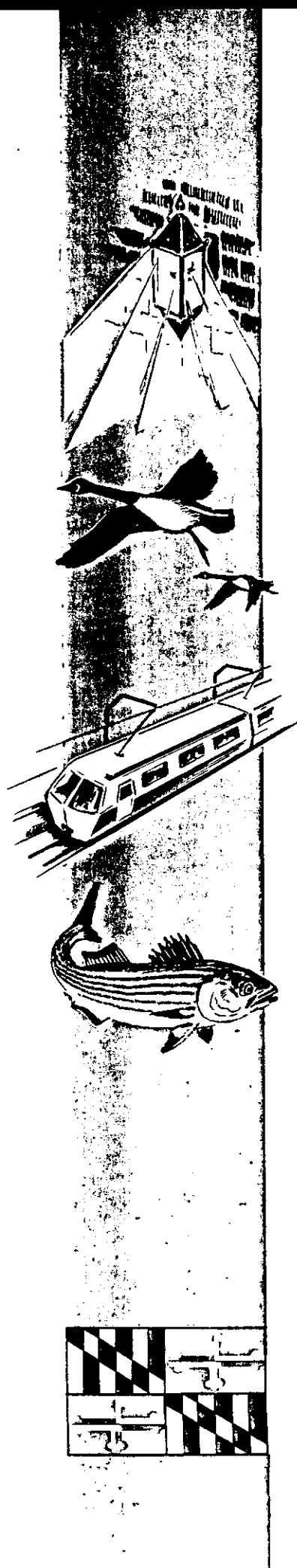
BY DONALD W. PRITCHARD
AND ROBERT E. WILSON

MARINE SCIENCES
RESEARCH CENTER
STATE UNIVERSITY OF NEW YORK
AT STONY BROOK

MARYLAND POWER PLANT SITING PROGRAM

DEPARTMENT OF NATURAL RESOURCES ■ DEPARTMENT OF HEALTH AND
MENTAL HYGIENE ■ DEPARTMENT OF ECONOMIC AND COMMUNITY DEVELOP-
MENT ■ DEPARTMENT OF STATE PLANNING ■ COMPTROLLER OF THE TREASURY
■ PUBLIC SERVICE COMMISSION ■

Versar INC.
ESM Operations
Library



1680-0809

MARINE SCIENCES RESEARCH CENTER
STATE UNIVERSITY OF NEW YORK
STONY BROOK, NEW YORK 11794

JHU-PPSE 8-10*

PHYSICAL HYDROGRAPHY OF THE VIENNA POWER PLANT SITE

PART I: COMPUTATIONS OF THE DISTRIBUTION OF EFFLUENT DISCHARGED
FROM THE VIENNA ELECTRIC GENERATING STATION INTO THE
NANTICOKE RIVER

PART II: COMPUTATIONS OF THE DISTRIBUTION OF CONTAMINANTS INTRODUCED
INTO CHICONE CREEK IN GROUNDWATER

by

Donald W. Pritchard and Robert E. Wilson

July 1980


Sponsored by the Power Plant Siting Program

Department of Natural Resources, State of Maryland

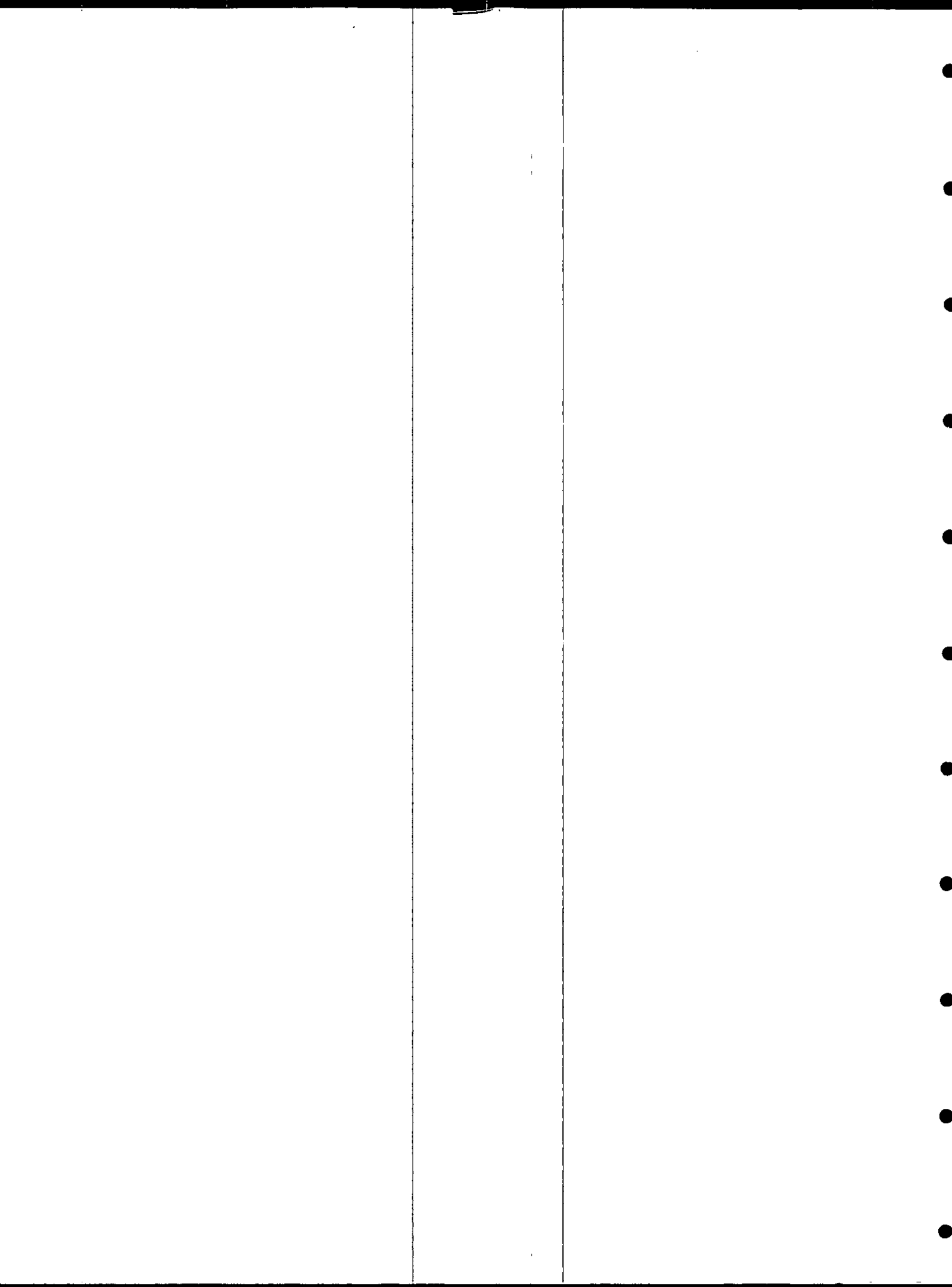
Special Report 37*
Reference 80-4

* Issued Concurrently

Approved for Distribution



J.R. Schubel, Director



Part I

Computations of the Distribution of Effluent Discharged
from the Vienna Electric Generating Station
into the Nanticoke River

INTRODUCTION

The purpose of this part of this report is to present the results of computer computations of the probable concentration of excess heat and contaminants in the Nanticoke River resulting from the combined discharge of blowdown water from existing Unit 8 and Proposed Unit 9 of the Vienna Electric Generating Station.

Computations are made herein for both the 400 MW new unit as originally proposed and for the 600 MW Unit 9 as now proposed in the amended Application for Certificate of Public Convenience and Necessity submitted by the Delmarva Power Company. Presentation of the results of both these cases allows an evaluation of the impact of the plant as now proposed and also the increment increase in impact resulting from the increase in unit size between that originally proposed and that now proposed.

In making the detailed calculations shown graphically in this report it was assumed that the blowdown water from Unit 8 and Unit 9 would be combined into a single discharge. Combining the discharges from the units would provide a smaller nearfield thermal plume than would be the case for the complex interacting plumes which would result from separate discharges. Computational difficulties have

prevented us from determining the shape of the two interacting plumes for the case of separate discharges. However, estimates of the area enclosed within specified isolines of contaminant concentration and of excess temperature have been made, and these results will be compared with the results of the more detailed analysis of the single, combined discharge for the two units.

The detailed results of computations of the character of the thermal plume given here make use of the original design for the discharge pipe, which called for an 8" inside diameter. The present plans call for a discharge pipe with a 10" orifice. The effects of this difference in discharge orifice size will also be discussed in a later section of this part of this report.

THE MODEL

The model used to obtain the information on the shape and dimensions of the thermal and contaminant plume presented herein is the MSRC Combined Field Thermal Plume Model. A detailed description of this model is given by Carter *et al.* (1979). The model combines a near field thermal plume model based on the work of Carter and Regier (1974) with a far field diffusion model described by Carter *et al.* (1977). The latter model makes use of the Okubo-Pritchard Diffusion Equations, Pritchard (1960).

The procedure involves the super-position of a large number of sequential small diffusing patches, each from an infinitesimal, instantaneous source, and all moving with the time varying ambient

velocity $u_a(t)$. The sequence of infinitesimal sources sum to the continuous rate of discharge of the power plant. The integration of the far field model is carried out over a number of tidal cycles until a pseudo-steady state far field distribution is attained; that is, until the time dependent variations in concentration over the tidal cycle are repeated from tidal cycle to tidal cycle.

The concentration distribution as computed from the far field model, while applicable for locations well removed from the source, is incorrect in the near field plume because the momentum and buoyant entrainment are not included. After pseudo-steady state in the far field computations is reached, the source is turned off, and computations made for several tidal cycles to obtain the background concentration distribution over the near field and intermediate field.

The near field model is then exercised and the distribution of concentration thus obtained is added to the far field distribution. In carrying out this combining of the two models care is taken such that excess heat and contaminant mass are conserved.

An important feature of this model is that it includes the interaction of the far field and near field distributions. In most near field models, the tacit assumption is made that there is an infinite supply of "clean" water available for entrainment into the plume. No account is taken of the fact that quite often some fraction of the water being entrained into the plume as dilution water contains a background of contaminants and excess heat built up from the previous continuous discharges from the plant.

Models are often used without verification that the computed results can be used with reasonable confidence for the specific purpose at hand. Usually this is because the data necessary for such verification are not available. The various parts of the MSRC Combined Field Thermal Plume Model have shown good comparisons with a number of direct plume measurements. The model has been used in its present full configuration in studies associated with an existing power plant on the Hudson River estuary. Good comparison was obtained between computed and observed values of recirculation at the plant, though no detailed comparison of computed and observed plume characteristics were made.

Fortunately, a set of data exists which allows verification of the model's use in the Vienna area of the Nanticoke River. In April 1974 the condenser discharges from the once-through cooling systems of Units 5, 6 and 7, together with the blowdown water from the cooling tower of Unit 8, were tagged with the fluorescent dye Rhodamine WT, as reported by Carter and Regier (1975). We have exercised the MSRC Combined Field Thermal Plume Model under the conditions applicable to the April 1974 field study, and have compared the computed values of dye concentration with the observed values of dye concentration with the observed values reported by Carter. This comparison is presented as final section to this part of this report.

INPUT PARAMETERS FOR THE MODEL

The model requires that certain geometric and flow dependent parameters be specified, including the time dependent velocity field.

For our purposes here the velocity was considered to be composed of a time dependent oscillatory component of semi-diurnal tidal period plus a time independent non-tidal mean velocity. An analysis of the current meter records made just upstream from the plant indicated that the amplitude of the oscillatory tidal current for the subject segment of the Nanticoke River is 55 cm s^{-1} . The mean non-tidal flow depends on the river flow, but the current meter records do not indicate any significant vertical shear in this mean flow.

Three river flow conditions were considered: (1) A low river flow of 445 cfs, which results in a non-tidal velocity of 0.84 cm s^{-1} for the average cross-section in the two-tidal excursion long reach of the river centered on the plant site; (2) a mean river flow of 810 cfs, which corresponds to a mean non-tidal velocity of 1.53 cm s^{-1} ; and (3) a high river flow of 1520 cfs, corresponding to a mean non-tidal velocity of 2.86 cm s^{-1} .

The diffusion velocity, a coefficient which enters the Okubo-Pritchard Diffusion Equations, was taken to be 1.5 cm s^{-1} . This value has been found applicable in other studies in the Chesapeake Bay estuarine system, and on the basis of the verification study described later in this report, this value appears applicable to the Nanticoke in the vicinity of the Vienna Electric Generating Station.

The mean width of the river in the area of interest was taken to be 410 meters, and the mean depth as 3.67 meters.

As pointed out earlier, it was assumed that the blowdown water from Unit 8 and Unit 9 would be combined into a single discharge.

The design features of the discharge structure were taken from the Application for Certificate of Public Convenience and Necessity as originally submitted by the Delmarva Power Company, for a shoreline submerged discharge for Unit 9. The details are given in Section 2.8C.1 and Figure 2.8C.1 of the above captioned document. Briefly, the discharged orifice is assumed to be located at a depth of 10 feet below MLW on the face of a vertical wall at the shoreline. This wall is assumed to extend downwards to a dredged bottom at 12 feet below MLW. The discharge port is taken to be a cylindrical pipe with an inside diameter of 8 inches. The effects on the results described here of increasing this pipe diameter to 10 inches will be discussed in a later section.

Computations were first made using the wintertime blowdown flow from Unit 9, as stated in the above captioned document for a 400 MWE unit, of 1332 gpm, combined with a blowdown discharge from Unit 8 of 381 gpm. This later figure was obtained by scaling the blowdown flow from Unit 9 by the ratio of the make-up flow for Unit 8 of 1460 gpm as given by Carter (1975) to the make-up flow for Unit 9 of 4892 gpm as given in the above captioned application. The total rate of flow to be discharged through the 8" diameter outfall was therefore taken to be $1713 \text{ gals min}^{-1}$ or $0.108 \text{ m}^3 \text{ sec}^{-1}$. The velocity at the discharge orifice was then taken to be 3.33 m sec^{-1} (or 10.9 ft sec^{-1}).

The Delmarva Power Company states in their Application for Certificate of Public Convenience and Necessity that the blowdown

water at point of discharge will have a temperature of 68°F in winter when the ambient temperature in the river is 34°F; while in summer the temperature of the discharge will be 85°F when the ambient temperature of the receiving water is 84°F. Hence the excess temperature at discharge in winter would be 34°F, and in summer only 1°F. The amended document gives slightly different values. However, these differences would not significantly alter the conclusions reached here.

The preliminary computations presented here are for the wintertime conditions of a 34°F excess temperature of the discharge. The summertime case for an excess temperature of 1°F is not treated for the following reasons. The distribution of relative concentration in the far field would not be significantly different between summer and winter, other things, such as river flow being equal. In the present form of the MSRC model, computational difficulties arise for the near field computations for very large densimetric Froude numbers such as occur for an excess temperature of only 1°F. We know that the near field plume will be smaller, that is, show more rapid dilution with distance from the source, as the densimetric Froude number increases, other factors being equal. Consequently the case considered here should be more severe in the near field than would occur for the summertime conditions of a 1°F excess temperature.

Intermediate conditions will exist in the spring months of April and May, when spawning of striped bass occur in this reach of the Nanticoke River. Excess temperatures of the discharge will be

about 15°F in April and 12°F in May. The size of the areas contained within specified isotherms of excess temperature in the thermal plume will thus be less than those computed here for the winter case, by a factor of two or more.

Note that in our computations we deal not with the absolute value of the excess temperature or of the concentration of a contaminant, but with the relative concentration; that is, the ratio of the concentration (or excess temperature) at any point in the plume to the concentration (or excess temperature) at the point of discharge. Thus, while the excess temperature in the summertime plume will obviously be much less than the excess temperature in the wintertime plume, since the initial undiluted values are 1°F for summer and 34°F for winter, the relative excess temperatures for the two cases will be approximately the same in the far field, and only fractionally lower in summer than in winter for the near field plume. This fact is important since the concentration of chemical contaminants in the undiluted blowdown water may be higher in summer than in winter.

RESULTS

The computed output from the model for these computations are in terms of the relative concentration, or inverse dilution. Thus, representing the dilution of the effluent by the symbol D , the concentration of a contaminant at the point of discharge by c_o and that at any other point in the river by c , and the excess temperature at the point of discharge by θ_o and that at any other point in the river

by θ , then the relative concentration is given by

$$D^{-1} = \frac{c}{c_o} = \frac{\theta}{\theta_o} \quad (1)$$

The relative concentration then varies from 1.0 at the discharge to 0.0 at positions sufficiently removed from the source so that no measurable constituents of the effluent occur.

Note that Equation (1) when applied to the excess temperature, θ , is correct only if surface cooling to the atmosphere is unimportant. This is certainly the case here where mixing in the near field plume results in a rapid reduction in excess temperature to very low values due to dilution. The integral of the excess temperature over the area of the plume results in a very low driving term for heat loss to the atmosphere.

Computations were made over a reach of the river extending upstream and downstream from the plant site a distance of 5 nautical miles (9.2 km) which is approximately the length of a tidal excursion. The complex geometry of this 10 nautical mile reach of the river was scaled to a rectilinear grid having a width of 410 meters, the mean width of the river over this segment. Values of the relative concentration were printed out at 561 grid positions for the far field computations. The grid points were separated by 0.2 nautical miles in the longitudinal direction and by 41 meters in the lateral direction. The rectilinear grid was distorted in the printout so that there appears to be an equal spacing in the lateral direction and in the

longitudinal direction; that is, the river appears to be wider in relation to its length by the factor of $370.6/41$ or 9.04 .

Printouts were obtained for each of the three river flows (high flow, or 1520 cfs; mean flow, or 810 cfs; and low flow, or 445 cfs), for four different stages of the tide (maximum ebb, maximum flood, near slack before ebb, and near slack before flood). Values are given for near the time of slack water rather than at slack water because the near field model fails to compute for exactly zero ambient current.

The computed relative concentration distributions were contoured by hand, and the resulting far field distributions on the distorted rectangular reach of the river are shown in Figures 1 through 6 for the twelve cases considered (3 river flows, each for 4 phases of the tide).

The near field plume on these figures is somewhat larger than it should be, since the far field computation does not take into consideration dilution by momentum entrainment close to the points of discharge. Near field calculations were carried out for mean river flow, for near slack before ebb and for maximum flood flow. These computations were made on an expanded rectangular grid of 1071 points extending longitudinally 0.2 nautical miles upstream and downstream from the point of discharge, and extending laterally from the western shore of the river outward a distance of only 82 meters. The longitudinal spacing between grid points for this near field calculation was 0.0080 nautical miles, and the lateral spacing was

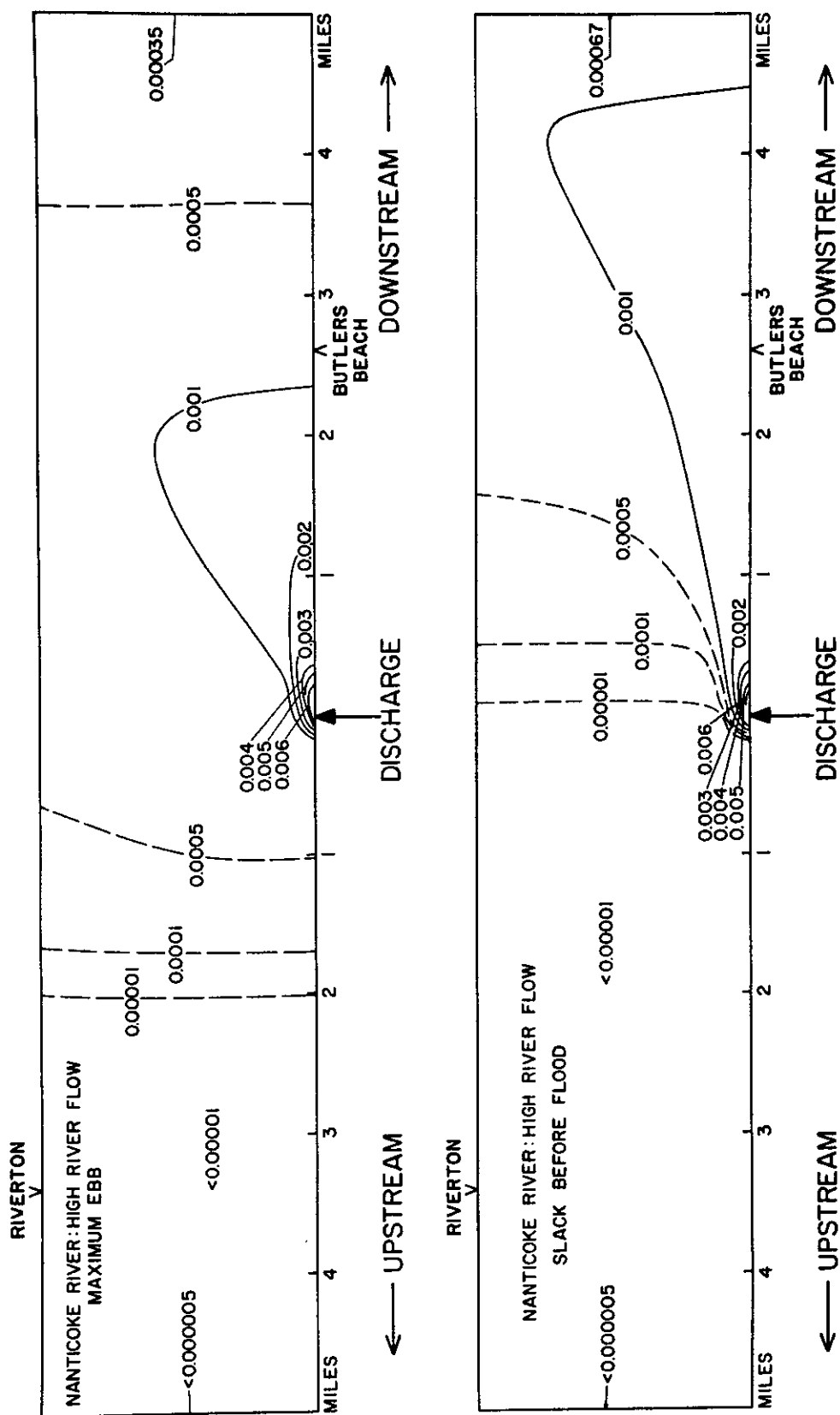


Figure 1. Isolines of relative concentration for high river flow (1520 cfs), for maximum ebb tidal flow and for near slack before flood.

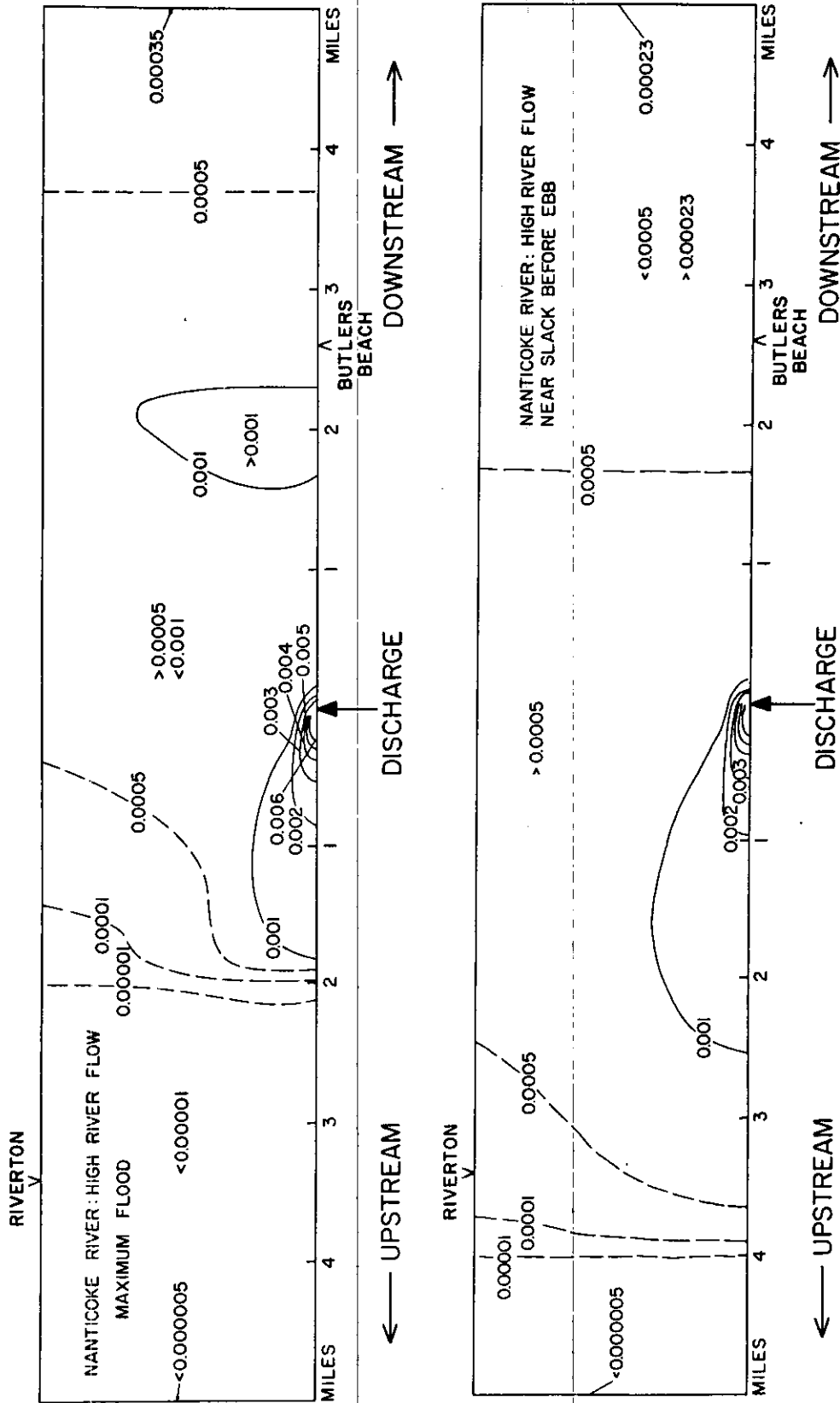


Figure 2. Isolines of relative concentration for high river flow (1520 cmfs), for maximum flood tidal flow and for near slack before ebb.

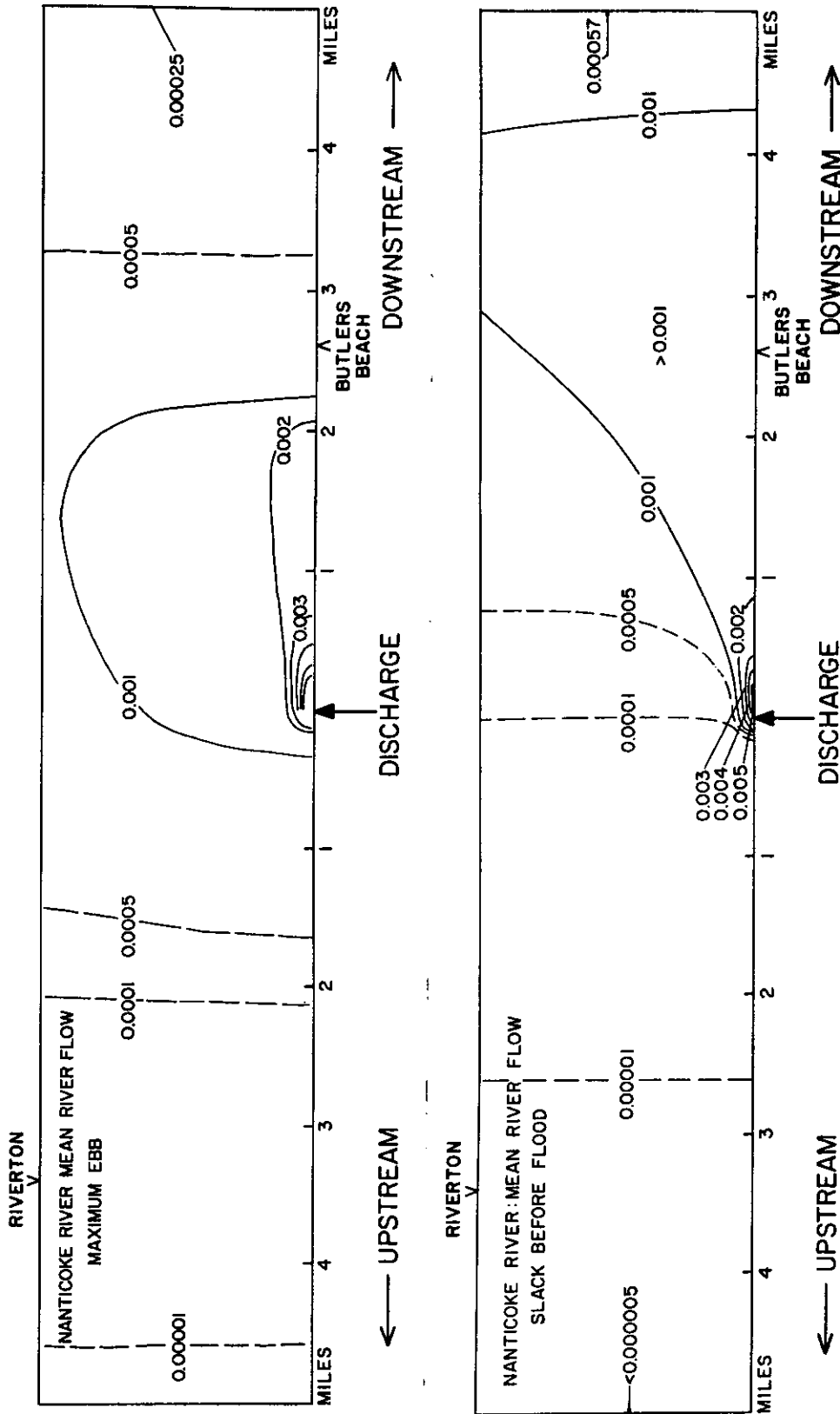
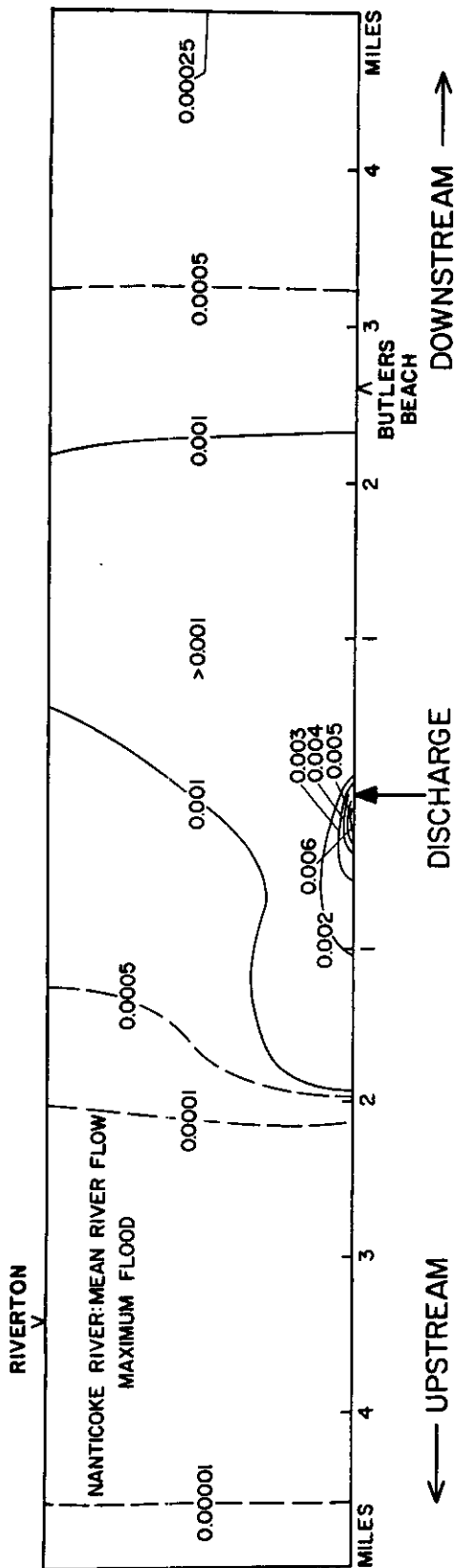


Figure 3. Isolines of relative concentration for mean river flow (810 cfs), for maximum ebb tidal flow and for near slack before flood.



-14-

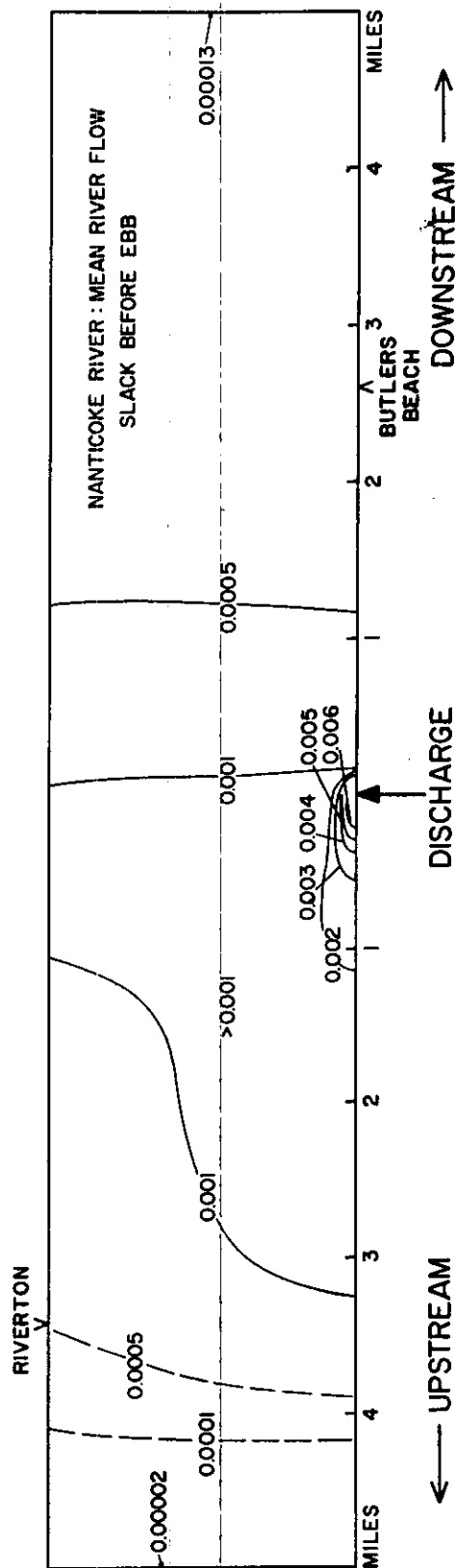


Figure 4. Isolines of relative concentration for mean river flow (810 cfs), for maximum flood tidal flow and for near slack before ebb.

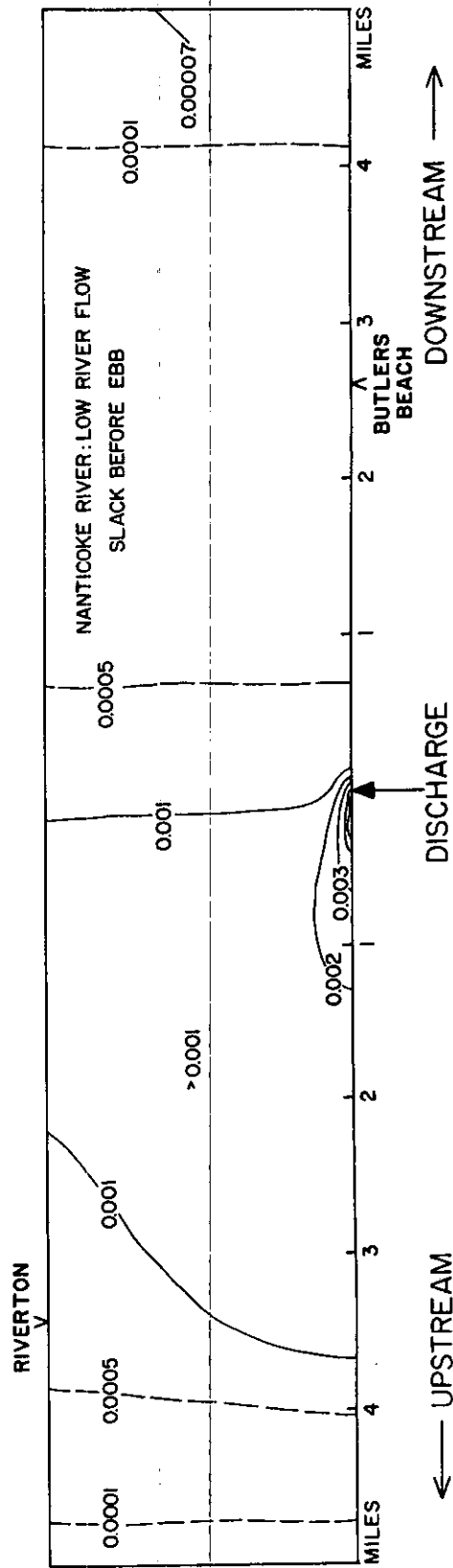


Figure 6. Isolines of relative concentration for low river flow (445 cfs), for maximum flood tidal flow and for near slack before ebb.

4.1 meters. The contoured distributions of relative concentration for these near field plumes are given in Figures 7 and 8.

The far field distributions of relative concentrations have been scaled back to the actual geometry of the river, and the twelve cases are given in Figures 9 through 32. A separate figure is given for the reach of the river up-stream from the point of discharge and for the reach of the river downstream from the point of discharge for each of the twelve cases considered.

Before going further we should mention that we accounted for the influence of the river banks on the far field concentrations by using the method of images. Reflection from the river bank which is on the same side of the river as the original source was accounted for by simply doubling the magnitude of the original source. Reflection from the distant river bank was accounted for by placing an image source behind this bank a distance equal to the width of the river. This image source must itself have an image appropriately placed, and so on. We used in total 6 image sources and the relative far field concentration fields presented in Figures 1 through 6 and 9 through 32 each represent a linear superposition of the field from the original source and the 6 image sources.

The concentration fields in Figures 1 through 6 and 9 through 32 show a well defined plume with relatively high concentrations superposed on a relatively uniform background. The plume is composed of material emitted from the source since the last change in direction of the tidal current. Concentrations within the plume decrease down

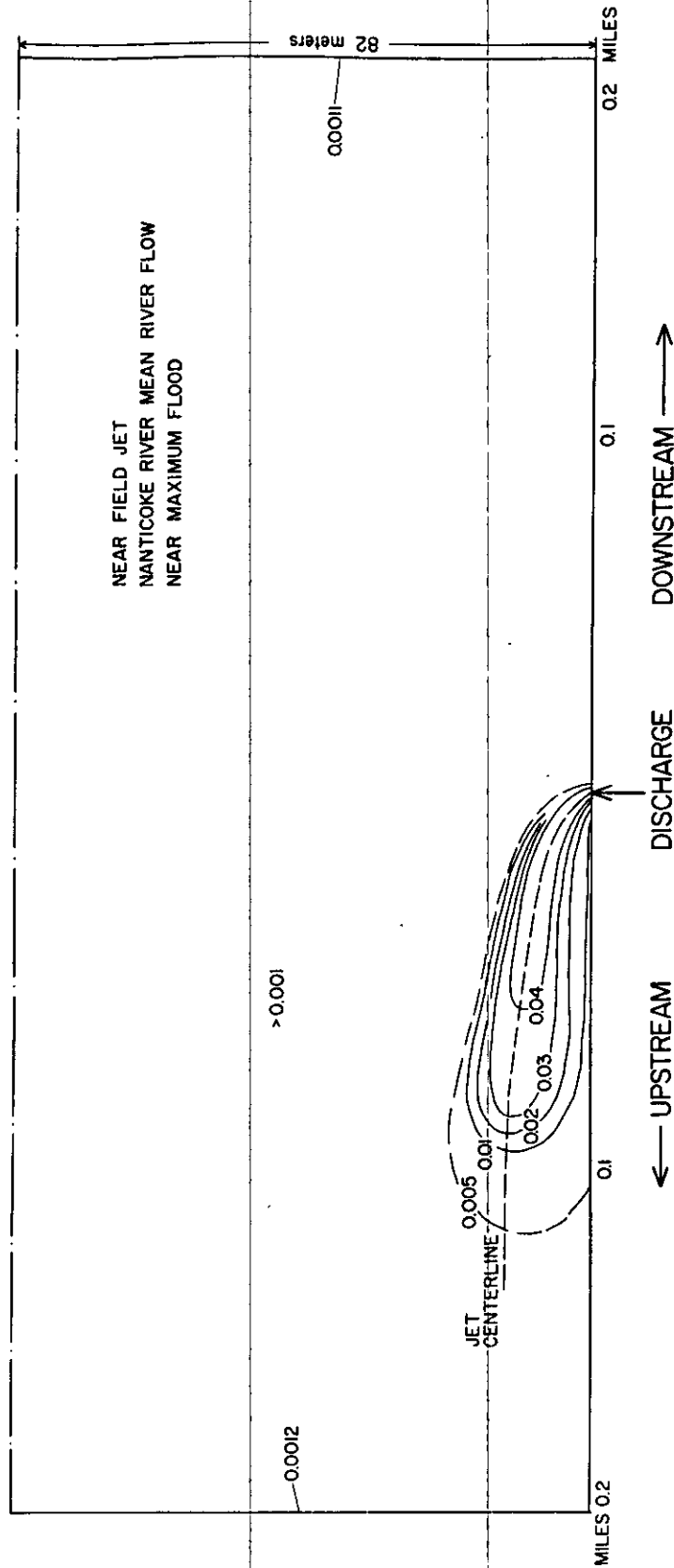


Figure 7. Isolines of relative concentration in the near field plume for mean river flow, for near maximum flood tidal flow.

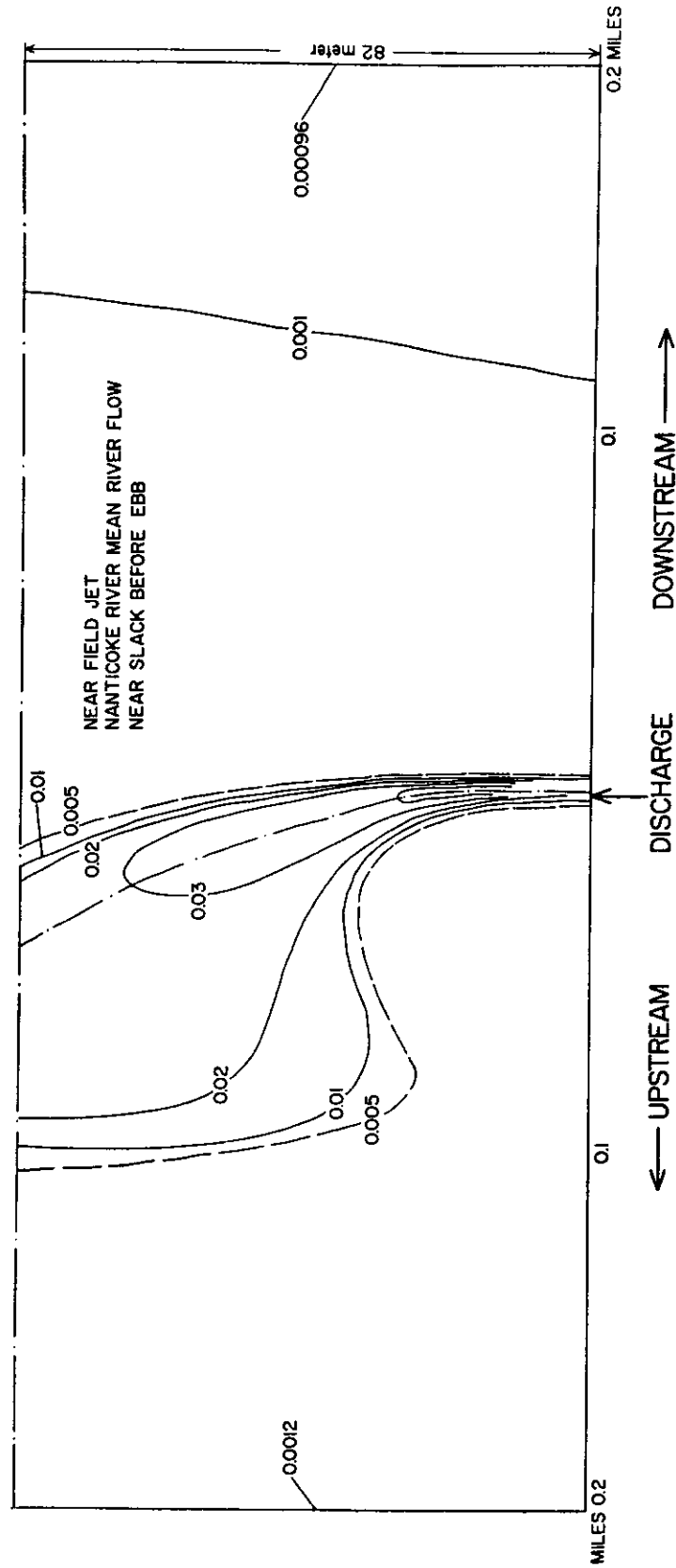


Figure 8. Isolines of relative concentration in the near field plume for mean river flow, for near slack before ebb.

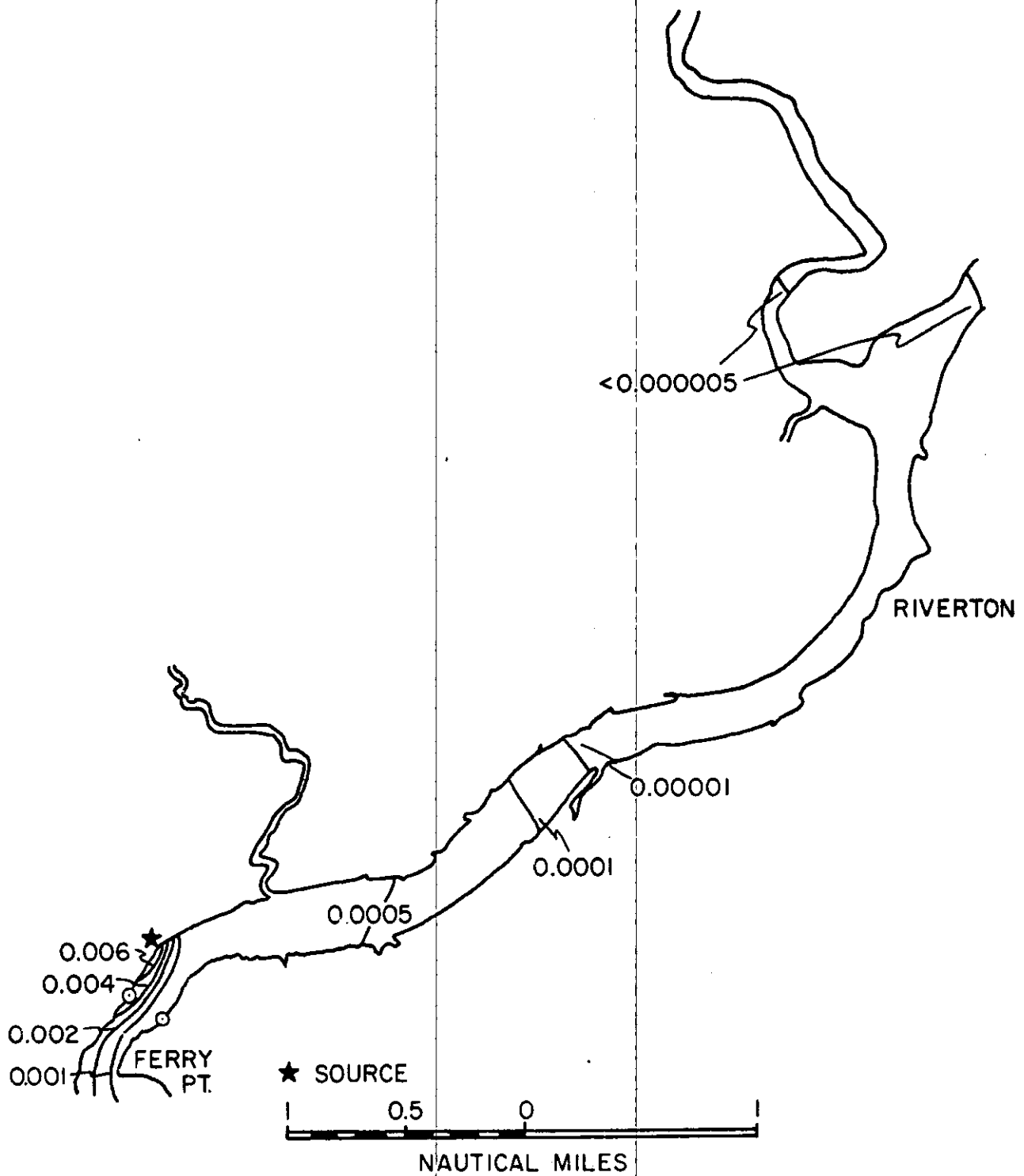


Figure 9. Distribution of relative concentration for a 400 MW plant, at maximum ebb, during high river flow, upstream from the source.

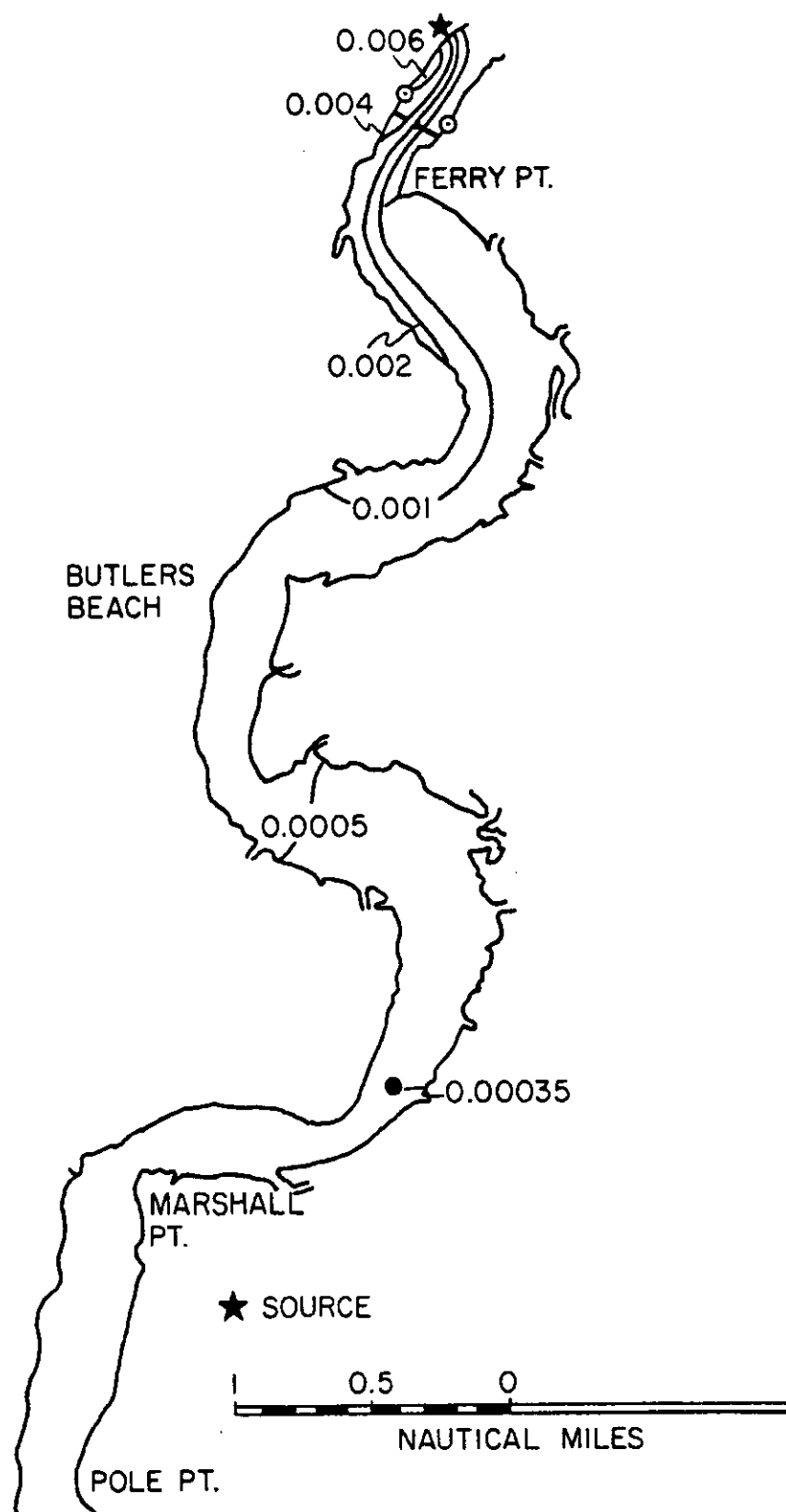


Figure 10. Distribution of relative concentration for a 400 MW plant, at maximum ebb, during high river flow, downstream from the source.

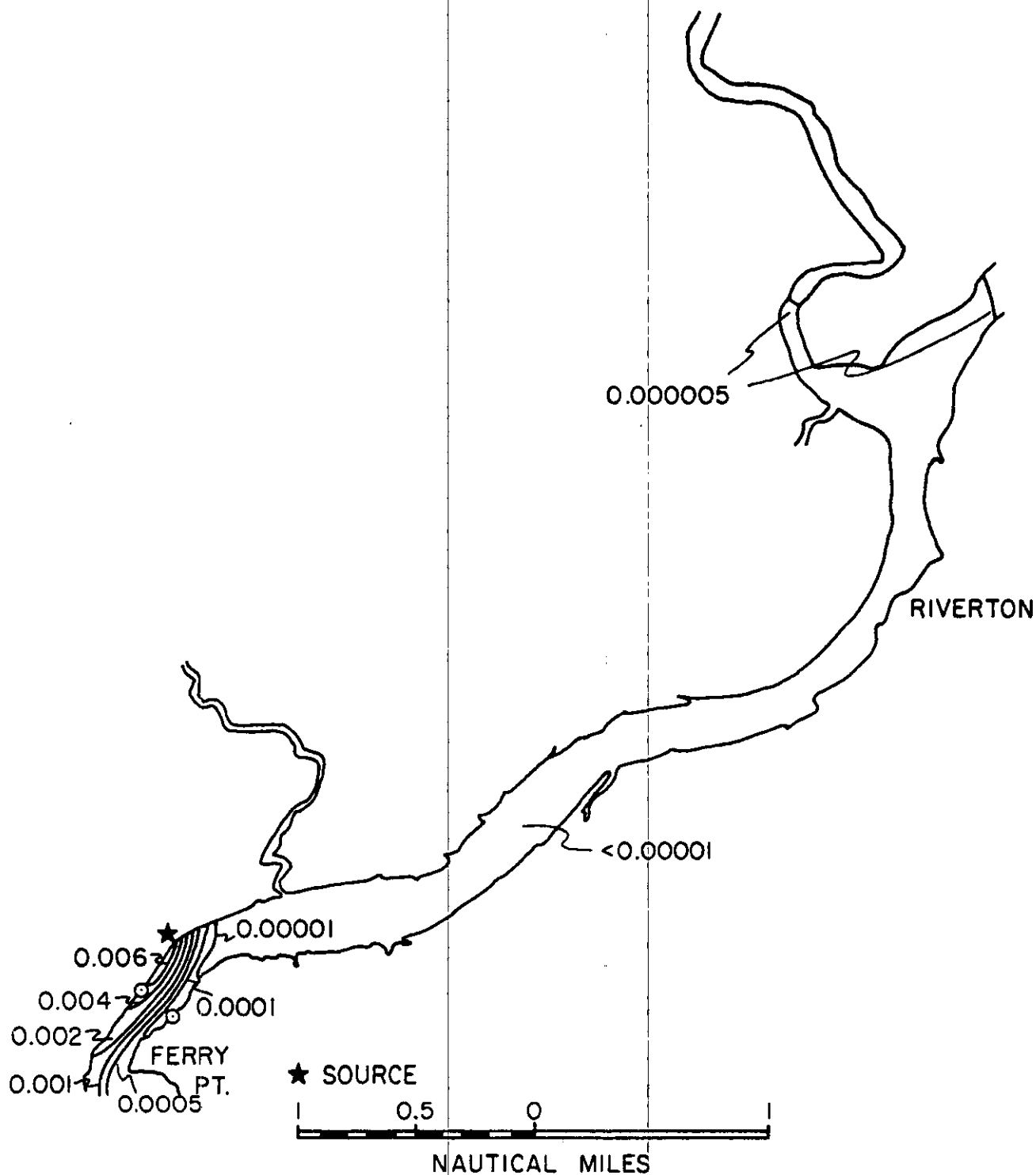


Figure 11. Distribution of relative concentration for a 400 MW plant, near slack before flood, during high river flow, upstream from the source.

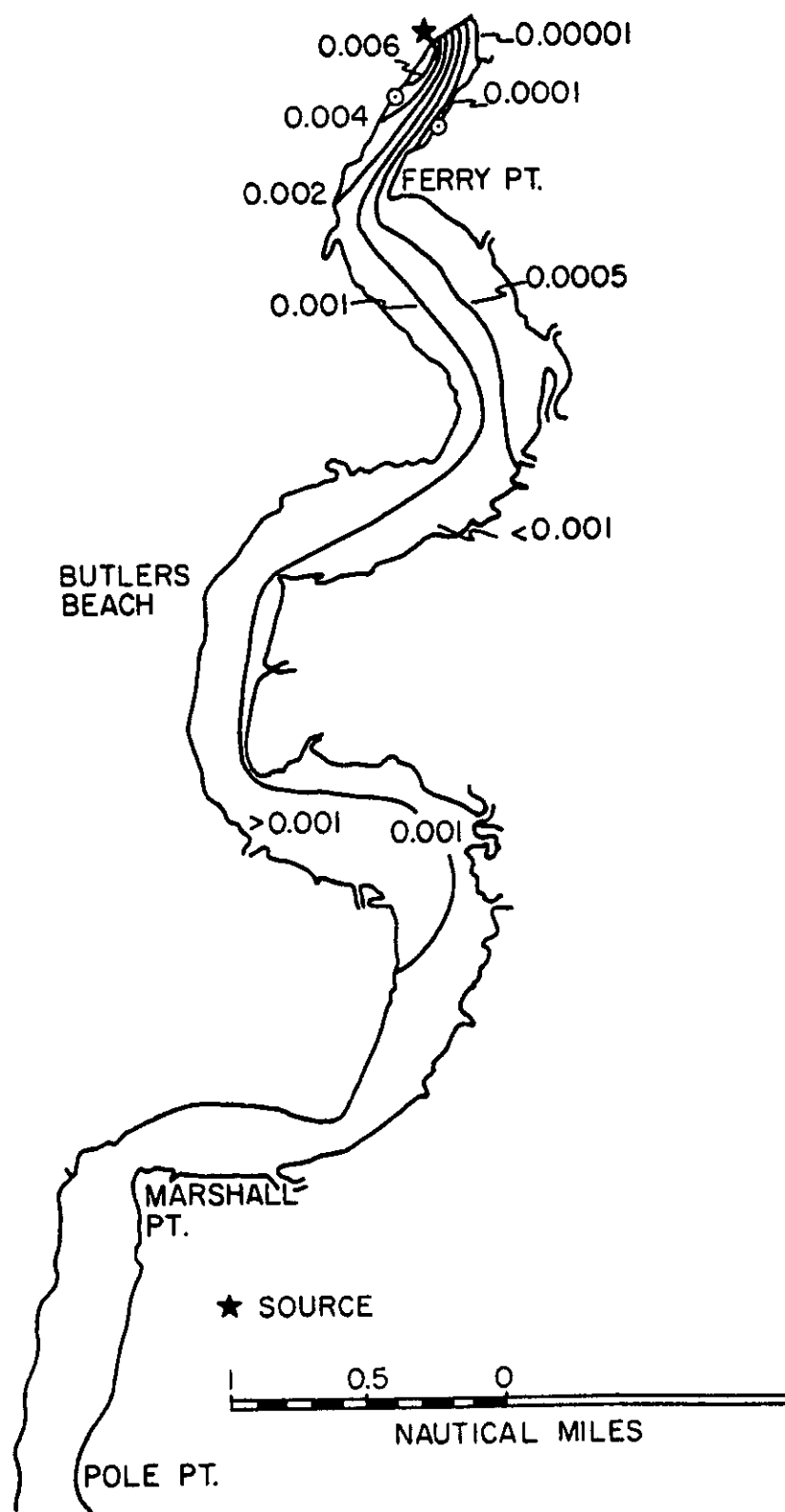


Figure 12. Distribution of relative concentration for a 400 MW plant, near slack before flood, during high river flow, downstream from the source.

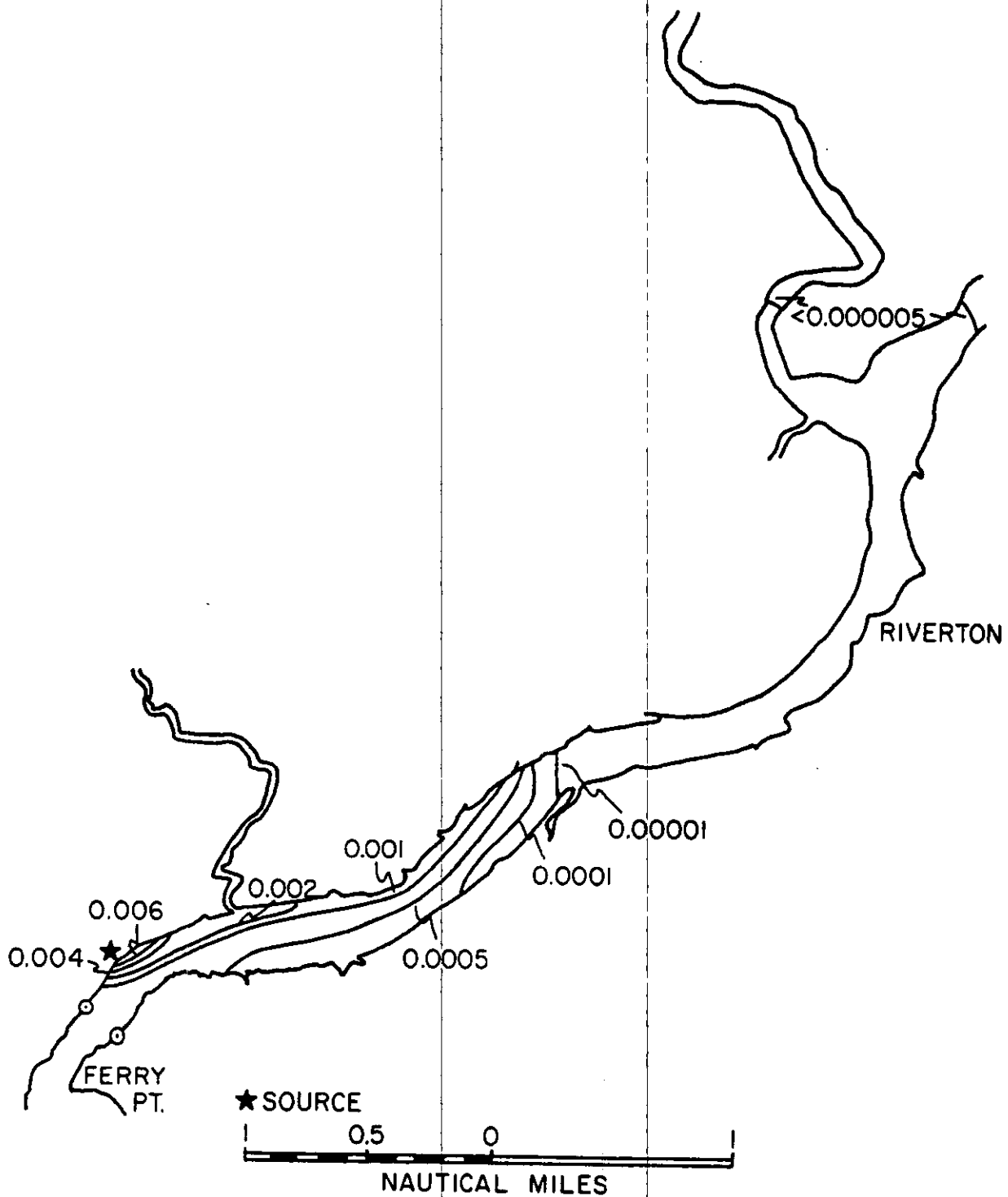


Figure 13. Distribution of relative concentration for a 400 MW plant, at maximum flood, during high river flow, upstream from the source.

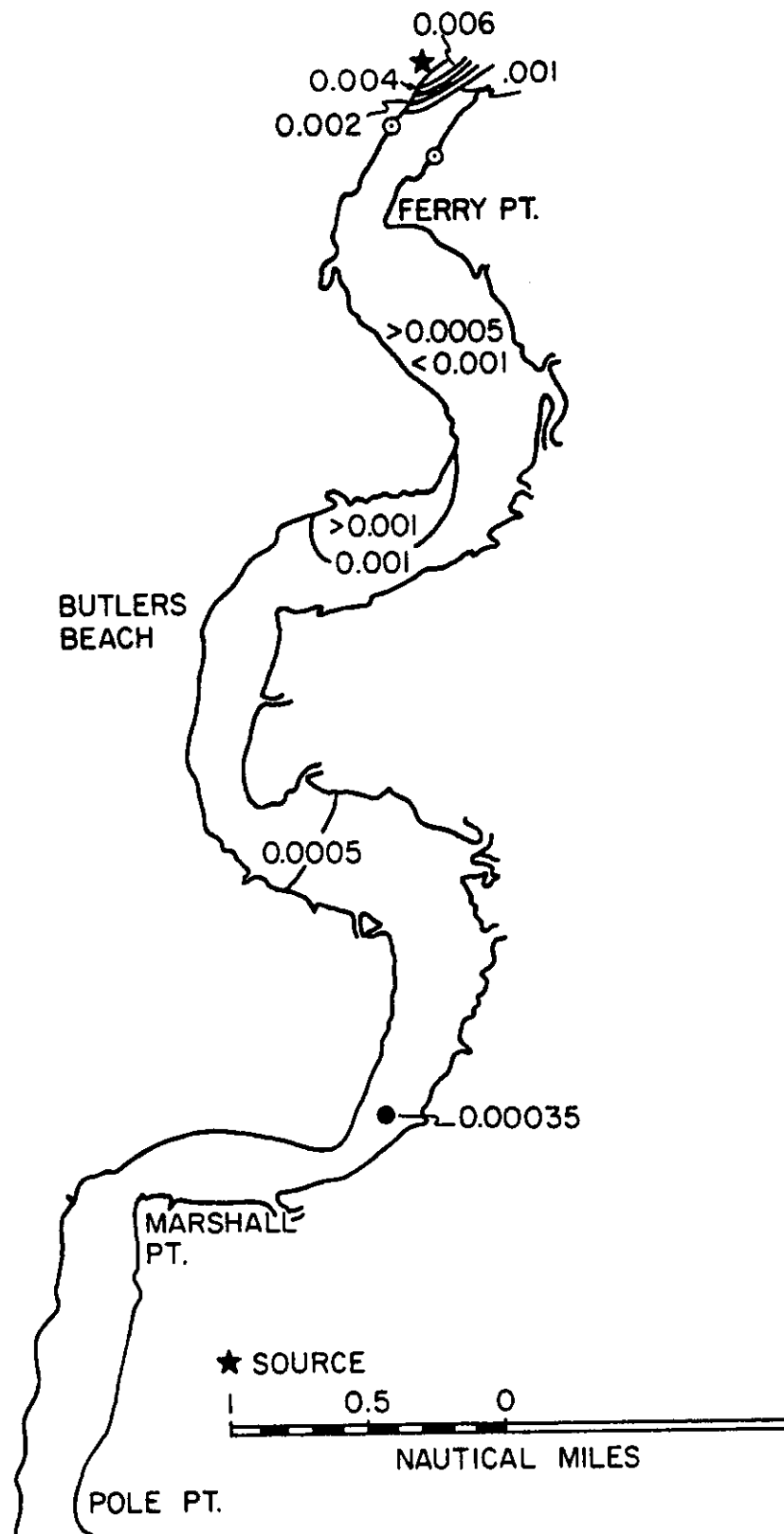


Figure 14. Distribution of relative concentration for a 400 MW plant, at maximum flood, during high river flow, downstream from the source.

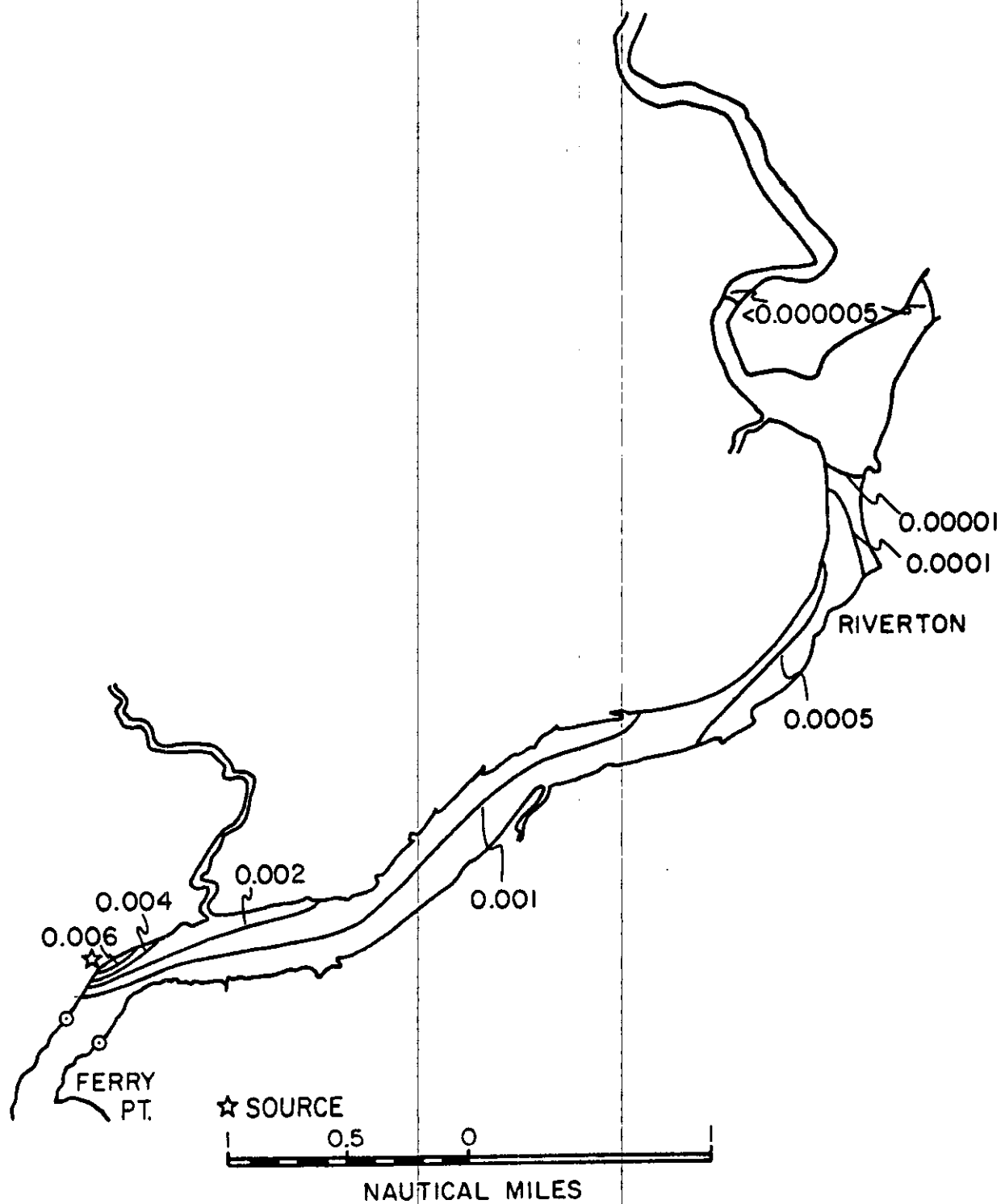


Figure 15. Distribution of relative concentration for a 400 MW plant, near slack before ebb, during high river flow, upstream from the source.

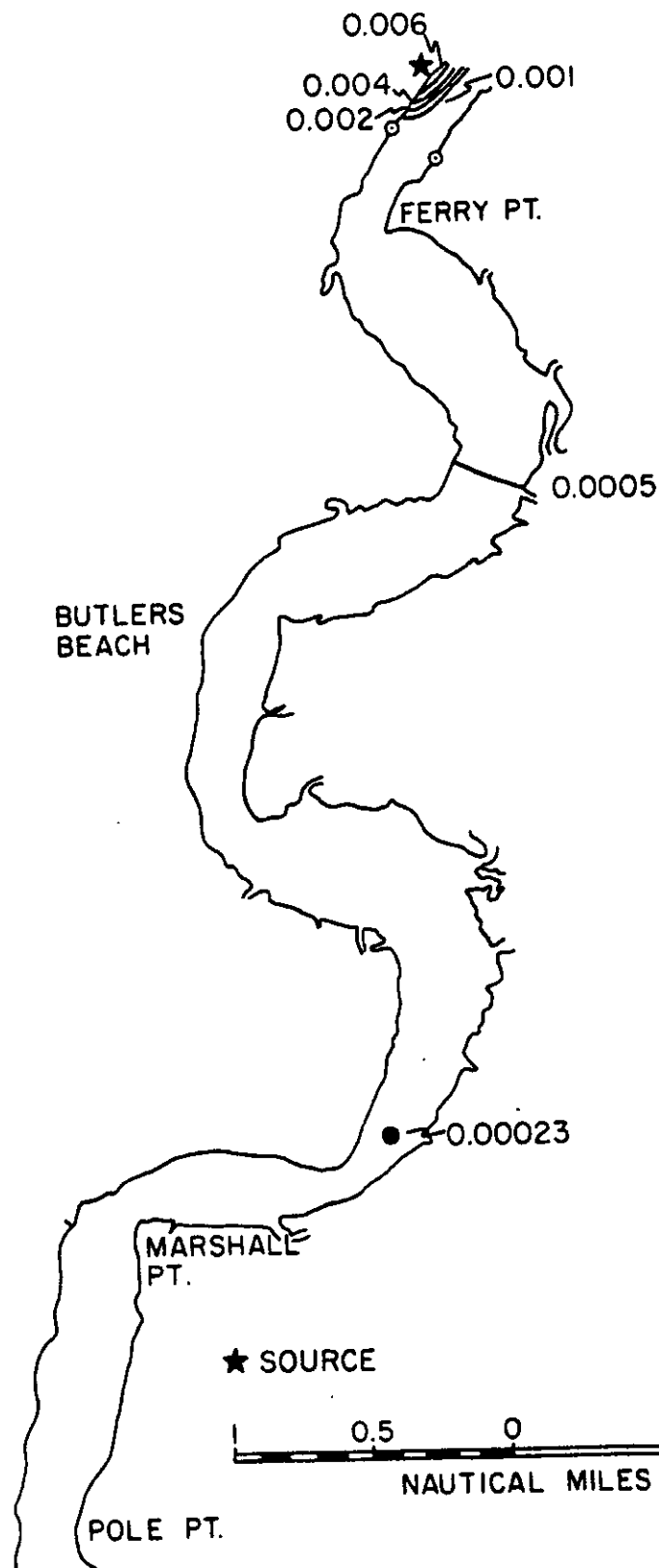


Figure 16. Distribution of relative concentration for a 400 MW plant, near slack before ebb, during high river flow, downstream from the source.

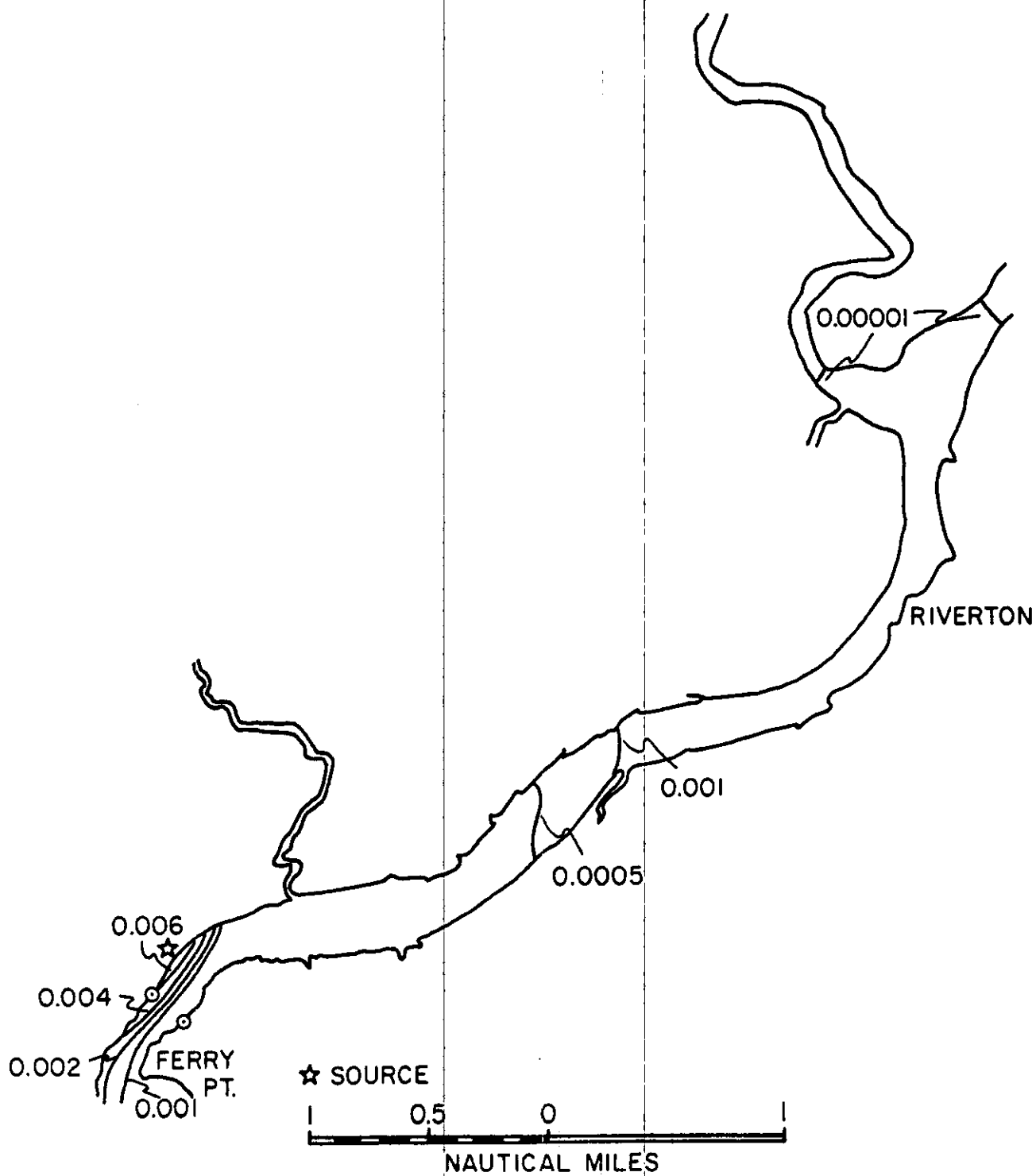


Figure 17. Distribution of relative concentration for a 400 MW plant, at maximum ebb, during mean river flow, upstream from the source.

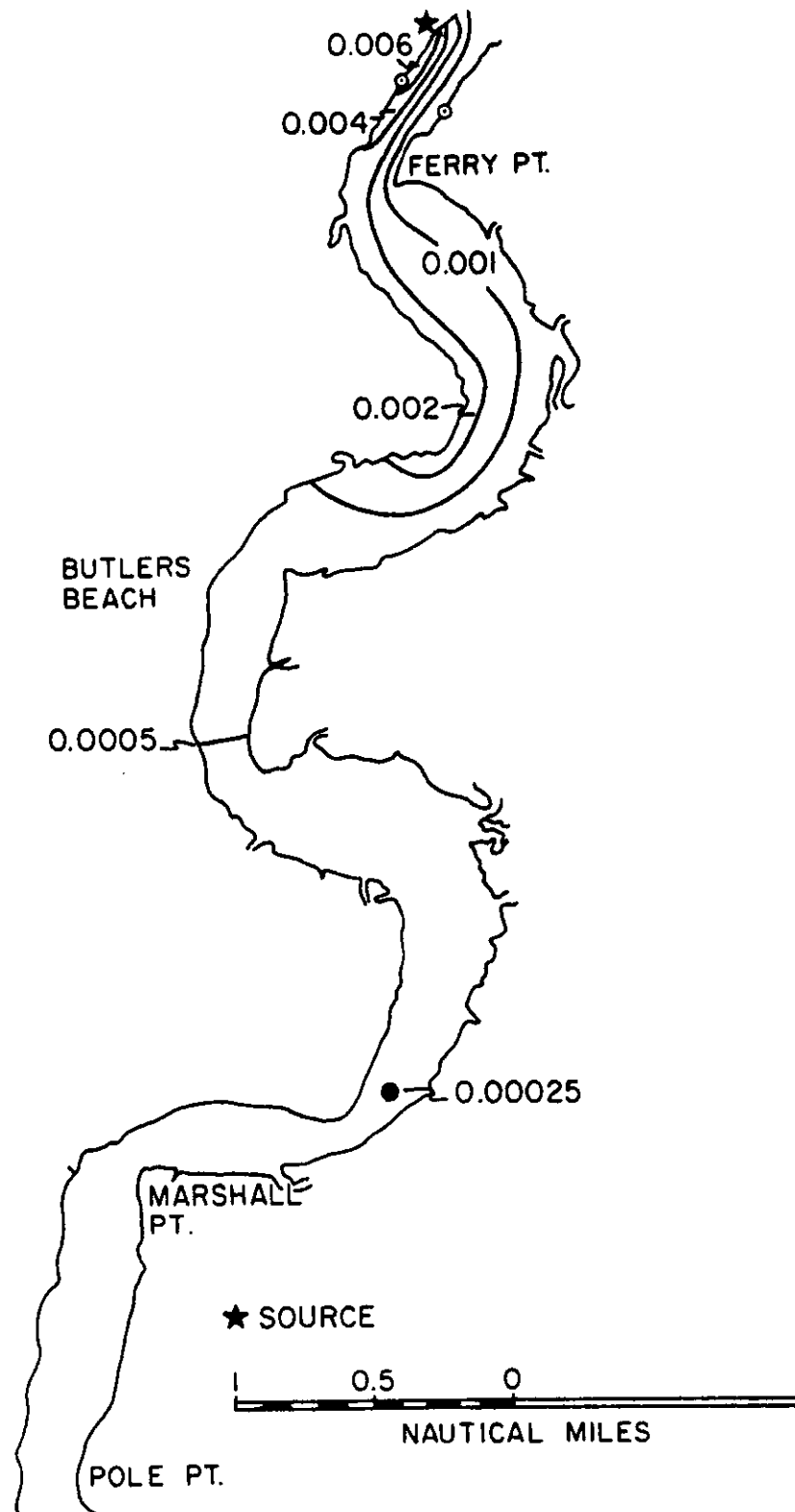


Figure 18. Distribution of relative concentration for a 400 MW plant, at maximum ebb, during mean river flow, downstream from the source.

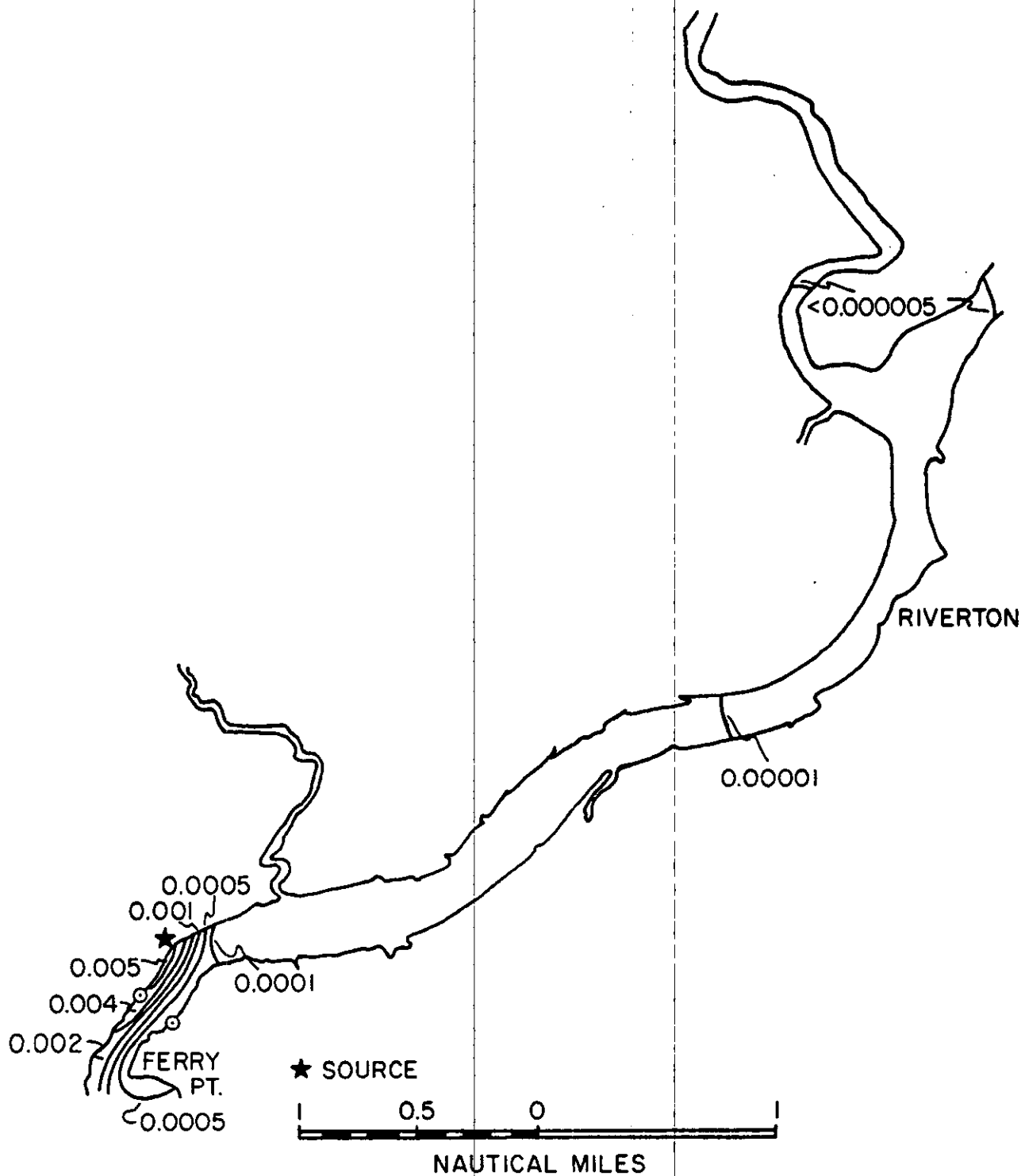


Figure 19. Distribution of relative concentration for a 400 MW plant, near slack before flood, during mean river flow, upstream from the source.

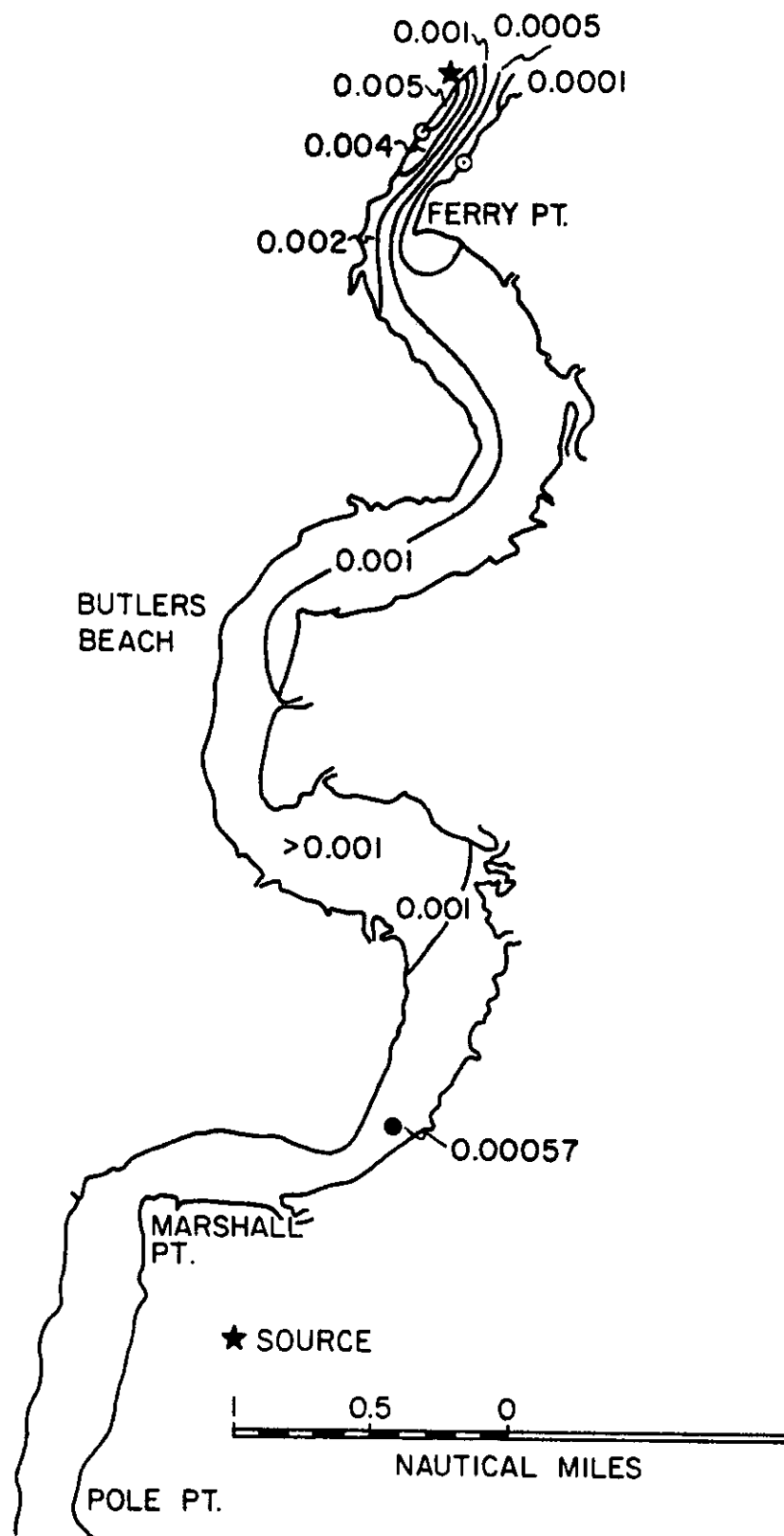


Figure 20. Distribution of relative concentration for a 400 MW plant, near slack before flood, during mean river flow, downstream from the source.

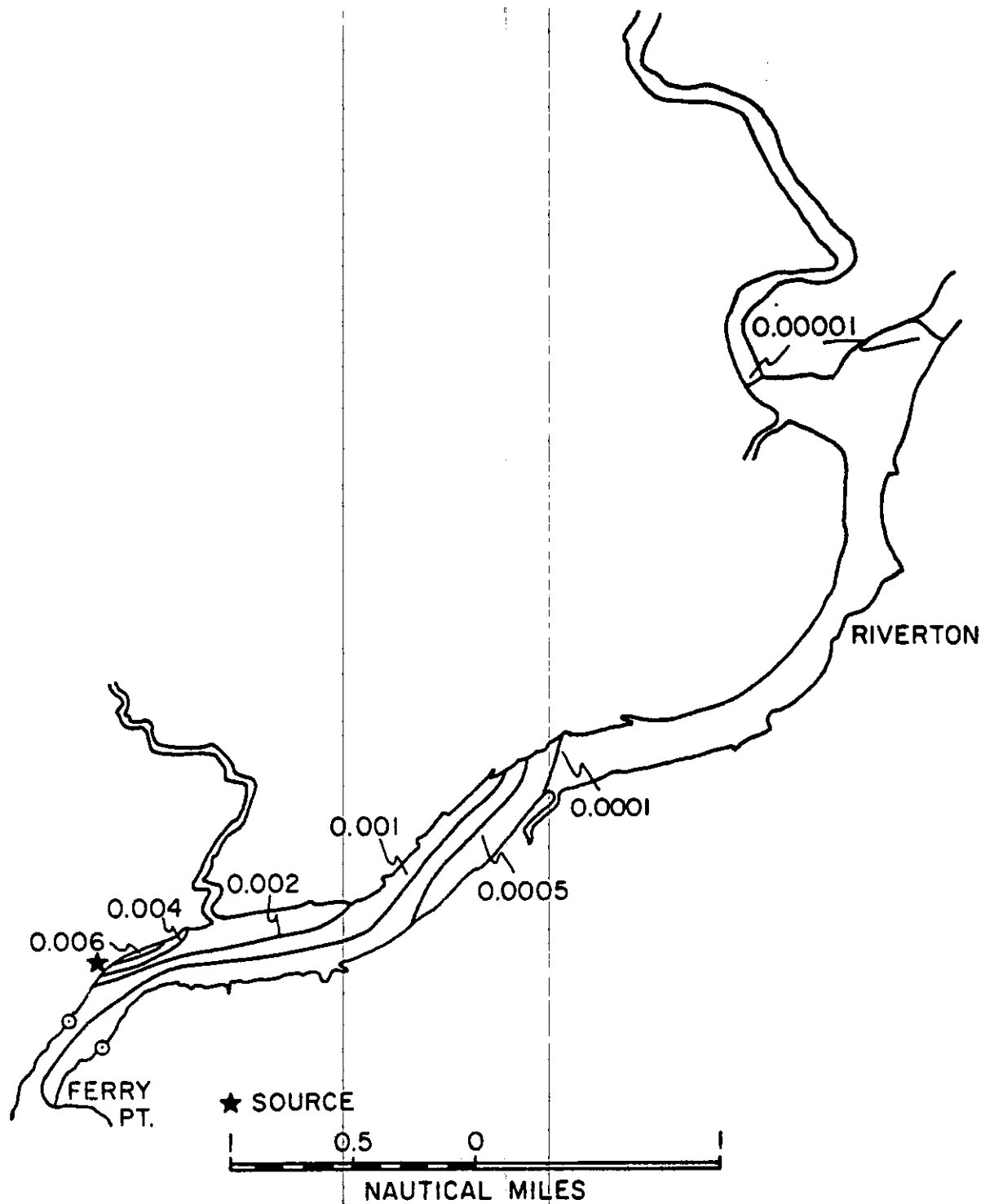


Figure 21. Distribution of relative concentration for a 400 MW plant, at maximum flood, during mean river flow, upstream from the source.

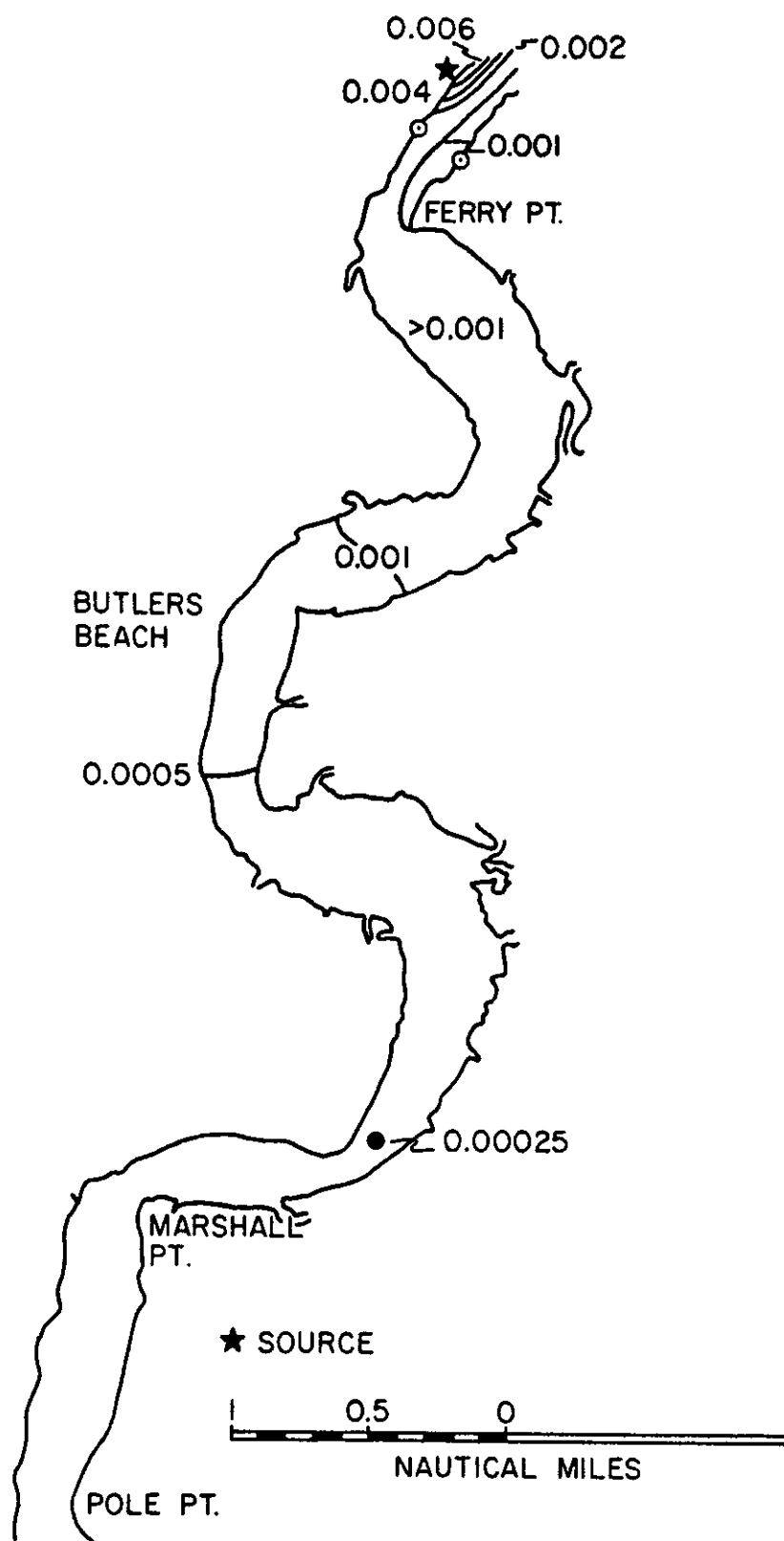


Figure 22. Distribution of relative concentration for a 400 MW plant, at maximum flood, during mean river flow, downstream from the source.

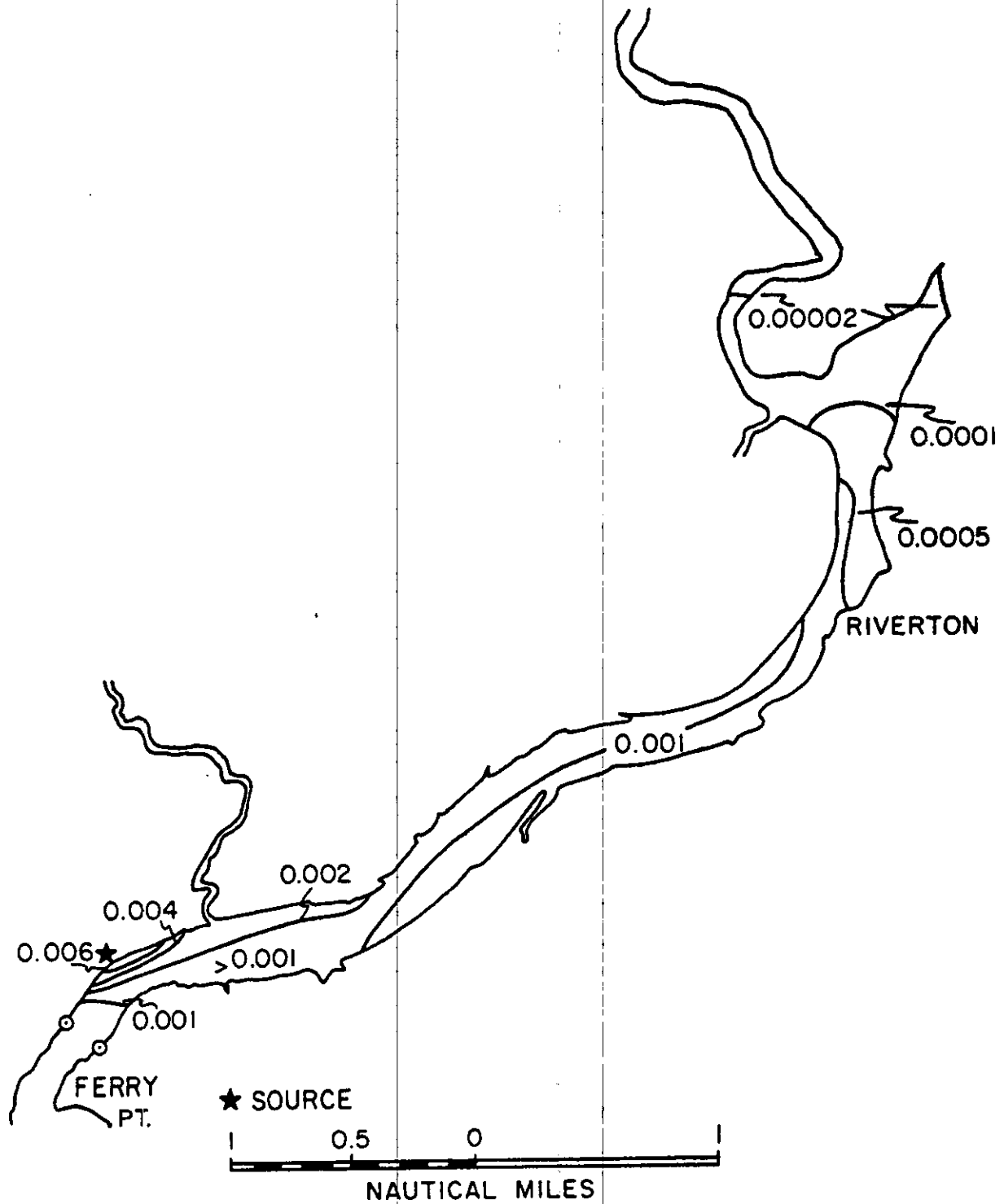


Figure 23. Distribution of relative concentration for a 400 MW plant, near slack before ebb, during mean river flow, upstream from the source.

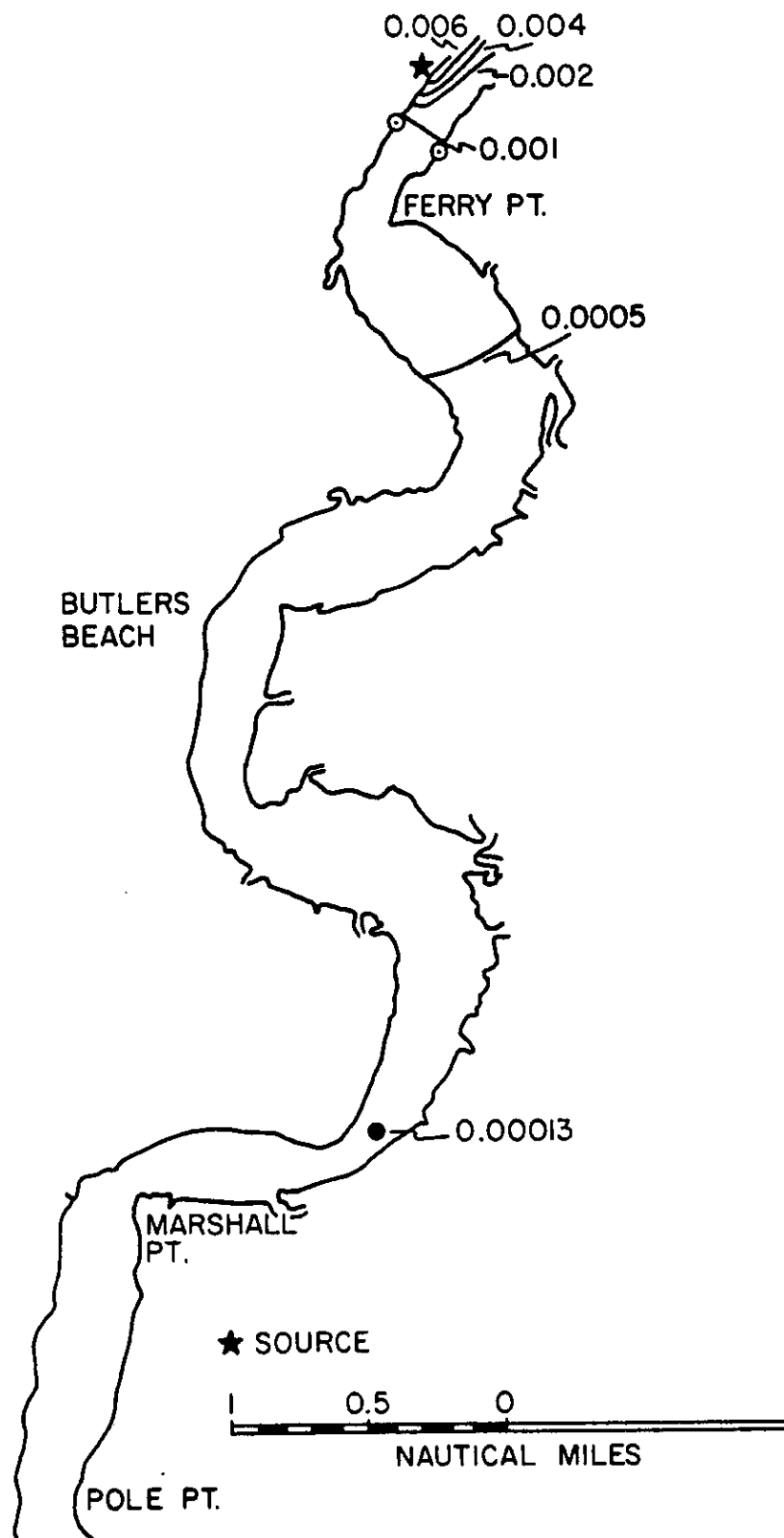


Figure 24. Distribution of relative concentration for a 400 MW plant, near slack before ebb, during mean river flow, downstream from the source.

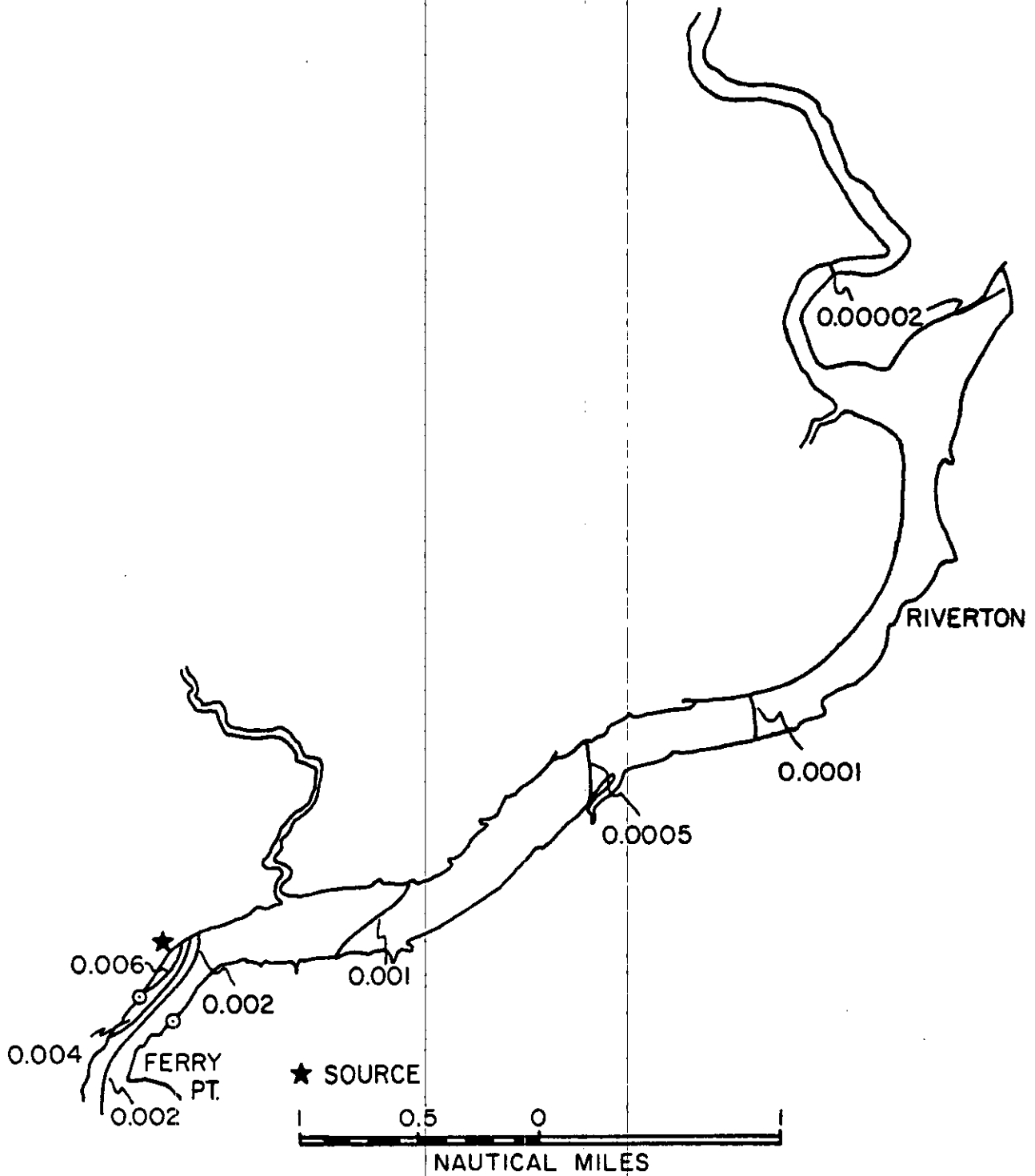


Figure 25. Distribution of relative concentration for a 400 MW plant, at maximum ebb, during low river flow, upstream from the source.

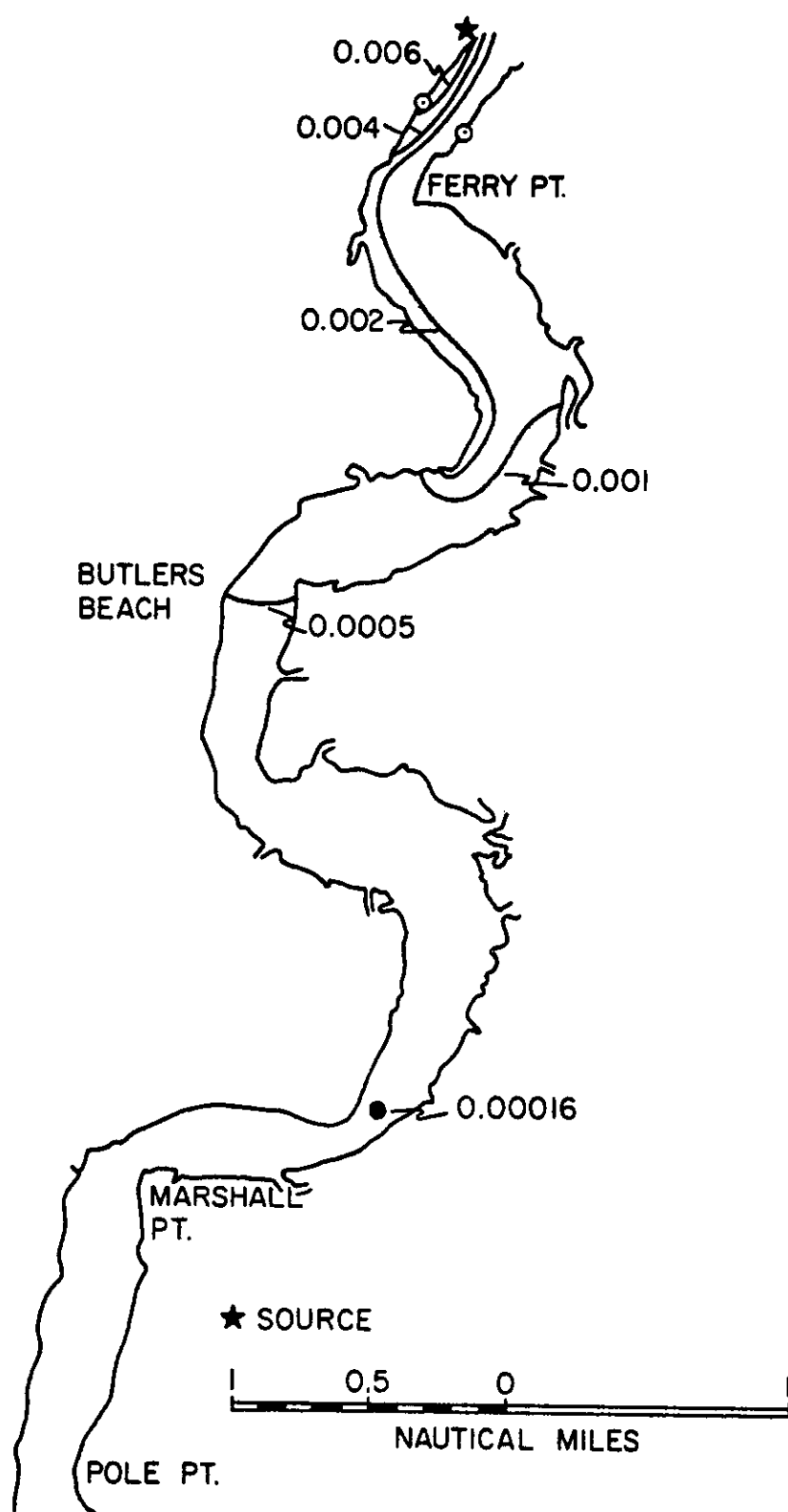


Figure 26. Distribution of relative concentration for a 400 MW plant, at maximum ebb, during low river flow, downstream from the source.

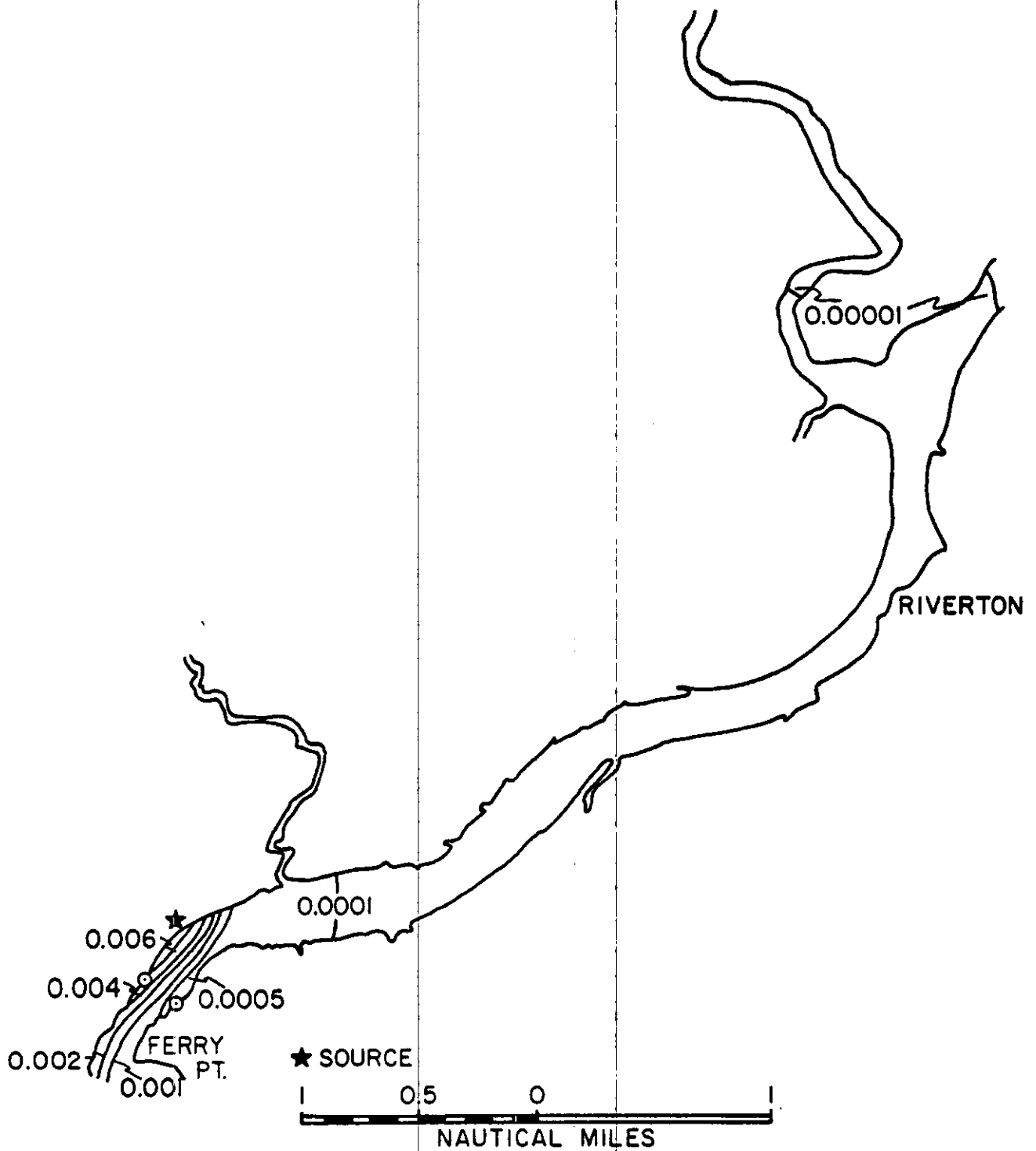


Figure 27. Distribution of relative concentration for a 400 MW plant, near slack before flood, during low river flow, upstream from the source.

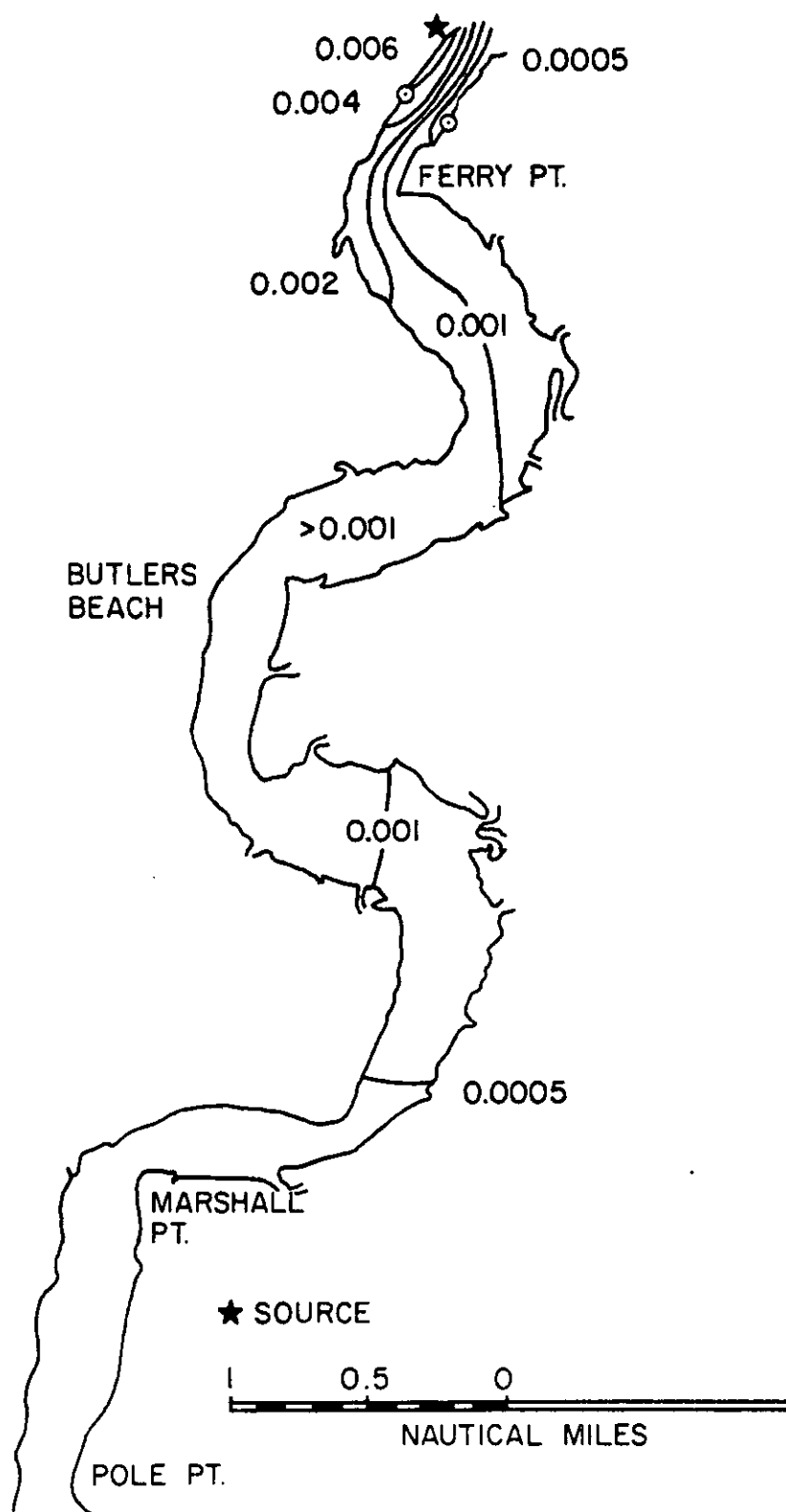


Figure 28. Distribution of relative concentration for a 400 MW plant, near slack before flood, during low river flow, downstream from the source.

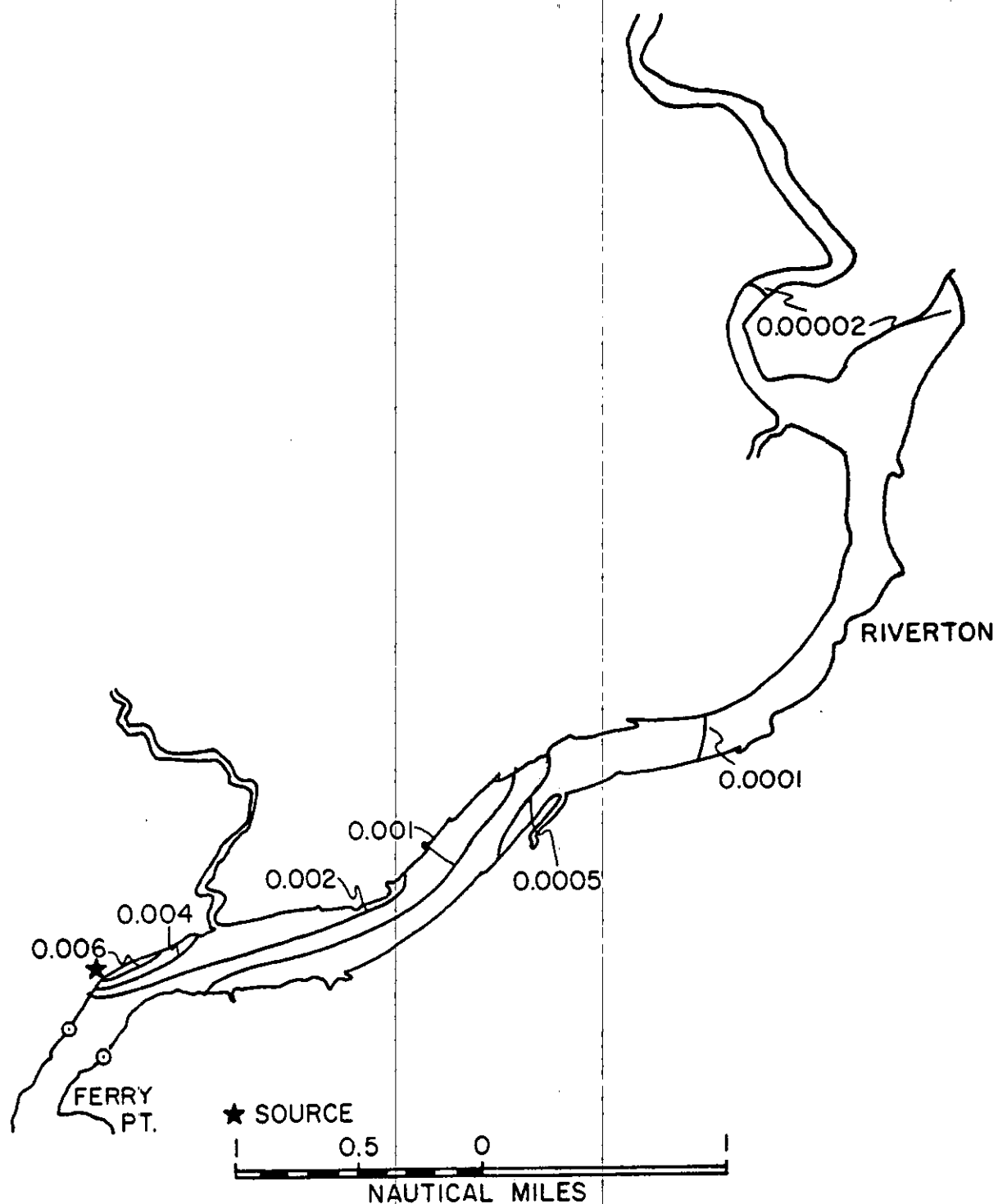


Figure 29. Distribution of relative concentration for a 400 MW plant, at maximum flood, during low river flow, upstream from the source.

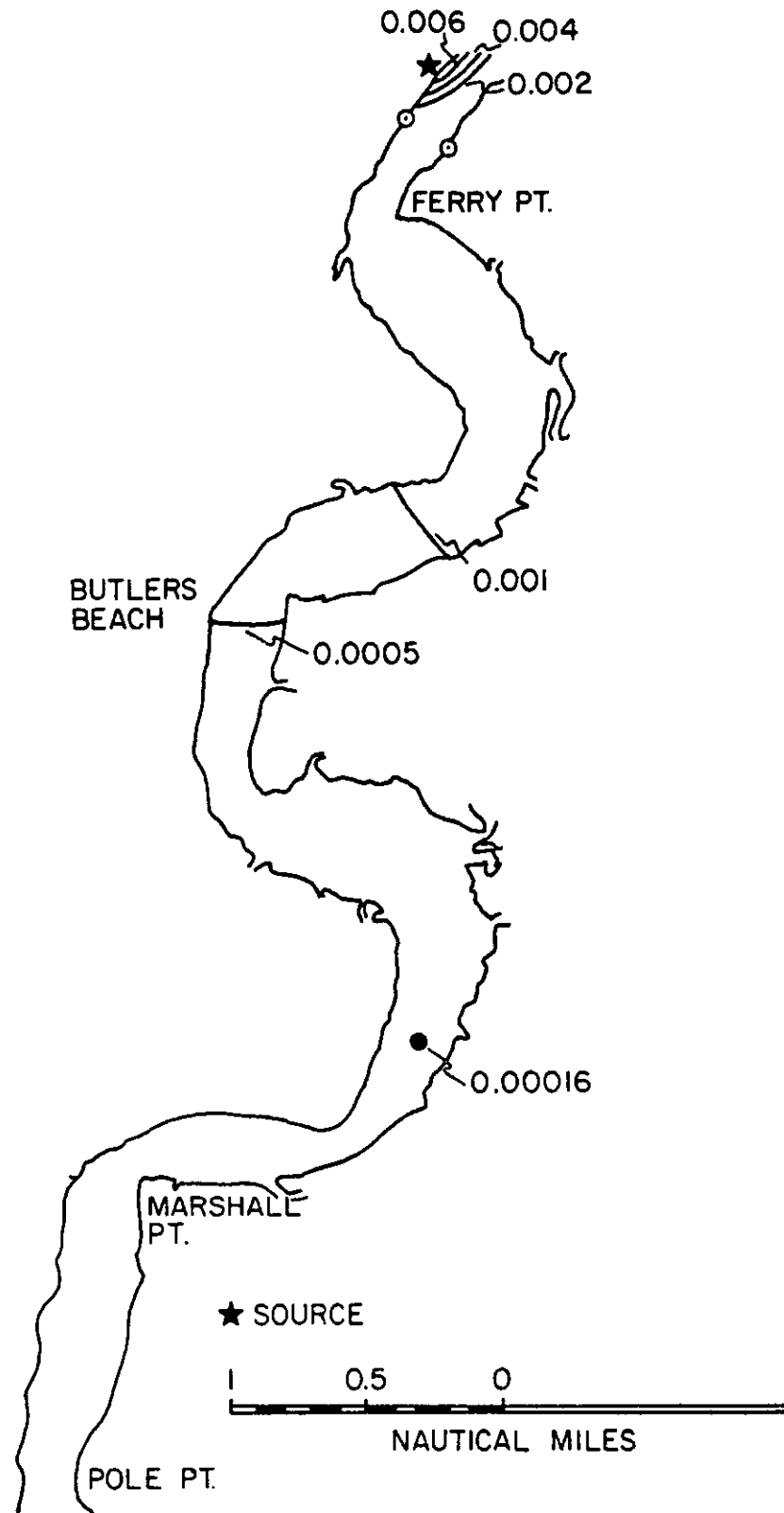


Figure 30. Distribution of relative concentration for a 400 MW plant, at maximum flood, during low river flow, downstream from the source.

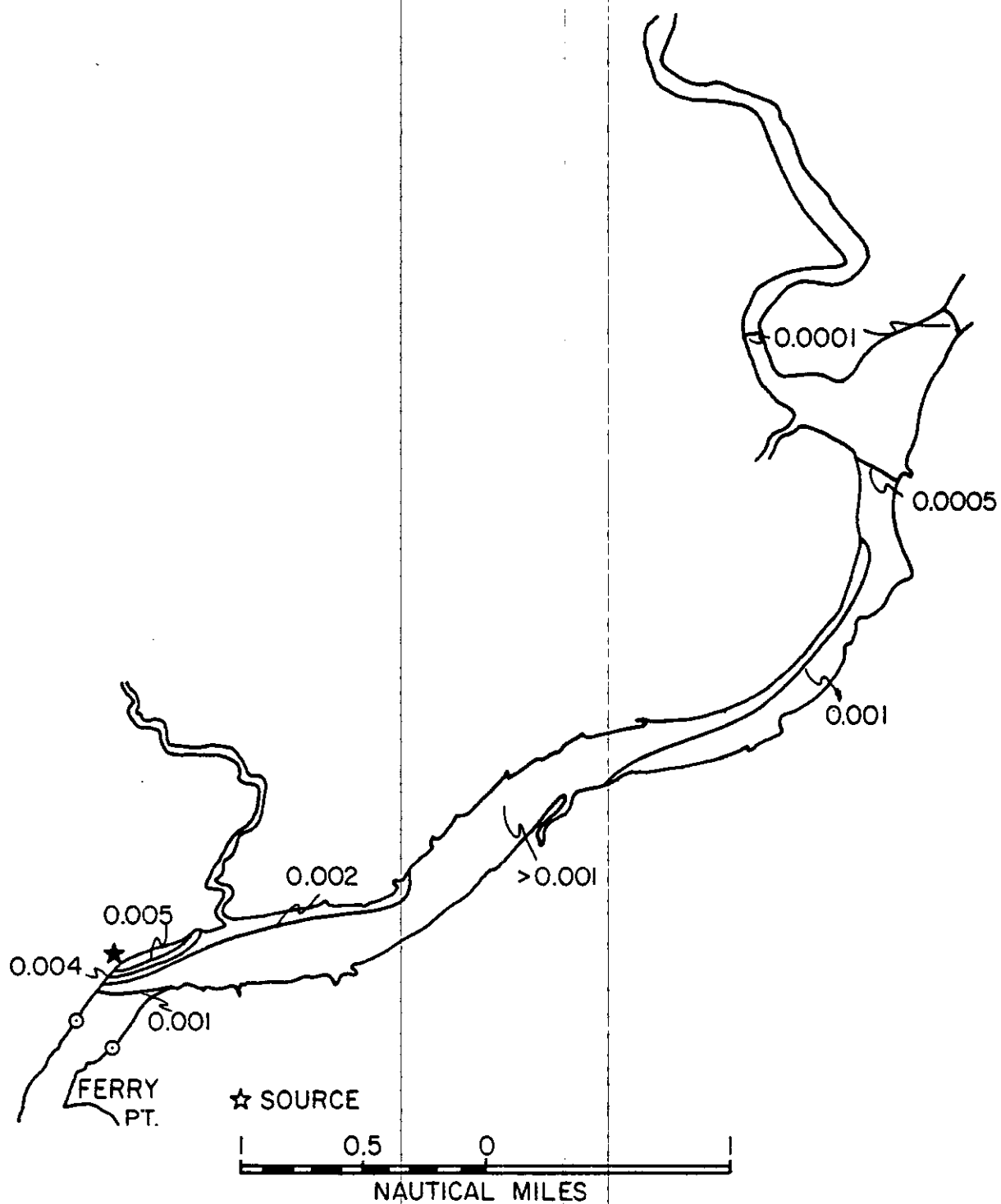


Figure 31. Distribution of relative concentration for a 400 MW plant, near slack before ebb, during low river flow, upstream from the source.

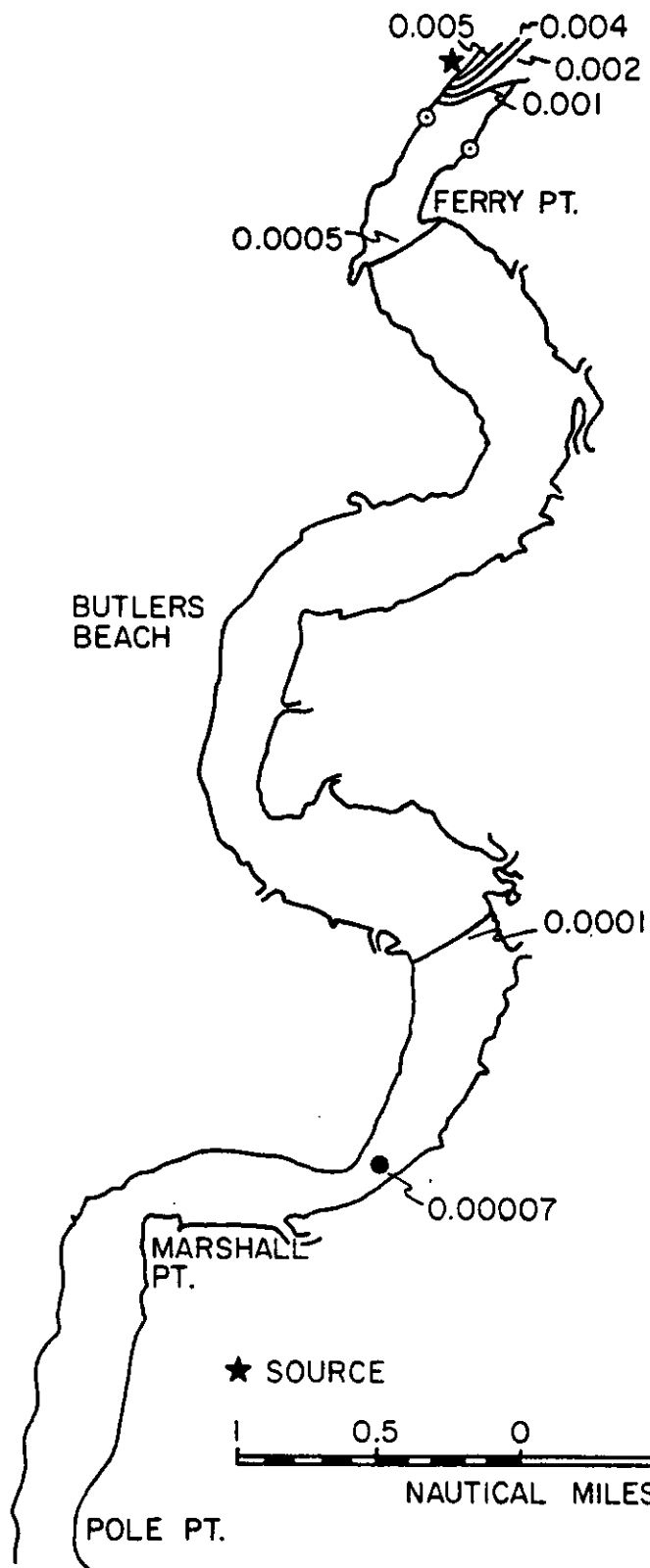


Figure 32. Distribution of relative concentration for a 400 MW plant, near slack before ebb, during low river flow, downstream from the source.

the centerline approximately as one over the distance from the source. The magnitude of concentrations within the plume depend primarily on the strength of the source and the ratio of the tidal current amplitude to the diffusion velocity. When the tide changes, a new plume begins to form and the plume created on the previous stage of the tide diffuses into the background.

The background concentration field is produced by the superposition of these diffusing remnant plumes over many tidal cycles. The background concentration field oscillates with the tidal current but it is very important to note that background concentration levels are dependent on the strength of the source and the magnitude of the *nontidal residual* current velocity rather than the tidal current velocity. Background concentrations are, therefore, quite sensitive to river flow.

As stated in the introduction, computations were also carried out for a source with a flow rate of 2570 gals. min., representing the discharge from Unit 8 combined with a new Unit 9 of 600 MWE.

The computed relative far field concentrations for this increased source on the distorted rectangular grid are presented in Figures 33 through 38. With the exception of the source strength, all input parameters for these computations were the same as those for the 400 MW plant. A comparison of the far field concentrations for the 400 MW and 600 MW plants is afforded by Figures 1 through 6 and 33 through 38. At any specific point, concentrations for the increased source are simply increased by a factor of 1.5 over those

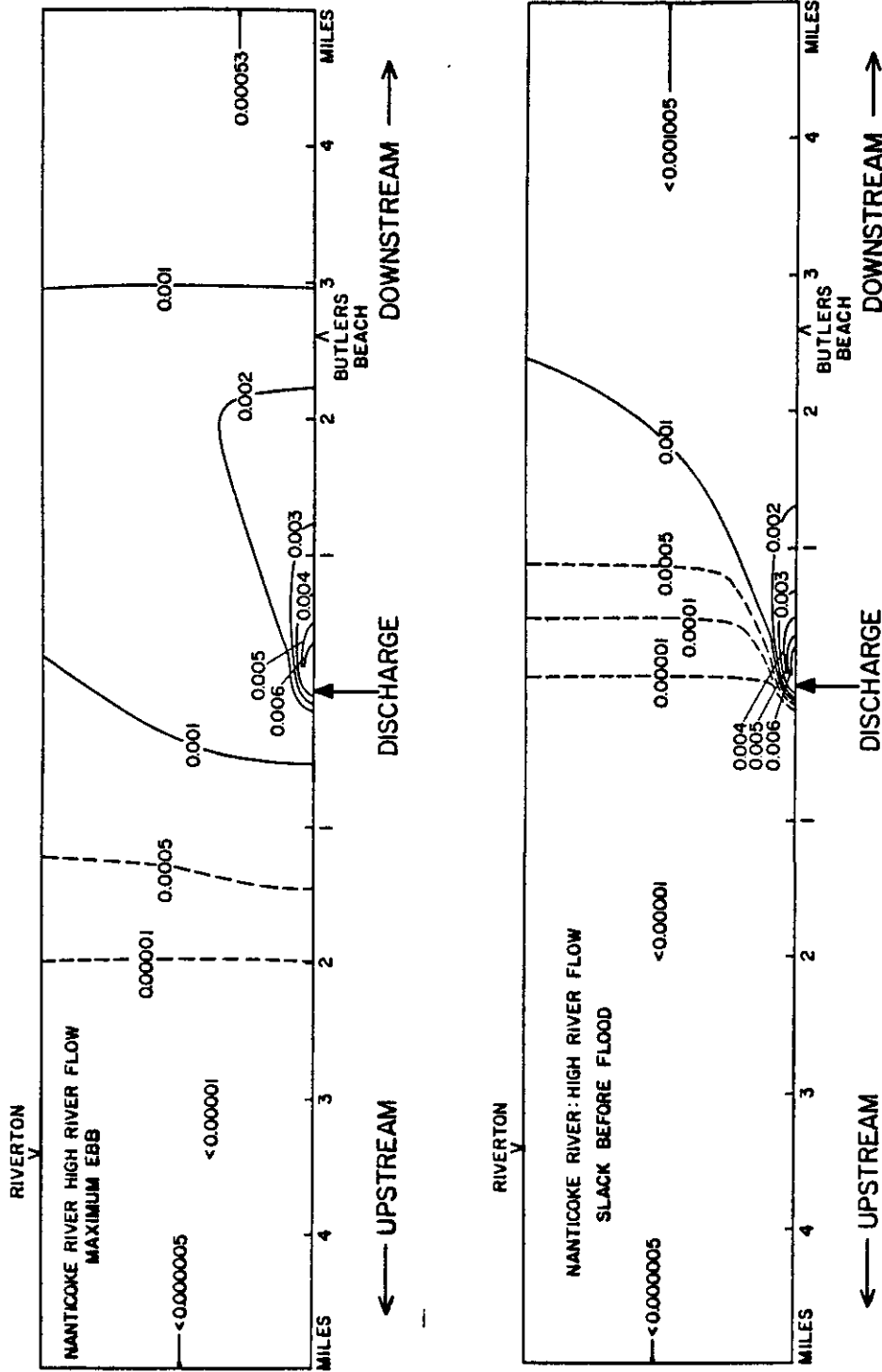


Figure 33. Isolines of relative concentration for high river flow (1520 cfs), for maximum ebb tidal flow and for near slack before flood. Computations are for a discharge flow of 2570 gpm representative of a 600 MW plant (compare with Figure 1 which is representative of a 400 MW plant).

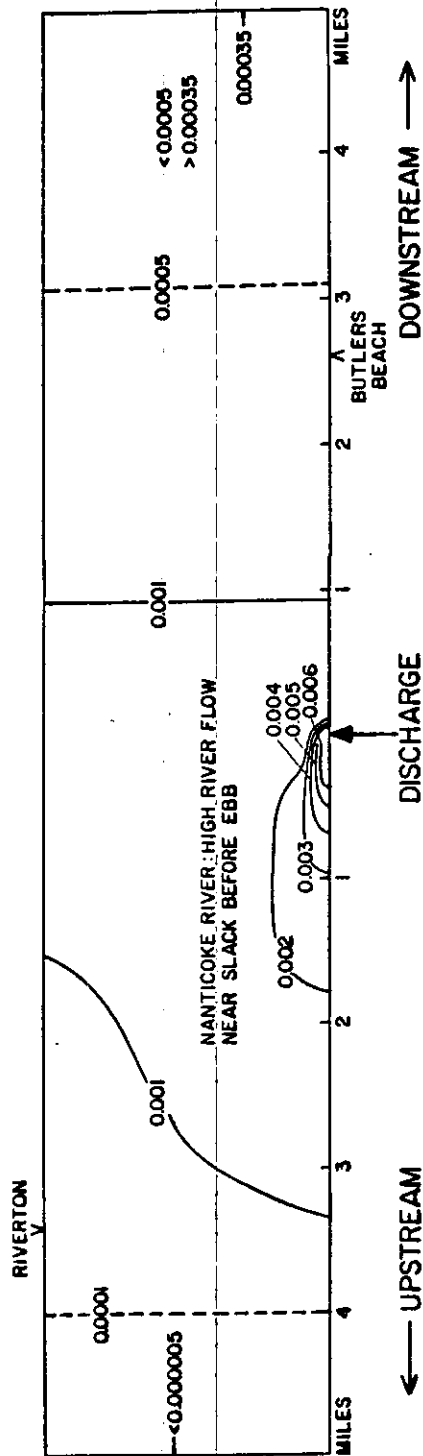
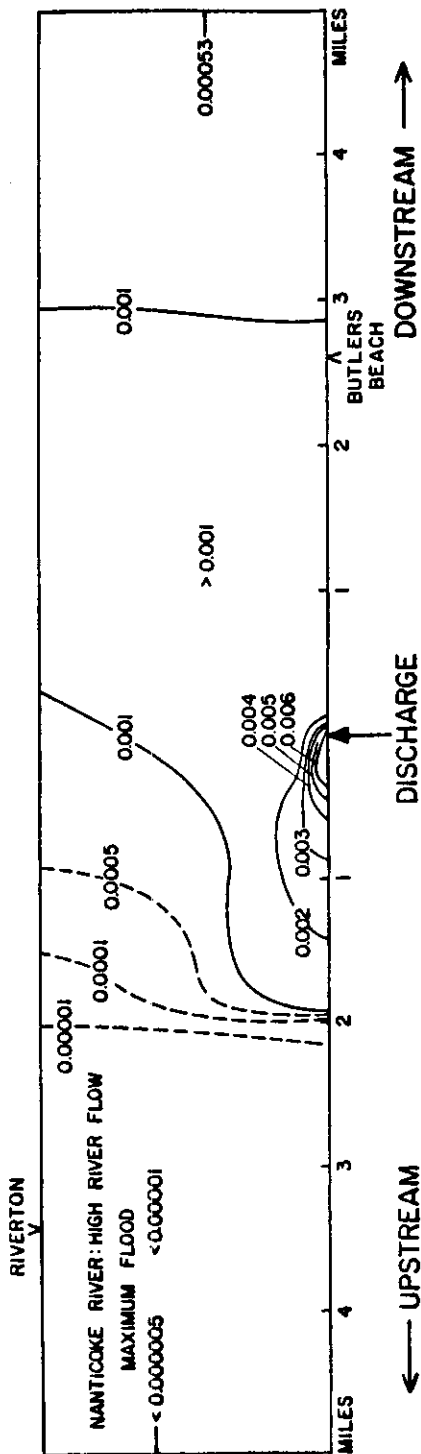


Figure 34. Isolines of relative concentration for high river flow (1520 cfs), for maximum flood tidal flow and for near slack before ebb. Computations are for a discharge flow of 2570 gpm representative of a 600 MW plant (compare with Figure 2 which is representative of a 400 MW plant).

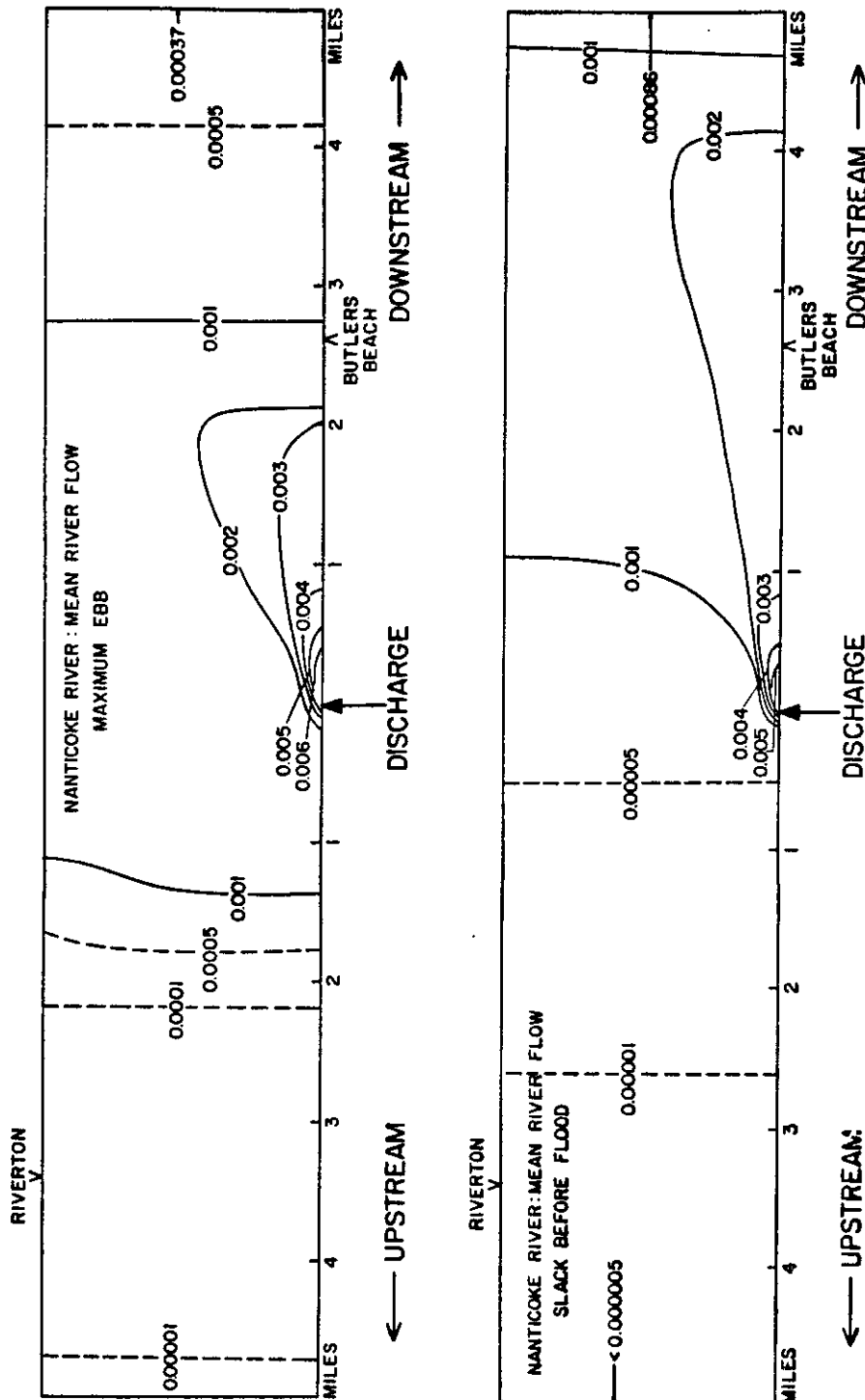


Figure 35. Isolines of relative concentration for mean river flow (810 cfs), for maximum ebb tidal flow and for near slack before flood. Computations are for a discharge flow of 2570 gpm representative of a 600 MW plant (compare with Figure 3 which is representative of a 400 MW plant).

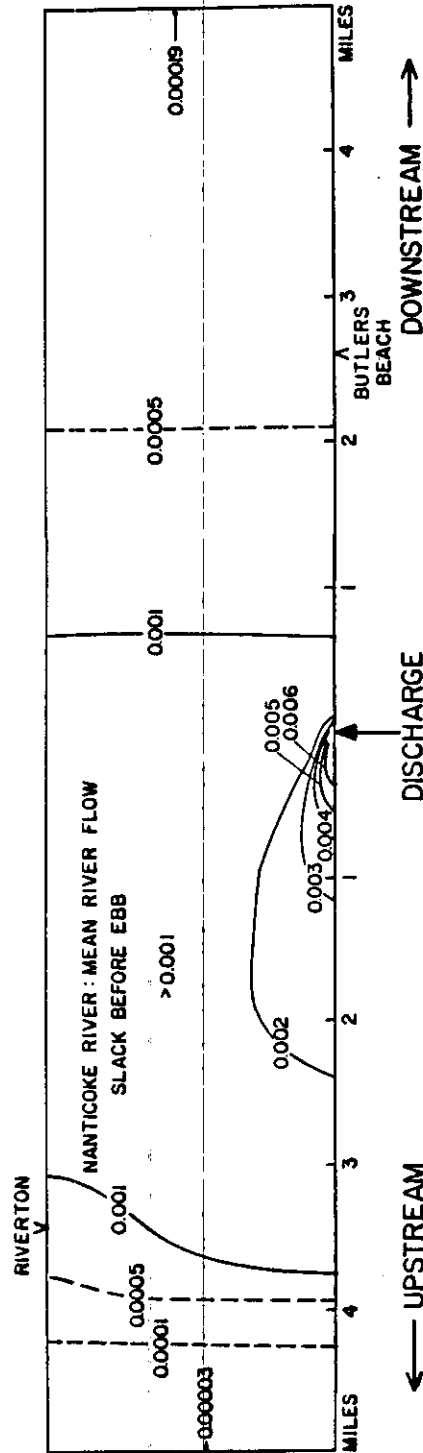
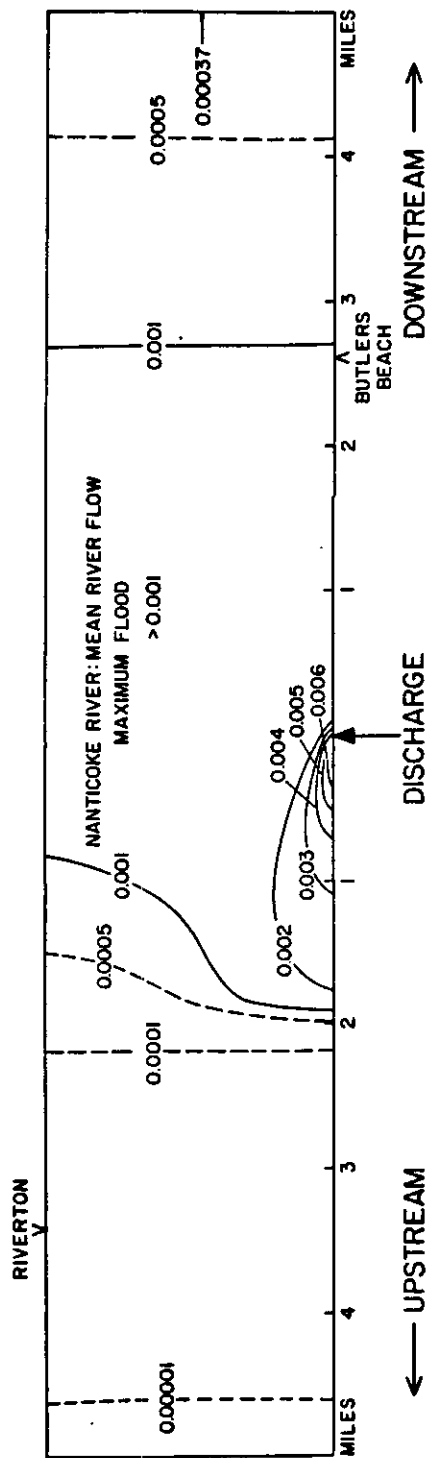


Figure 36. Isolines of relative concentration for mean river flow (810 cfs), for maximum flood flow for near slack before ebb. Computations are for a discharge flow of 2570 gpm representative of a 600 MW plant (compare with Figure 4 which is representative of a 400 MW plant).

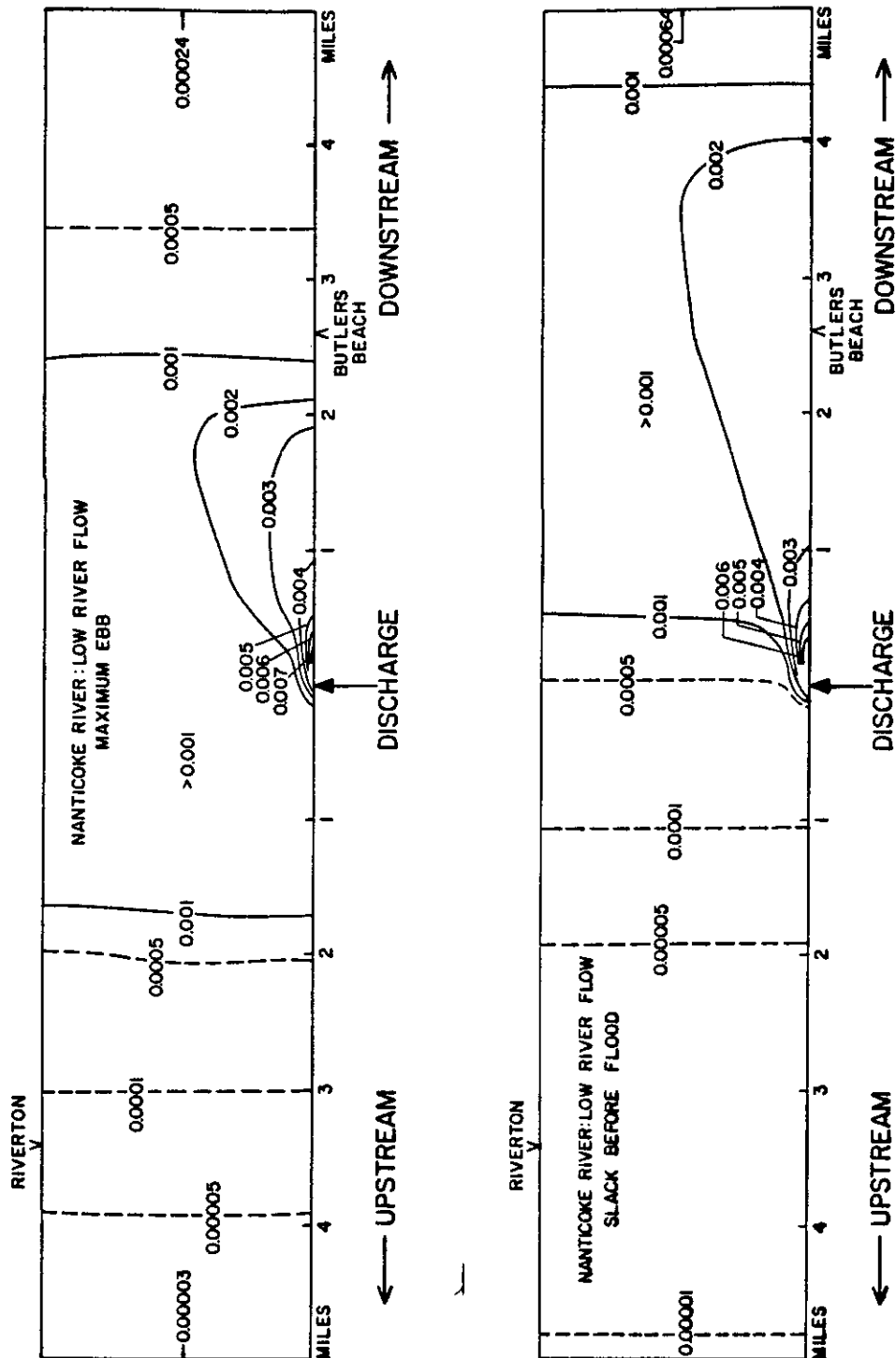


Figure 37. Isolines of relative concentration for low river flow (445 cfs), for maximum ebb tidal flow and for near slack before flood. Computations are for a discharge flow of 2570 gpm representative of a 600 MW plant (compare with Figure 5 which is representative of a 400 MW plant).

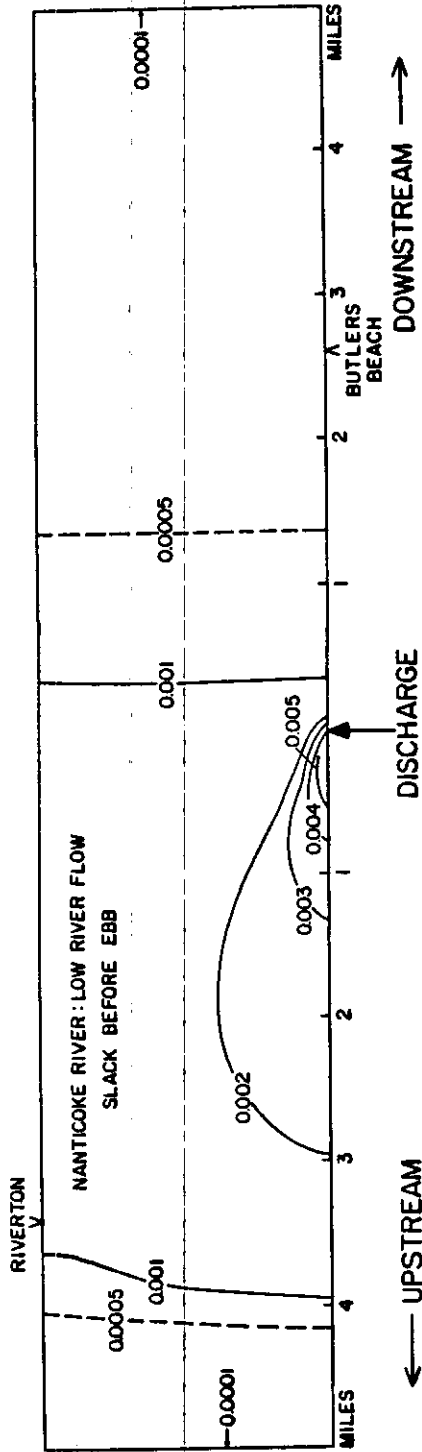
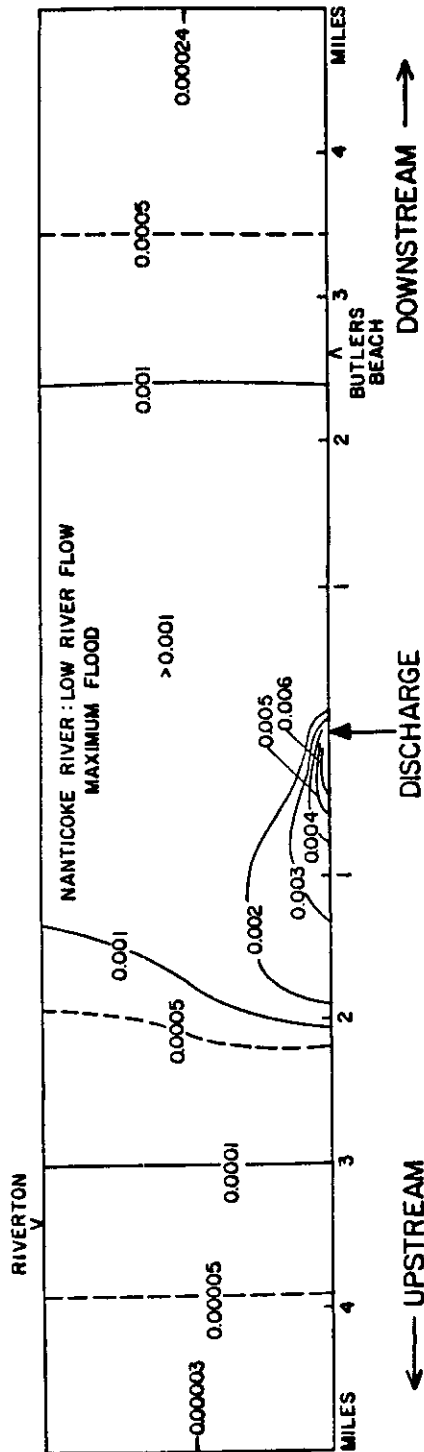


Figure 38. Isolines of relative concentration for low river flow (445 cfs), for maximum flood tidal flow and for near slack before ebb. Computations are for a discharge flow of 2570 gpm representative of a 600 MW plant (compare with Figure 6 which is representative of a 400 MW plant).

concentrations computed for the original source; concentrations at a fixed point are linearly proportional to source strength. The area enclosed by a given isoline of concentration is not, however, linearly proportional to source strength and may exhibit very significant increases which are greater than a factor of 1.5.

The far field distributions of relative concentration computed for the increased source have been scaled back to the actual river geometry; they are presented in Figures 39 through 62. These figures are to be compared to Figures 9 through 32 for the 400 MW plant.

The near field distribution for this 600 MW case are given in Figures 63 and 64. It is evident that these figures are not markedly different from Figures 7 and 8, which give the nearfield distributions of relative concentration for the 400 MW case. The only clear difference between these two sets of figures is that in the 600 MW case (Figure 63), the plume extends further offshore before bending to become parallel to the axis of the estuary.

The reasons for both the similarities and the differences can be found in the assumed input conditions for the two cases. In making the computation for the larger discharge the diameter of the discharge orifice was kept the same as in the 400 MW case. The consequent larger velocity and momentum of the discharge resulting in extending the plume further offshore and also in increasing the densimetric Froude number, and hence increasing the relative rate of mixing in the near field.

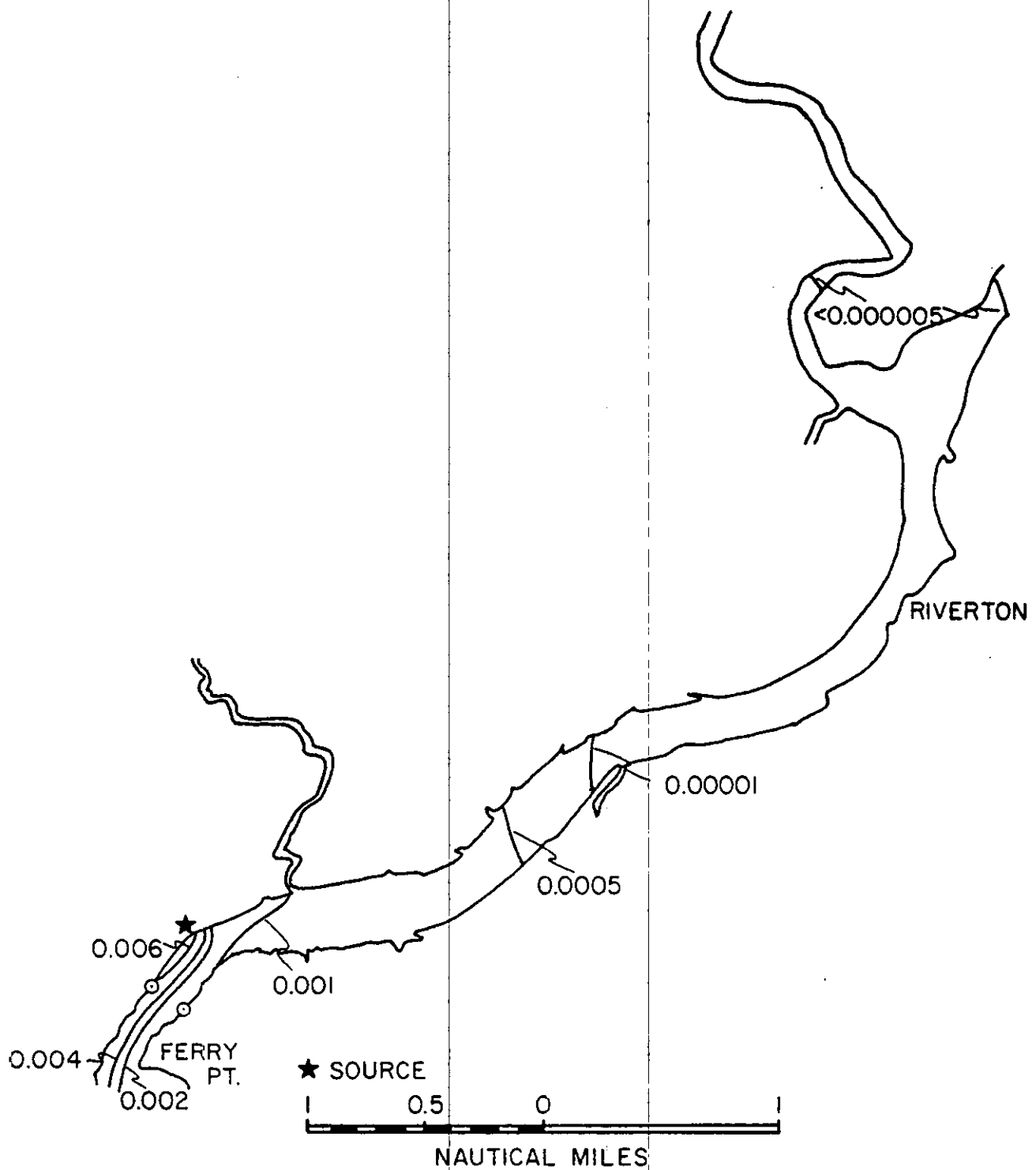


Figure 39. Distribution of relative concentration for a 600 MW plant, at maximum ebb, during high river flow, upstream from the source.

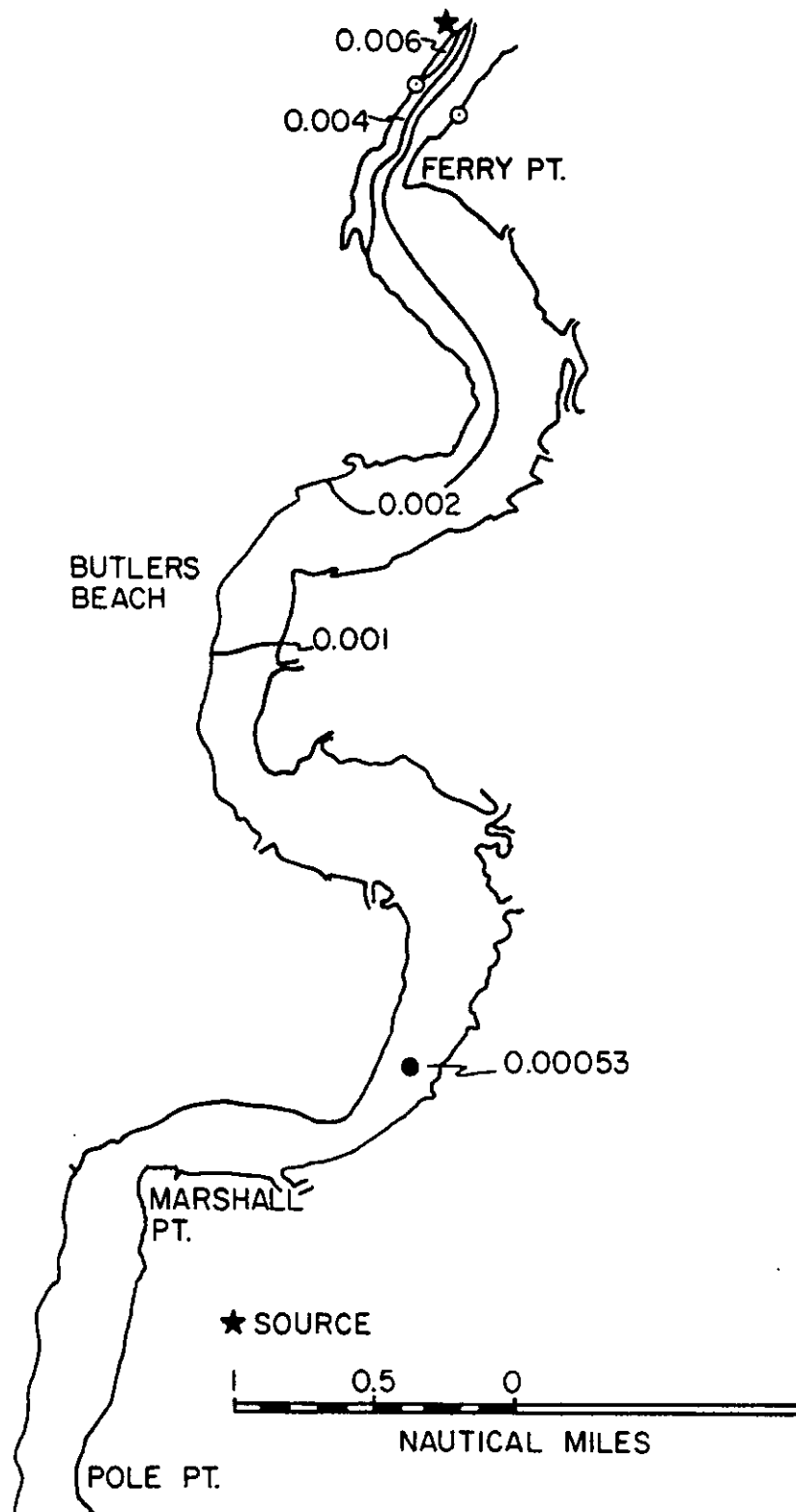


Figure 40. Distribution of relative concentration for a 600 MW plant, at maximum ebb, during high river flow, downstream from the source.

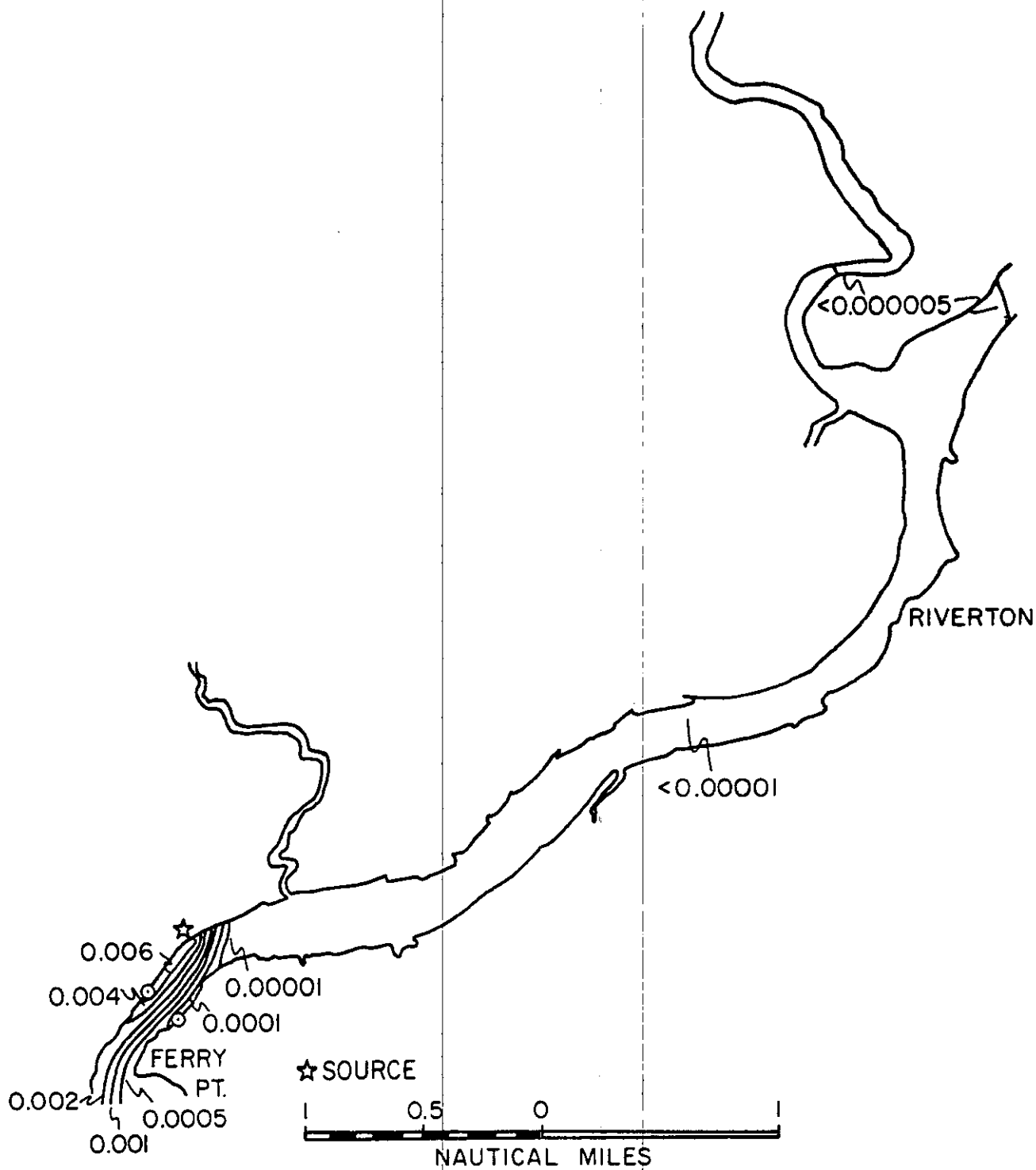


Figure 41. Distribution of relative concentration for a 600 MW plant, near slack before flood, during high river flow, upstream from the source.

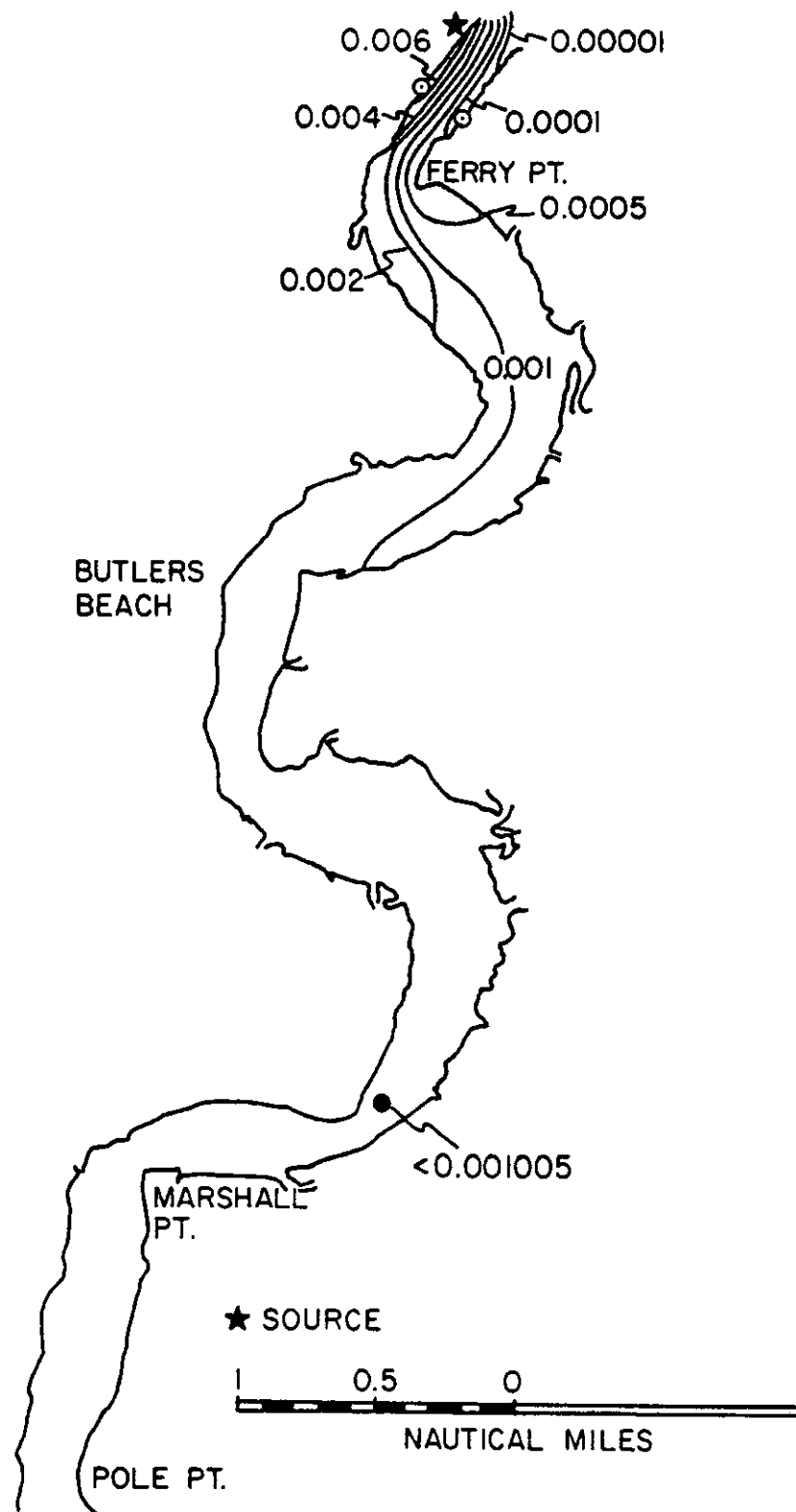


Figure 42. Distribution of relative concentration for a 600 MW plant, near slack before flood, during high river flow, downstream from the source.

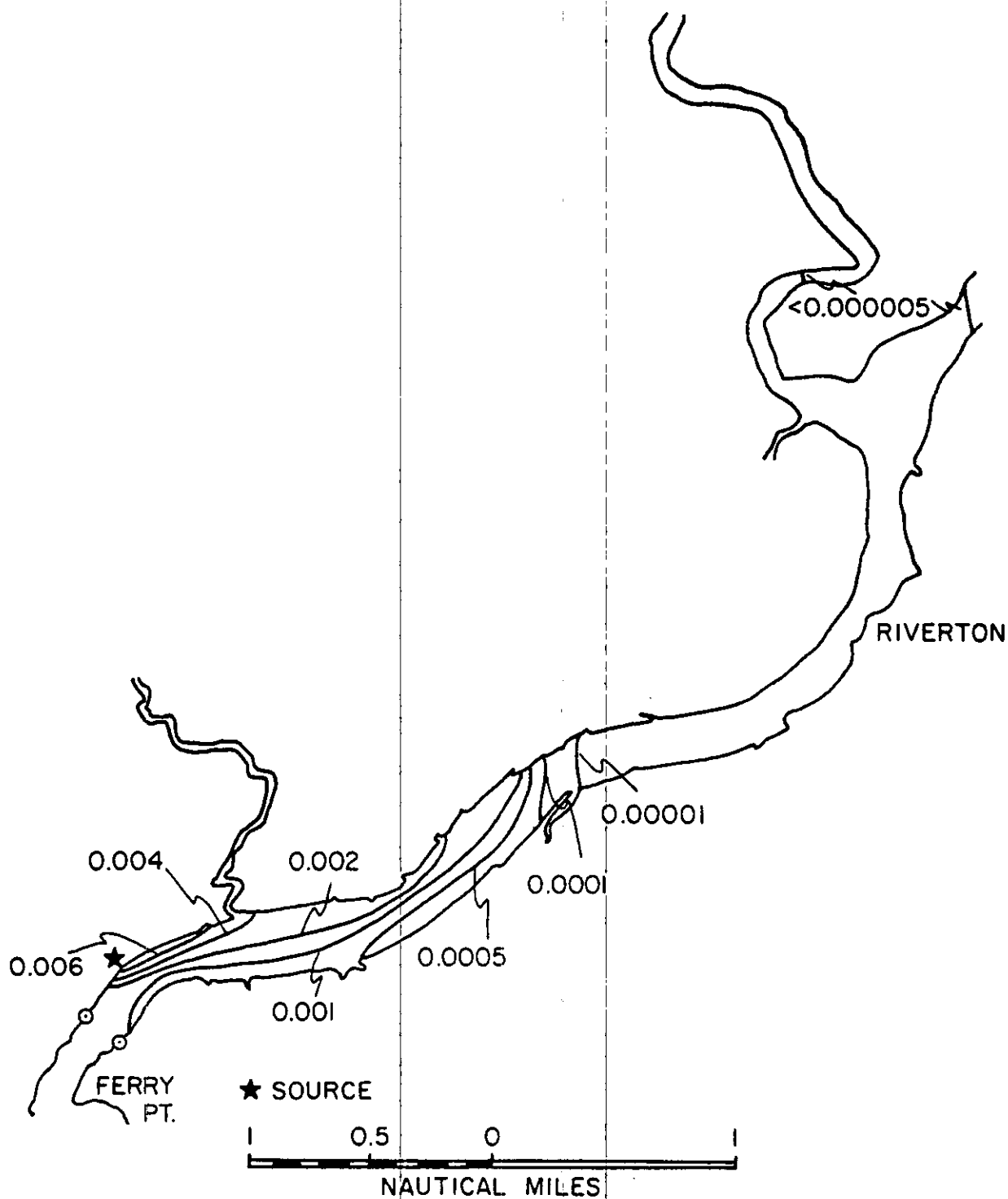


Figure 43. Distribution of relative concentration for a 600 MW plant, at maximum flood, during high river flow, upstream from the source.

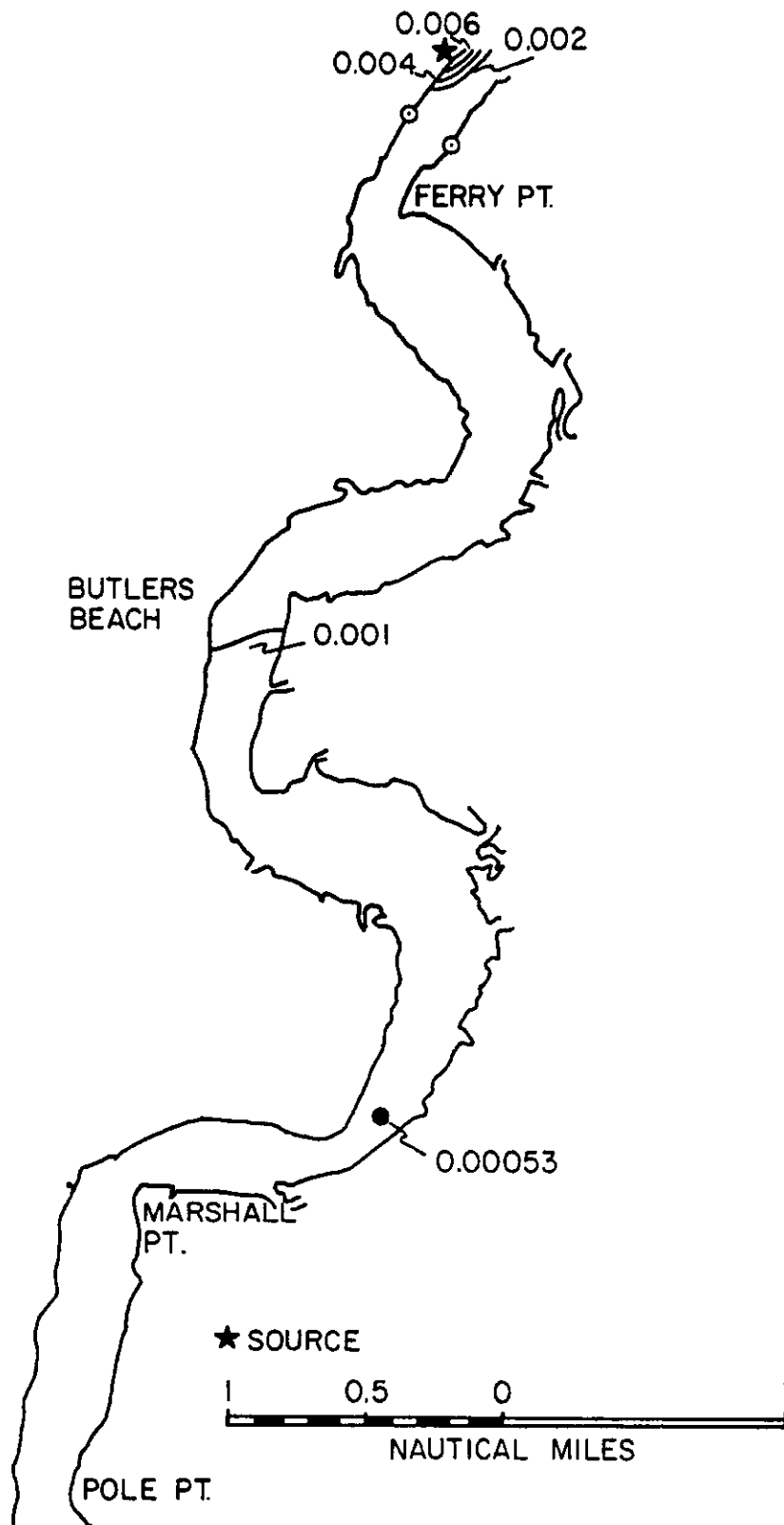


Figure 44. Distribution of relative concentration for a 600 MW plant, at maximum flood, during high river flow, downstream from the source.

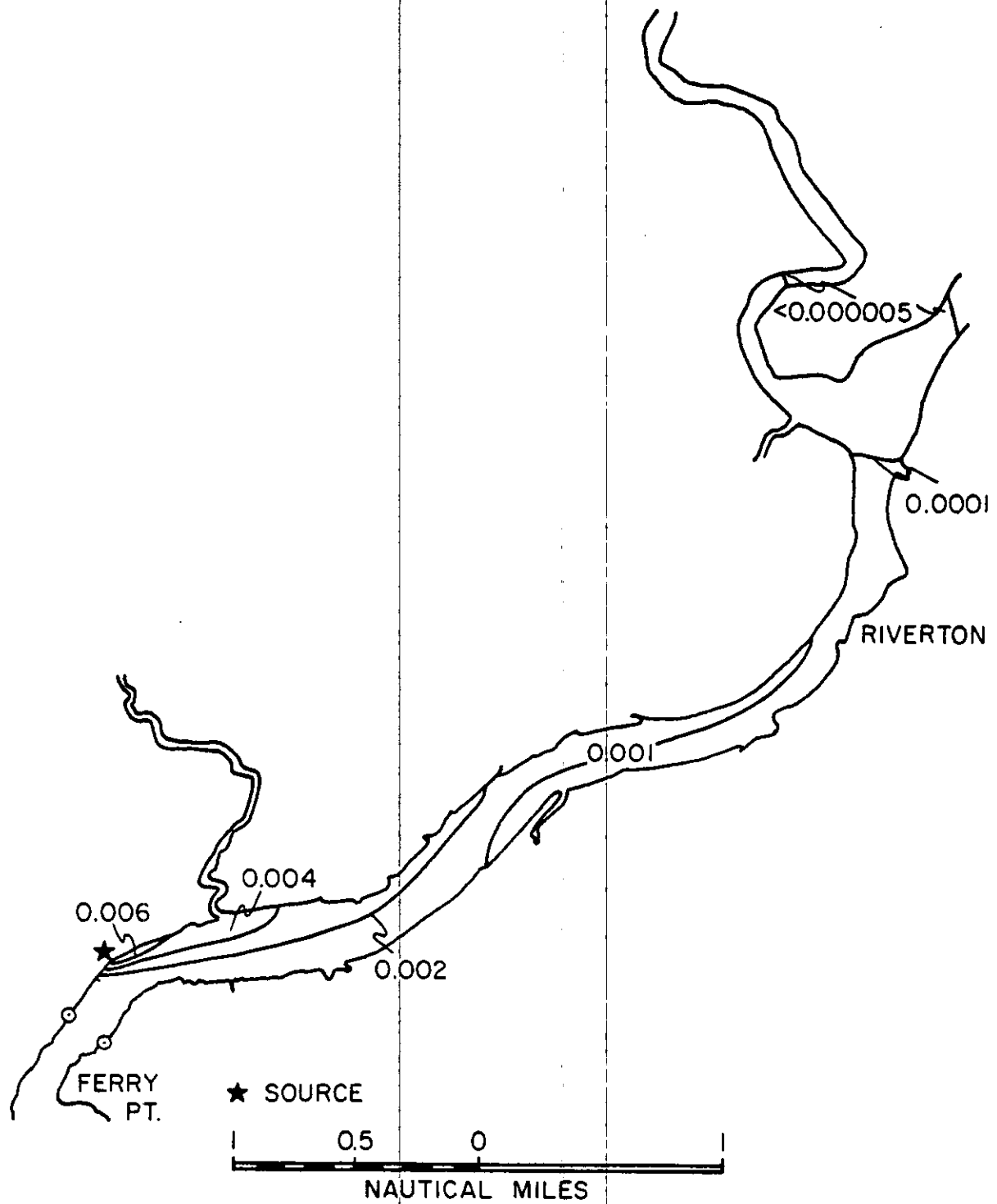


Figure 45. Distribution of relative concentration for a 600 MW plant near slack before ebb, during low river flow, upstream from the source.

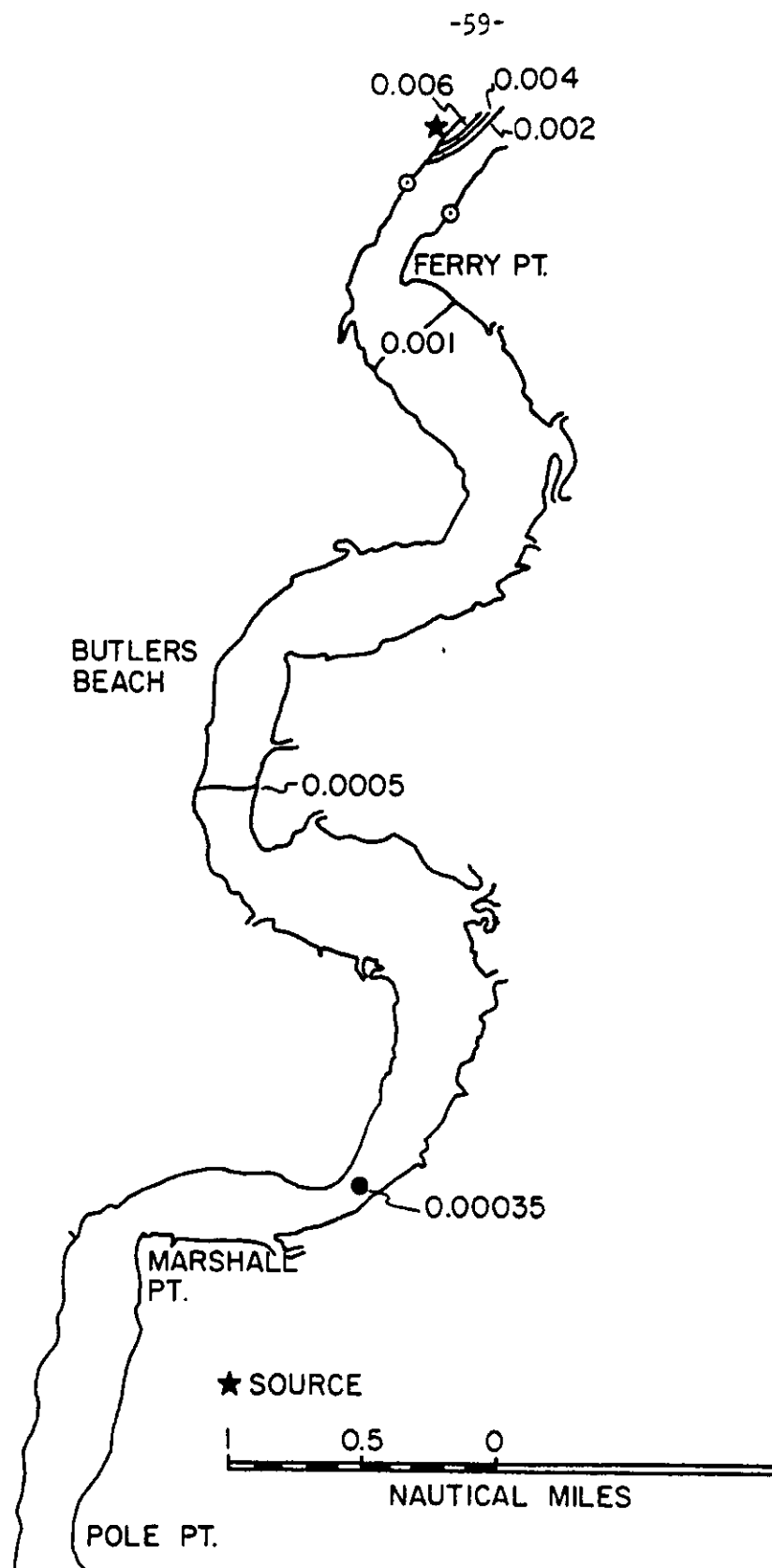


Figure 46. Distribution of relative concentration for a 600 MW plant, near slack before ebb, during high river flow, downstream from the source.

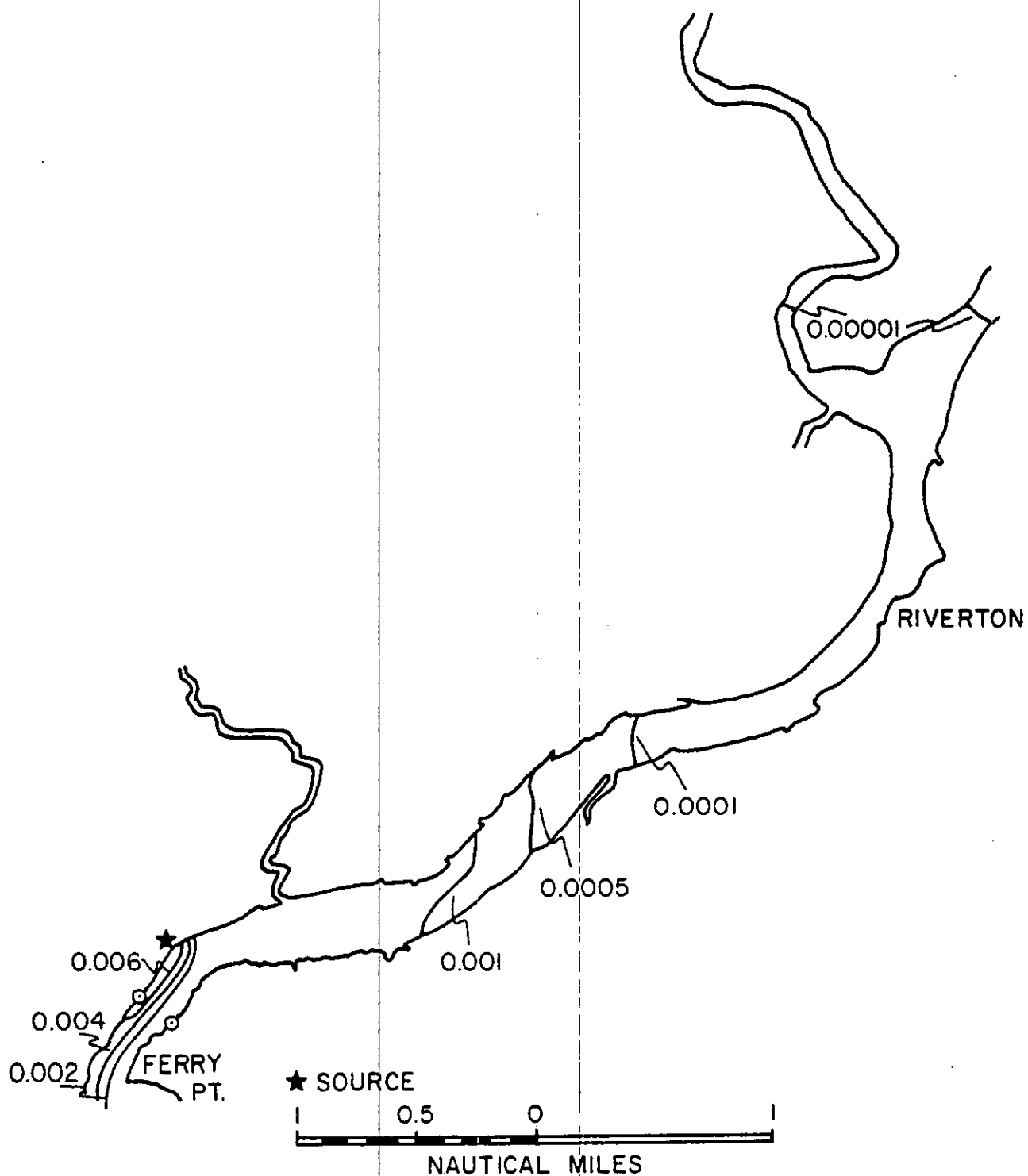


Figure 47. Distribution of relative concentration for a 600 MW plant, at maximum ebb, during mean river flow, upstream from the source.

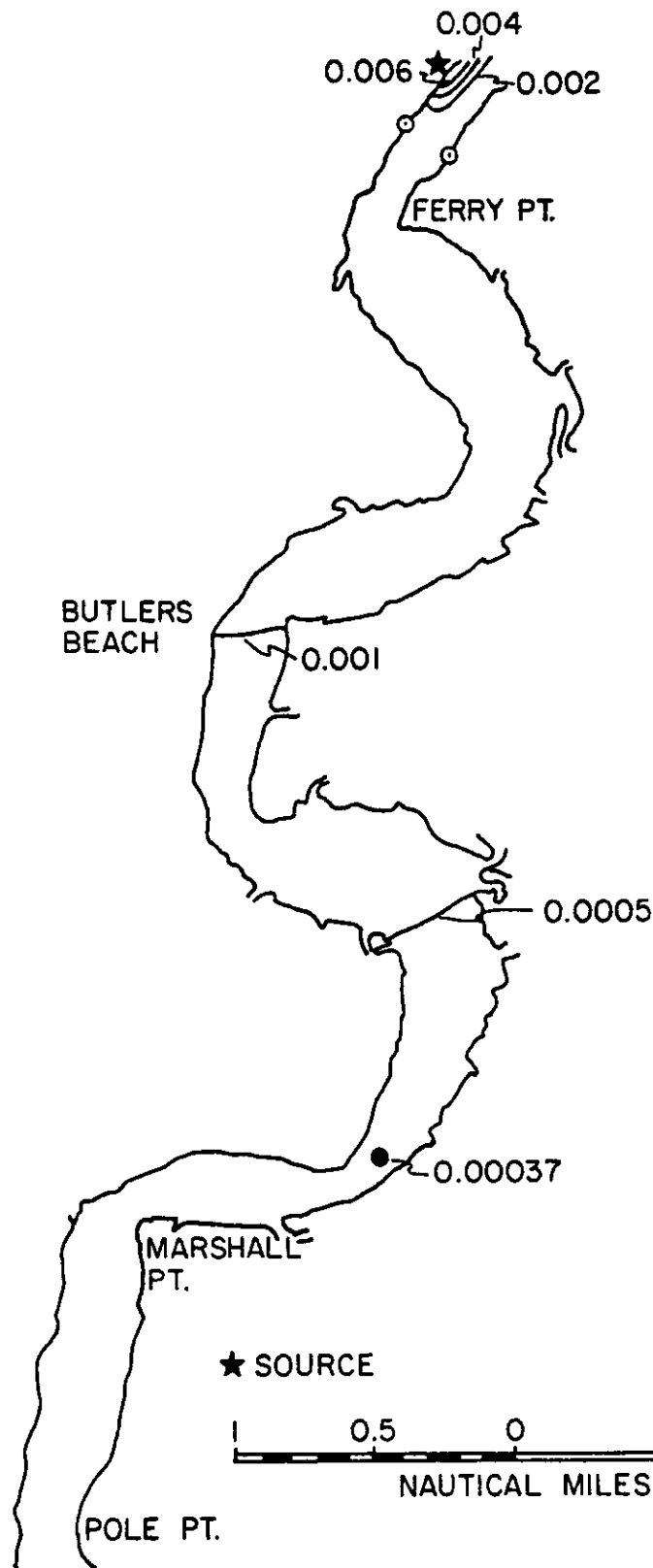


Figure 48. Distribution of relative concentration for a 600 MW plant, at maximum ebb, during mean river flow, downstream from the source.

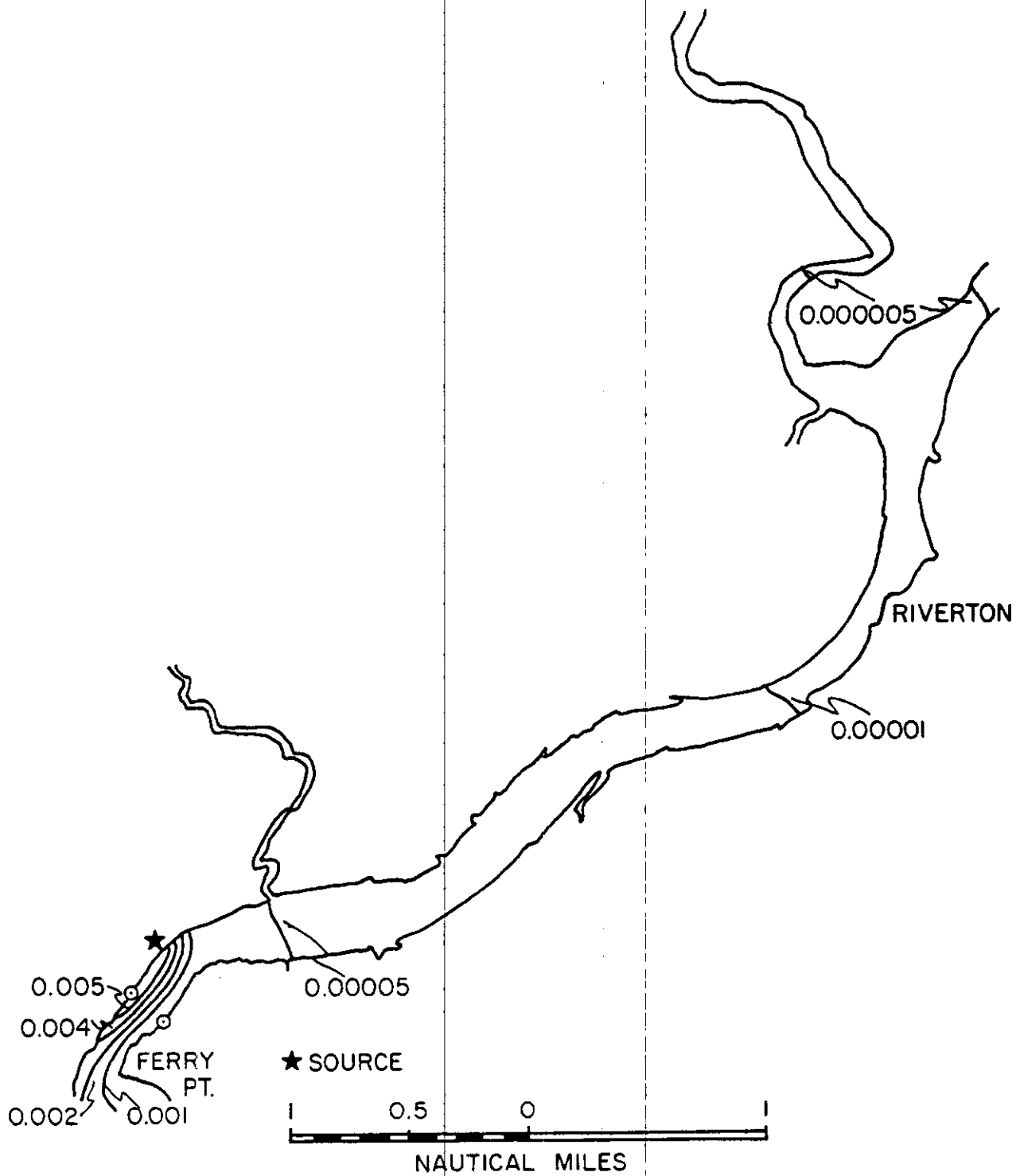


Figure 49. Distribution of relative concentration for a 600 MW plant, near slack before flood, during mean river flow, upstream from the source.

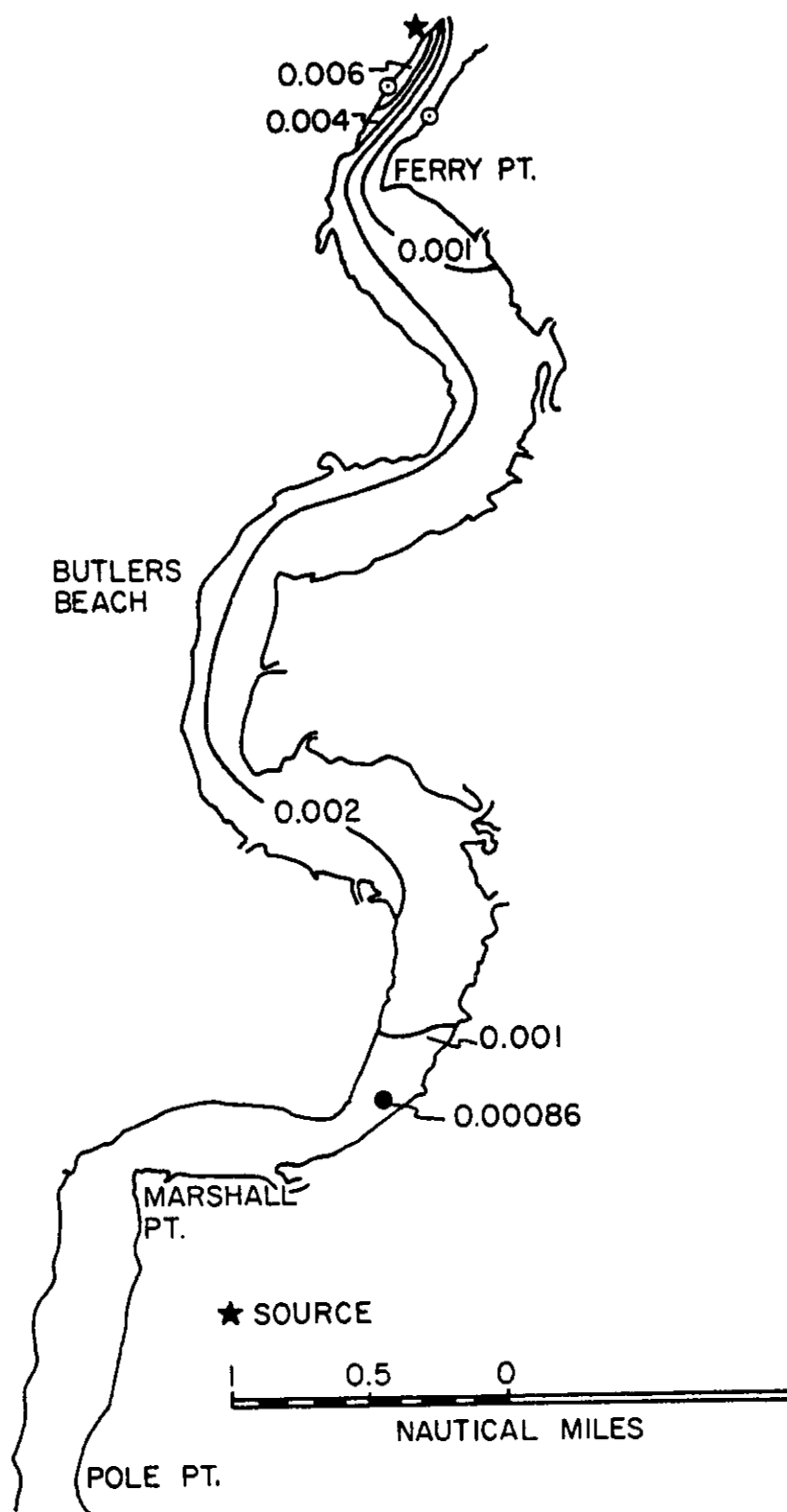


Figure 50. Distribution of relative concentration for a 600 MW plant, near slack before flood, during mean river flow, downstream from the source.

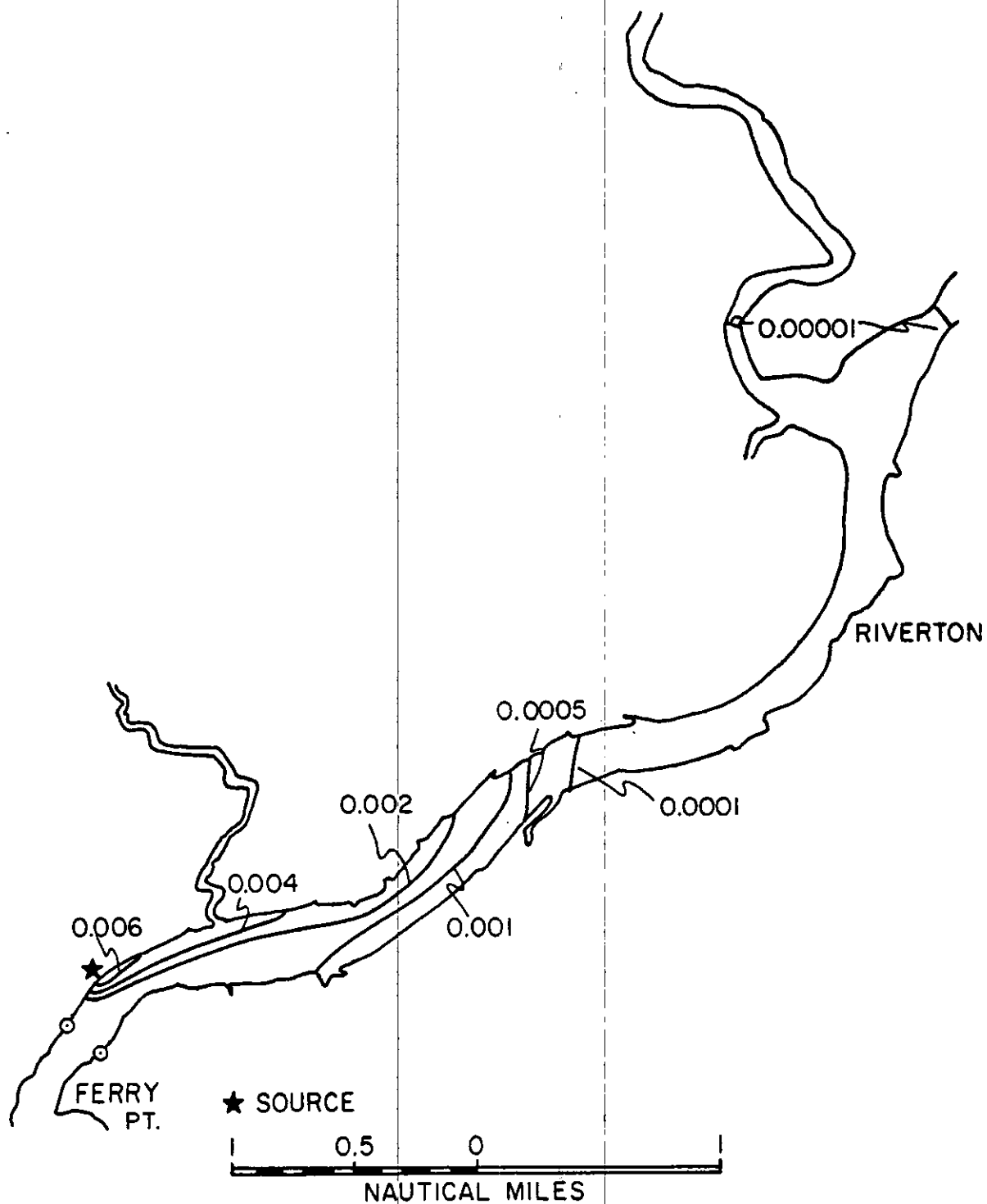


Figure 51. Distribution of relative concentration for a 600 MW plant, at maximum flood, during mean river flow, upstream from the source.

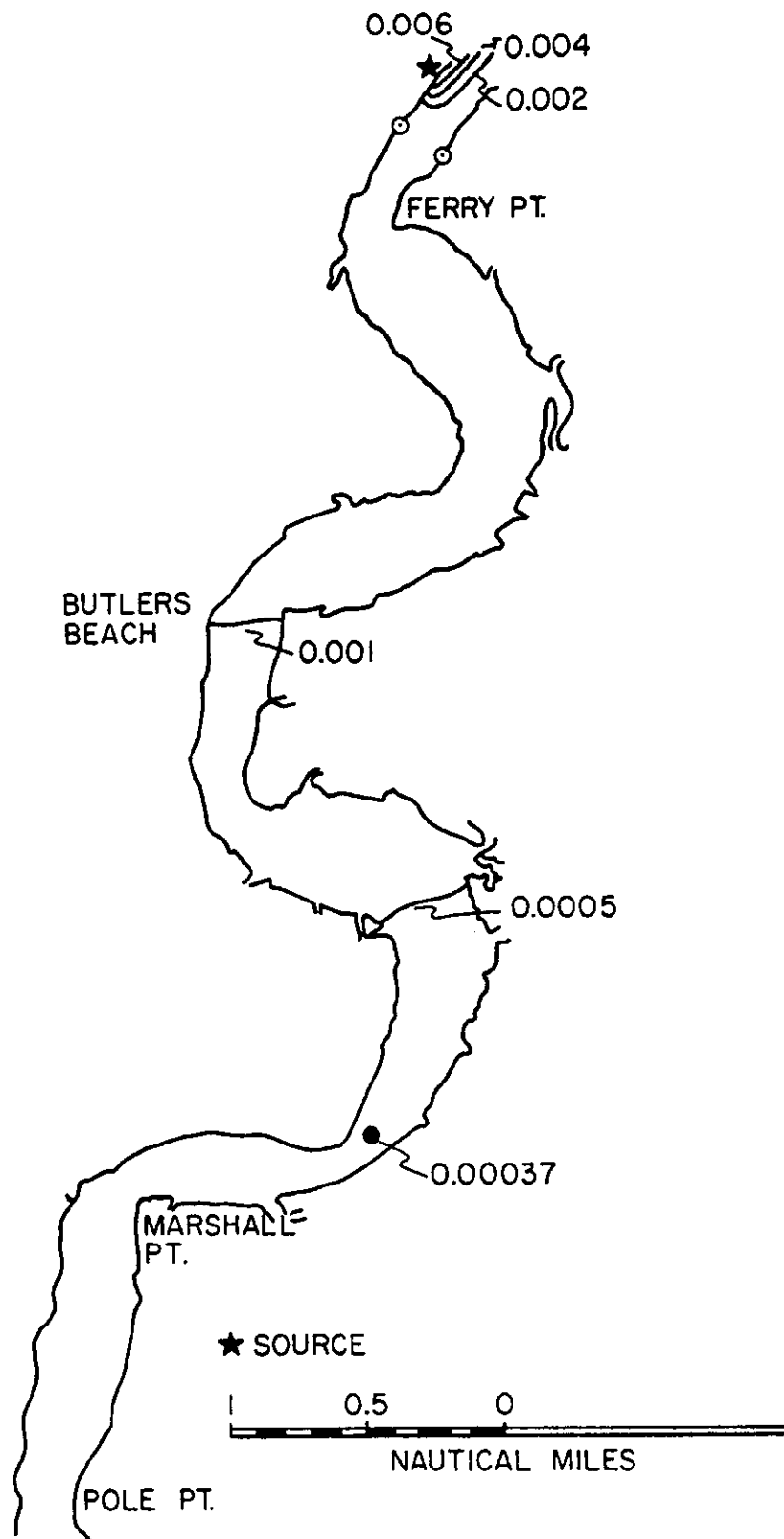


Figure 52. Distribution of relative concentration for a 600 MW plant, at maximum flood, during mean river flow, downstream from the source.

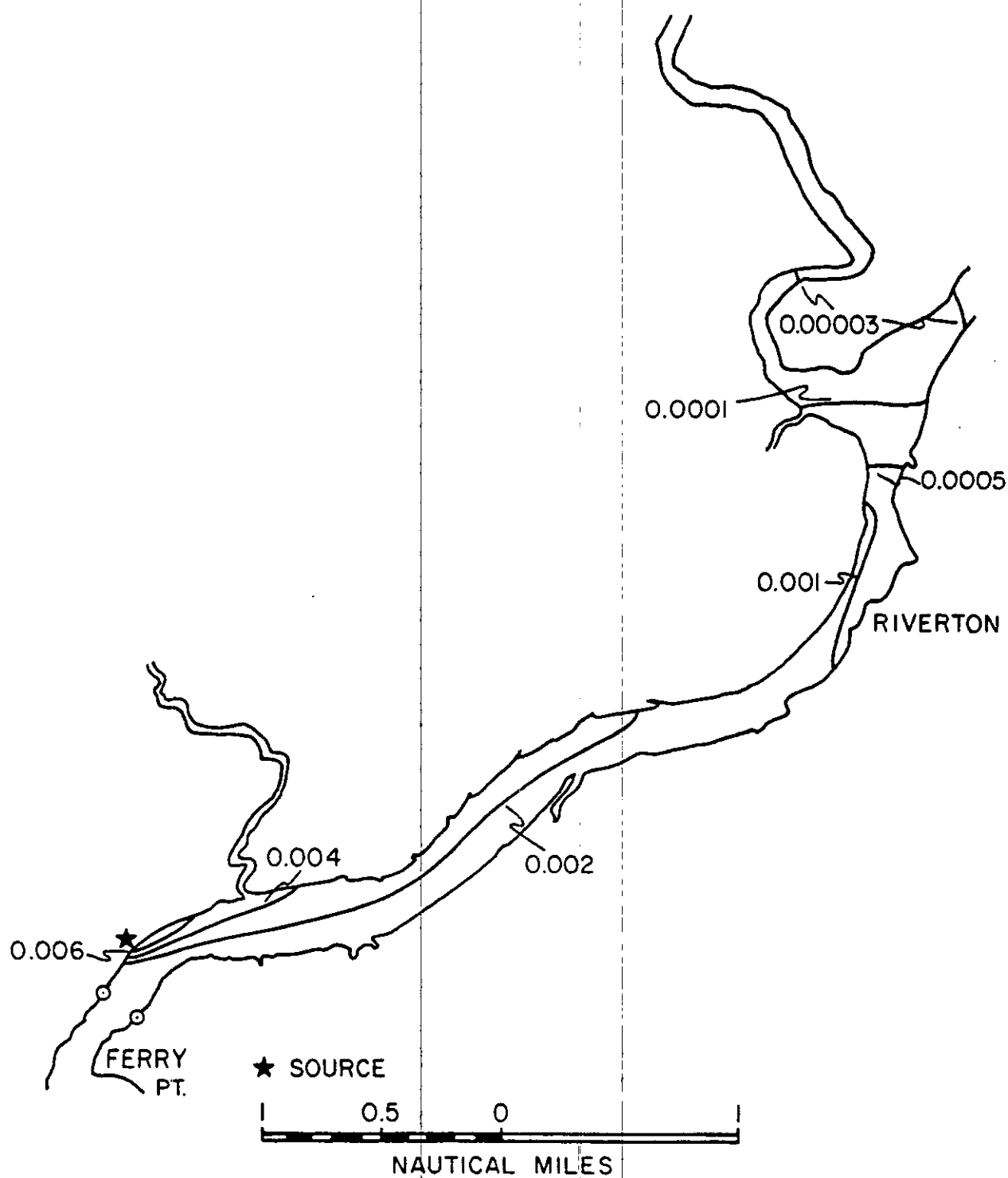


Figure 53. Distribution of relative concentration for a 600 MW plant, near slack before ebb, during mean river flow, upstream from the source.

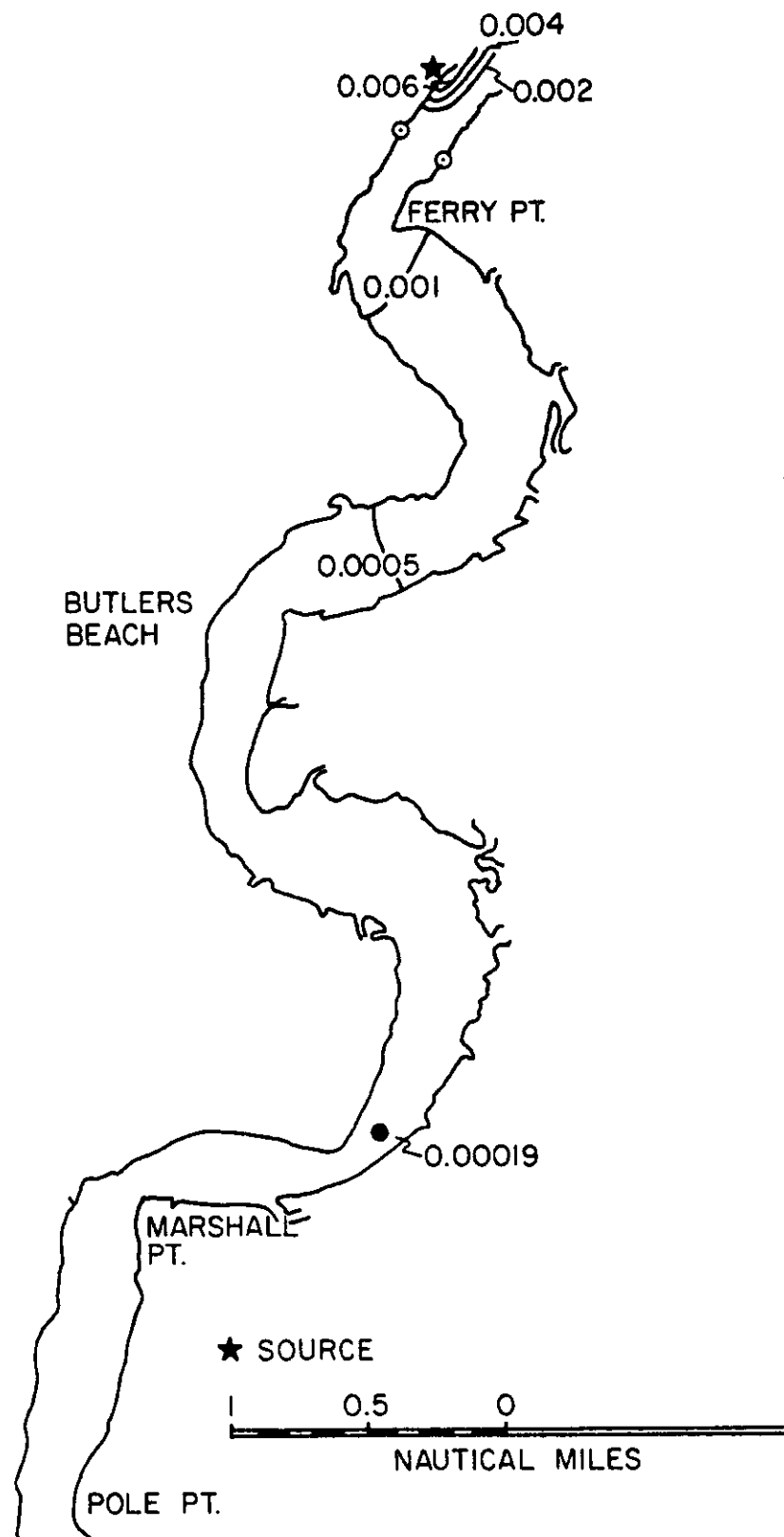


Figure 54. Distribution of relative concentration for a 600 MW plant, near slack before ebb, during mean river flow, downstream from the source.

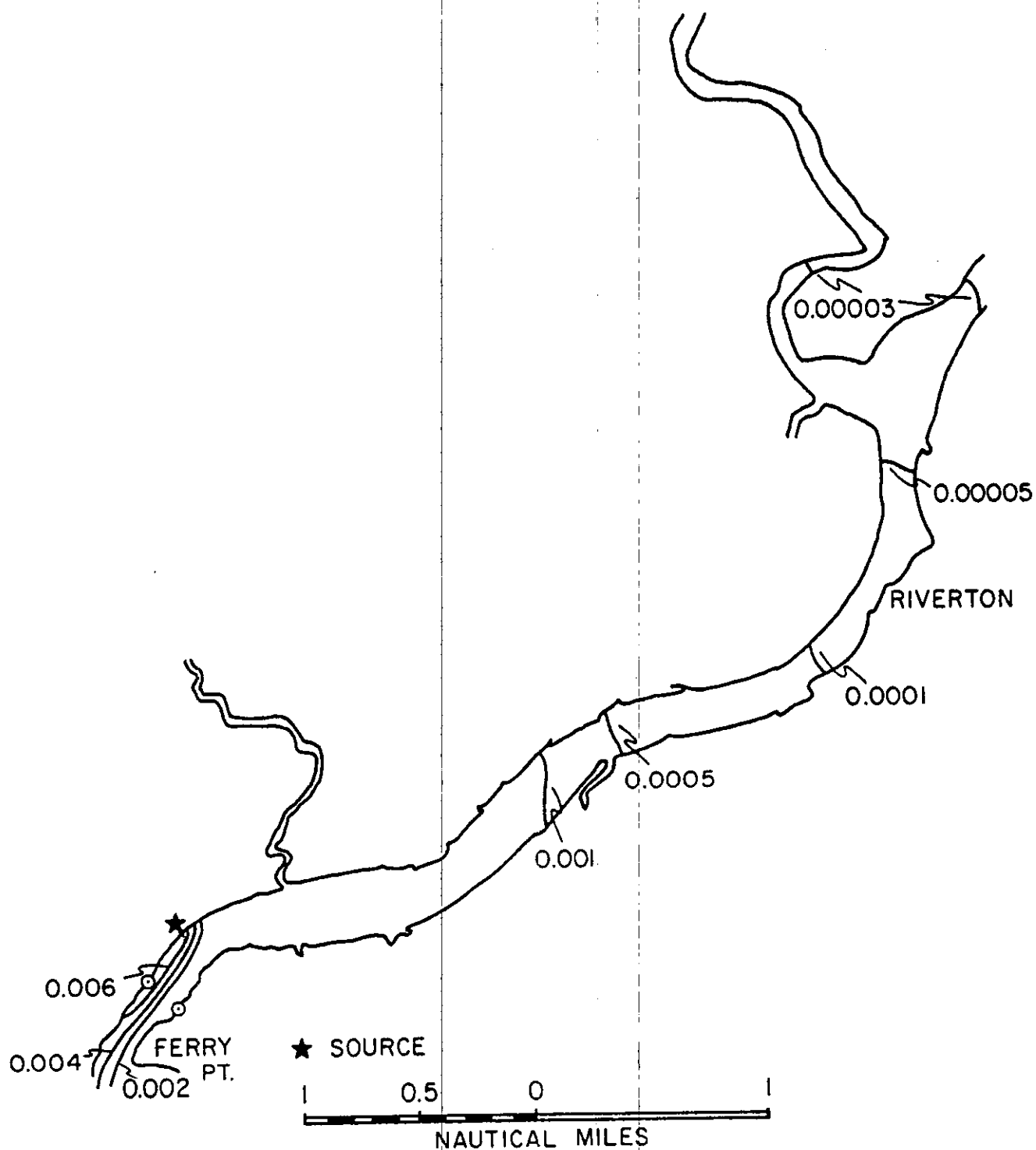


Figure 55. Distribution of relative concentration for a 600 MW plant, at maximum ebb, during low river flow, upstream from the source.

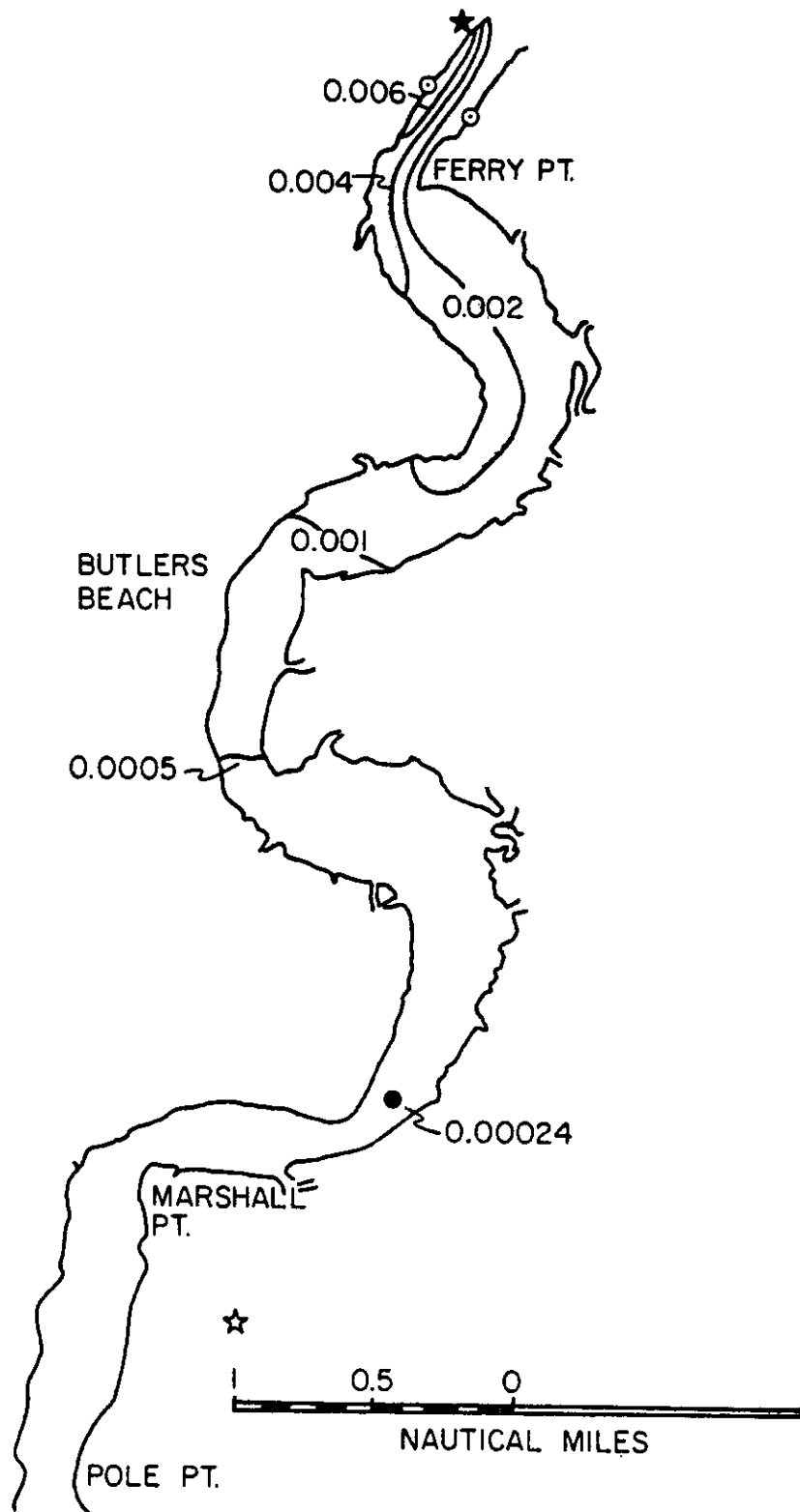


Figure 56. Distribution of relative concentration for a 600 MW plant, at maximum ebb, during low river flow, downstream from the source.

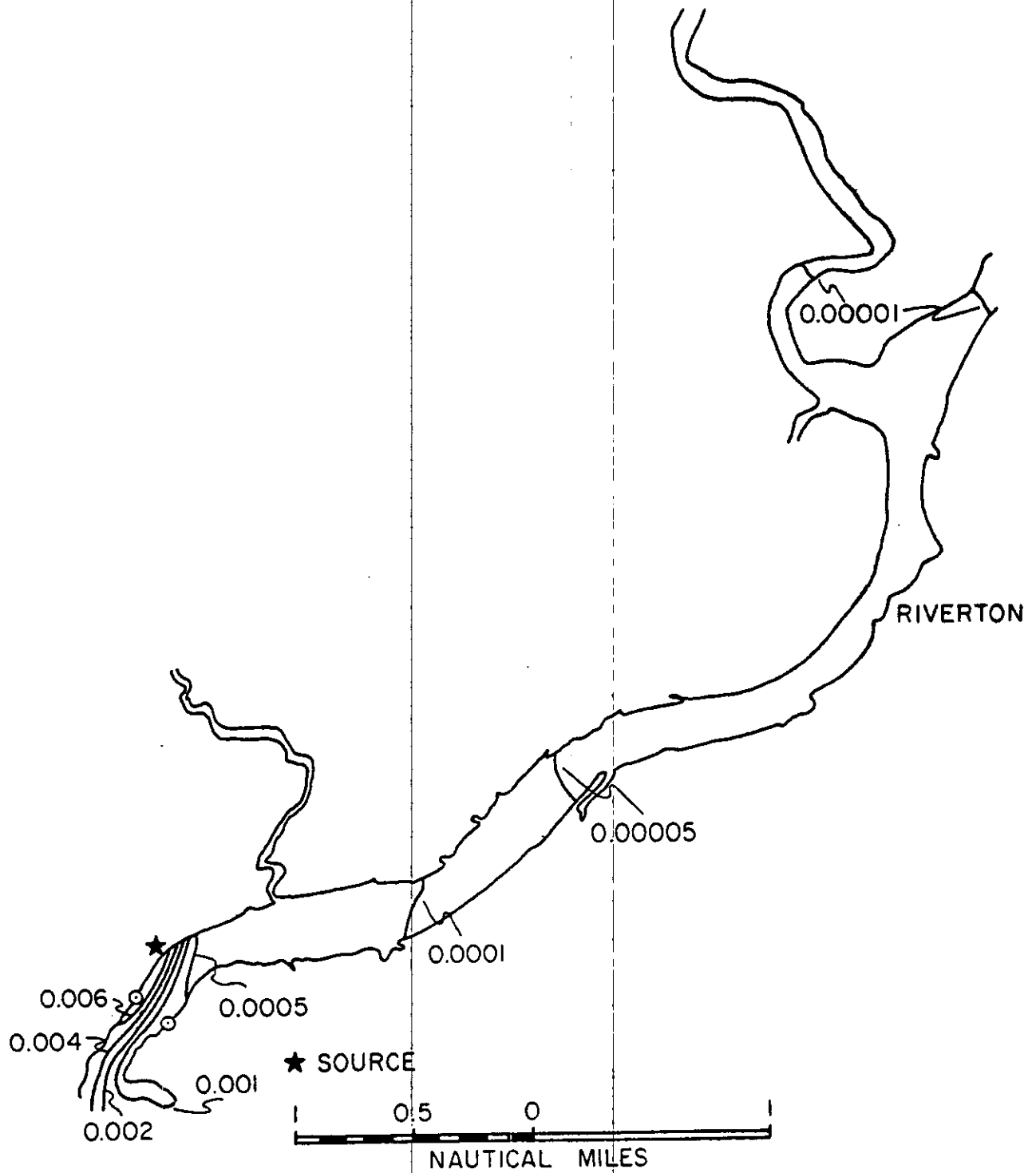


Figure 57. Distribution of relative concentration for a 600 MW plant, near slack before flood, during low river flow, upstream from the source.

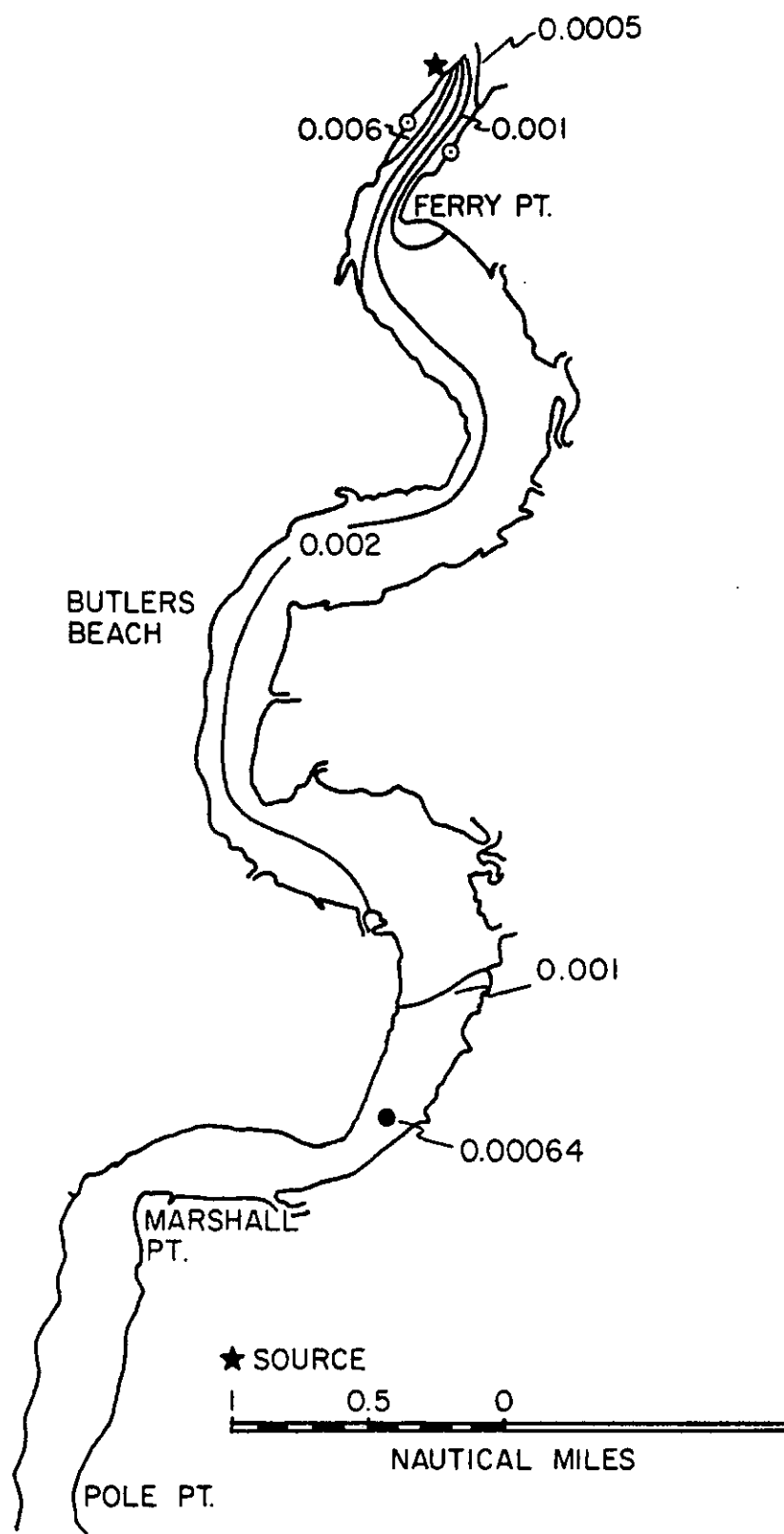


Figure 58. Distribution of relative concentration for a 600 MW plant, near slack before flood, during low river flow, downstream from the source.

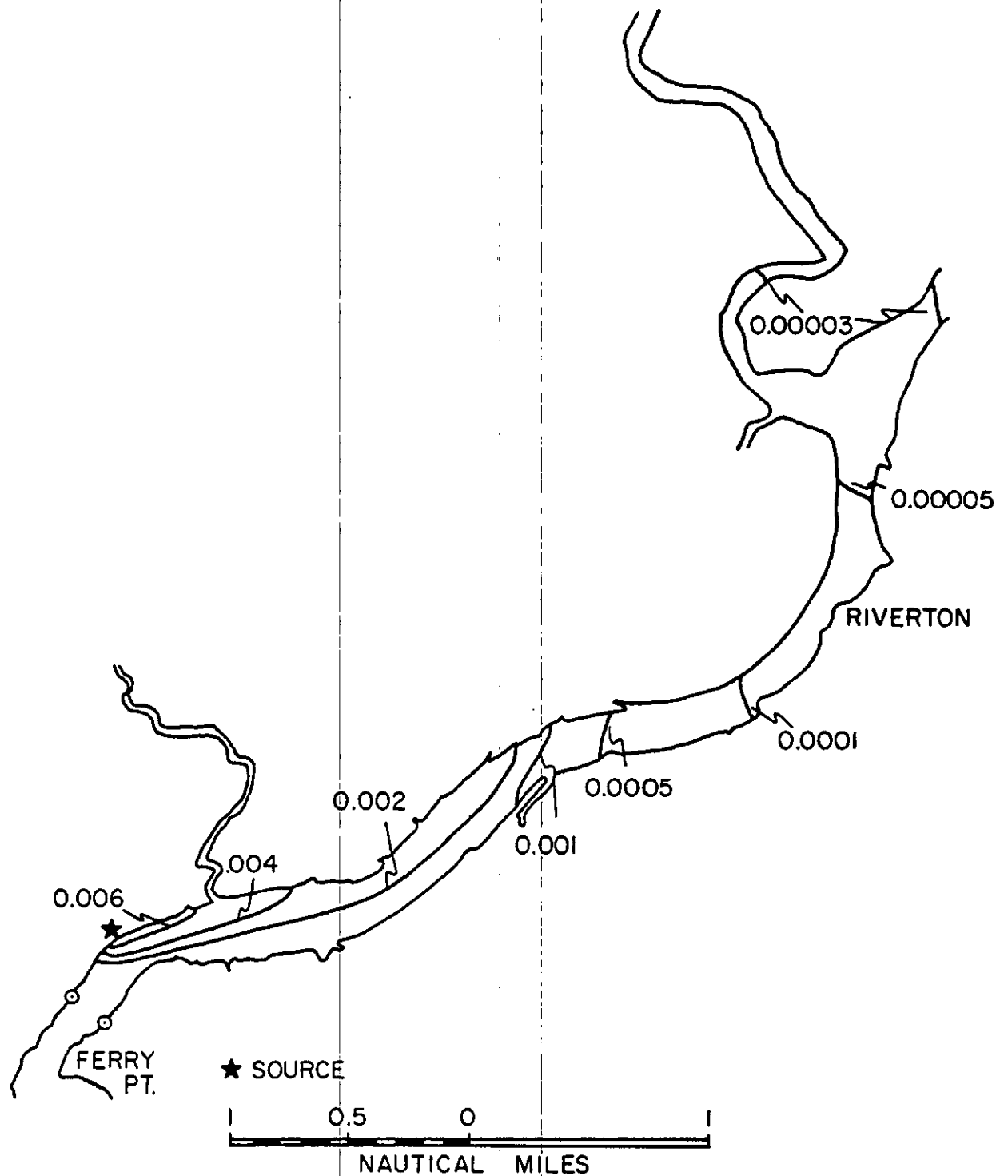


Figure 59. Distribution of relative concentration for a 600 MW plant, at maximum flood, during low river flow, upstream from the source.

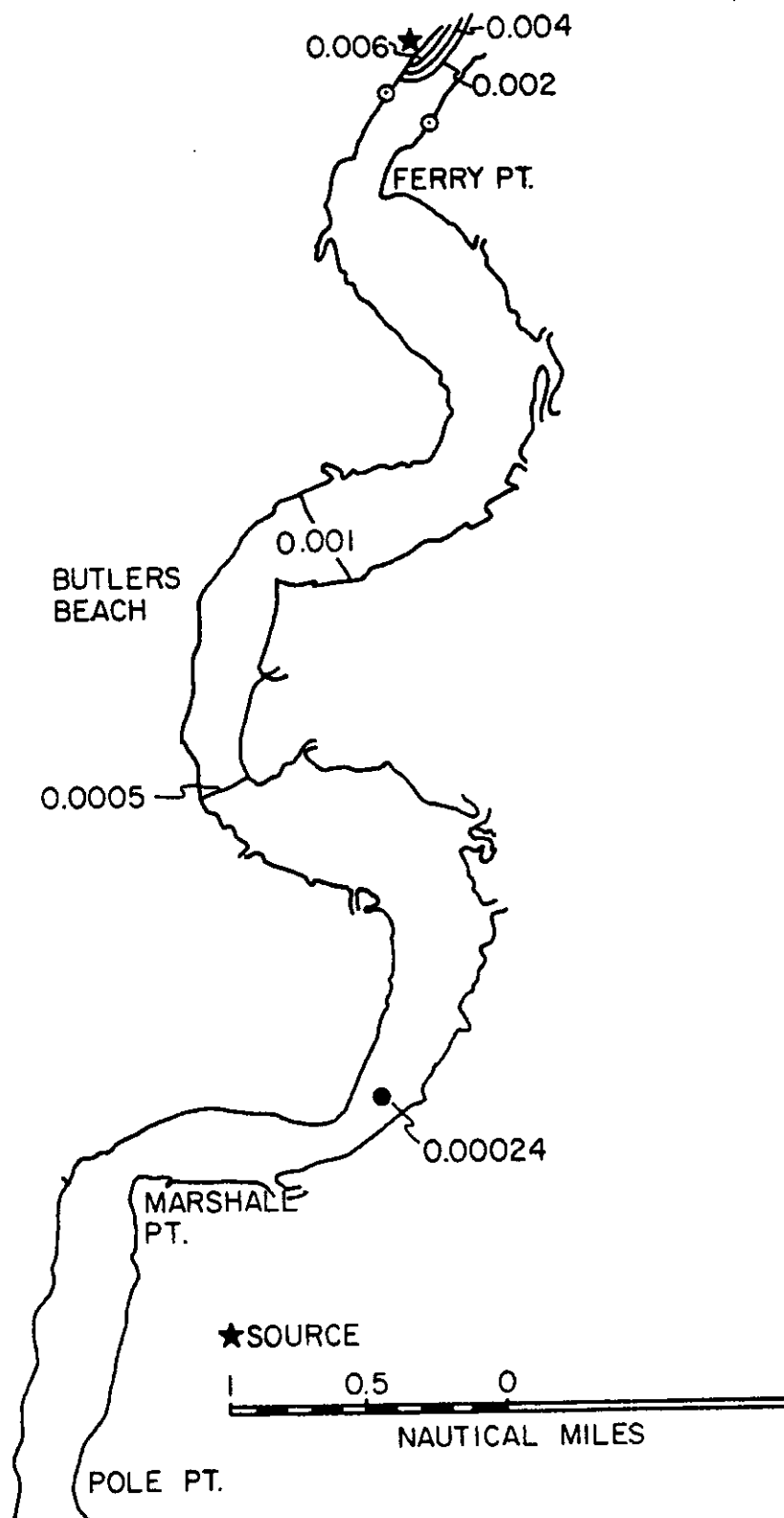


Figure 60. Distribution of relative concentration for a 600 MW plant, at maximum flood, during low river flow, downstream from the source.

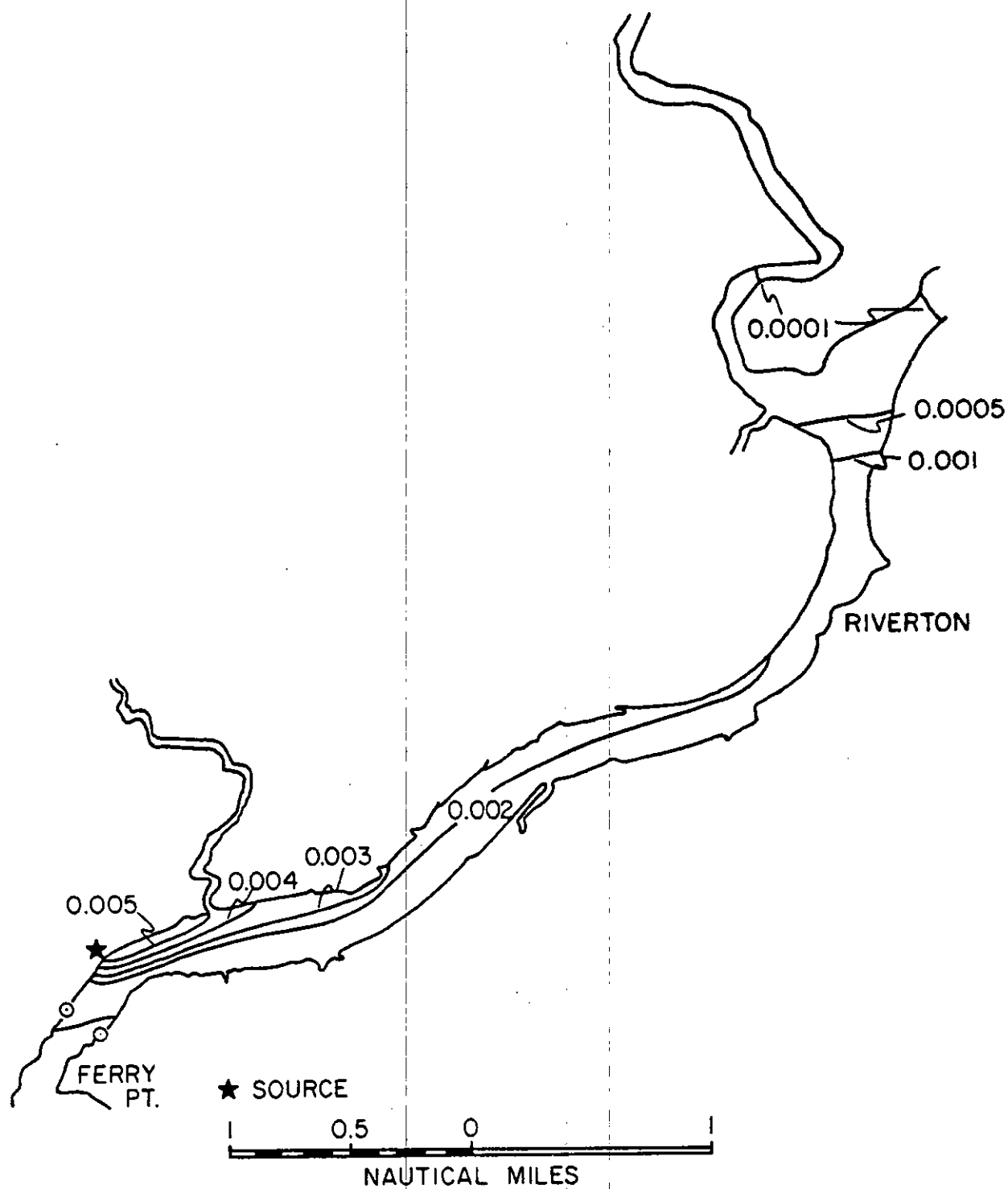


Figure 61. Distribution of relative concentration for a 600 MW plant, near slack before ebb, during low river flow, upstream from the source.

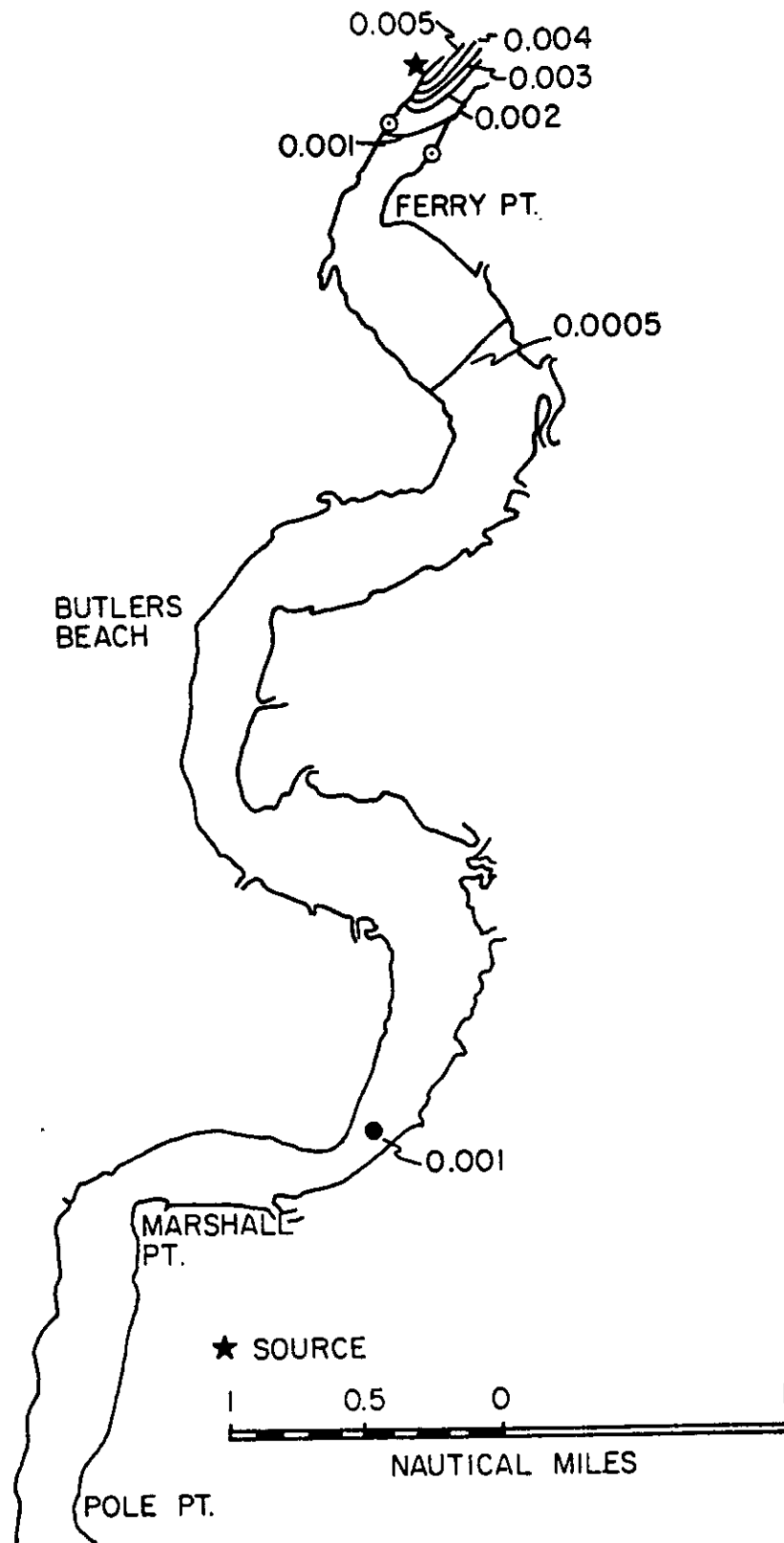


Figure 62. Distribution of relative concentration for a 600 MW plant, near slack before eff, during low river flow, downstream from the source.

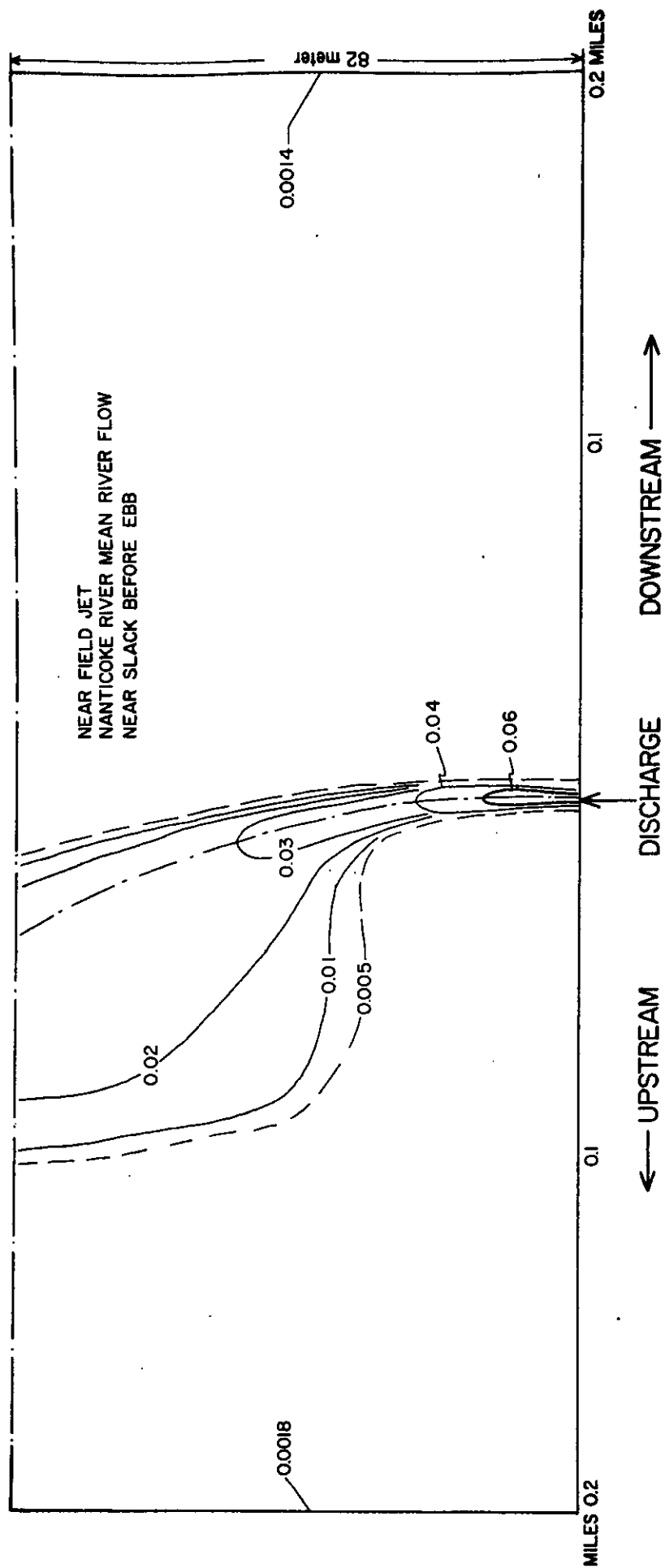


Figure 64. Isolines of relative concentration in the near field plume for a 600 MW plant for mean river flow, for near slack before ebb.